

Distribution Agreement

In presenting this thesis or dissertation as a partial fulfillment of the requirements for an advanced degree from Emory University, I hereby grant to Emory University and its agents the non-exclusive license to archive, make accessible, and display my thesis or dissertation in whole or in part in all forms of media, now or hereafter known, including display on the world wide web. I understand that I may select some access restrictions as part of the online submission of this thesis or dissertation. I retain all ownership rights to the copyright of this thesis or dissertation. I also retain the right to use in future works (such as articles or books) all or part of this thesis or dissertation.

Signature:

Jill Seladi-Schulman

Date

Contribution of viral morphology to influenza virus fitness

By

Jill Seladi-Schulman
Doctor of Philosophy

Graduate Division of Biological and Biomedical Sciences
Microbiology and Molecular Genetics

Anice Lowen, Ph.D.
Advisor

Marty Moore, Ph.D.
Committee Member

Richard Plemper, Ph.D.
Committee Member

Sam Speck, Ph.D.
Committee Member

Dave Steinhauer, Ph.D.
Committee Member

Accepted:

Lisa A. Tedesco, Ph.D.
Dean of the James T. Laney School of Graduate Studies

Date

Contribution of viral morphology to influenza virus fitness

By

Jill Seladi-Schulman
B.S., Georgia Institute of Technology, 2008

Advisor: Anice Lowen, Ph.D.

An abstract of
A dissertation submitted to the Faculty of the
James T. Laney School of Graduate Studies of Emory University
in partial fulfillment of the requirements for the degree of
Doctor of Philosophy
in Microbiology and Molecular Genetics
2014

Abstract

Contribution of viral morphology to influenza virus fitness

By Jill Seladi-Schulman

Influenza viruses come in two shapes – spheres and filaments. Laboratory strains that have been grown extensively in embryonated chicken eggs or in MDCK cells are made up of predominantly spherical and ovoid virions. Filament-producing strains are generally found in low-passage or clinical isolates. Previous work has shown that the filamentous morphology can be gradually lost upon continued passage in embryonated chicken eggs in favor of a predominantly spherical morphology. The fact that filaments are maintained in nature but not in the laboratory suggests the hypothesis that filament-producing viruses have a selective advantage within the infected host that is not necessary for growth in the laboratory. Through serial passage of two filament-producing viruses – A/Netherlands/602/2009 (H1N1) [NL602] and A/Georgia/M5081/2012 (H1N1) [M5081] – in embryonated chicken eggs and MDCK cells, we found that a conversion to a predominantly spherical morphology is not necessary for improved growth in laboratory substrates. However, we did identify two individual point mutations in the M1 matrix protein within the egg-passaged NL602 virus that conferred a spherical morphology as well as a growth advantage in eggs. Additionally, we observed that a filamentous morphology was selected for through passaging of a spherical laboratory strain – A/Puerto Rico/8/1934 (H1N1) [PR8] – in guinea pigs. Through sequencing of the guinea pig passage twelve virus pool, we identified several point mutations within the M1 matrix protein that conferred a filament-producing morphology when introduced individually. The selection for filament production through passaging in an animal host indicated that filament formation *in vivo* is in some way advantageous to the virus. Using a panel of *in vitro* assays, we compared the functional properties of PR8wt and two of the filament-producing M1 single mutants identified through guinea pig passage. Results indicated that filament-producing viruses have a higher neuraminidase activity than their spherical counterparts. No differences were observed in red blood cell binding avidity, hemagglutination inhibition, plaque reduction, or thermostability. Taken together, we have demonstrated that while filament formation can be lost upon passage in laboratory substrates, this trait is selected for within an animal host, and the observed selective advantage may relate to the increased neuraminidase activity of filament-producing viruses.

Contribution of viral morphology to influenza virus fitness

By

Jill Seladi-Schulman
B.S., Georgia Institute of Technology, 2008

Advisor: Anice Lowen, Ph.D.

A dissertation submitted to the Faculty of the
James T. Laney School of Graduate Studies of Emory University
in partial fulfillment of the requirements for the degree of
Doctor of Philosophy
in Microbiology and Molecular Genetics
2014

Acknowledgements

The work contained herein would not have been possible without the help and support of many people both inside and outside of the laboratory:

First and foremost, thank you to my thesis advisor, Anice, for being a great mentor to me over the past three years. You have truly made me a better scientist in every way. Also thank you for your patience and understanding at times when I was frustrated. It was a pleasure being a graduate student in your lab.

A very big thank you to my thesis committee for your continued support, feedback, and valuable suggestions.

To all members of the Lowen and Steel labs – thank you many times over for any help, suggestions, or feedback that you may have provided over the past three years. I enjoyed doing science with all of you.

The support of numerous friends was indispensable throughout this entire journey.

Several members of my entering class became very close, both celebrating each other's successes and helping each other through the bad times. Justin, Lynsey, Bree, Elizabeth, Tim, and Grant – thank you, thank you, thank you! Another special thank you to Alex.

Despite being separated by hundreds of miles throughout my graduate school career, you were a constant source of support and laughter.

My family has been instrumental in providing so much encouragement and support throughout my time in graduate school. They have always been interested in and inquired about the work I am doing (despite not understanding half of the science words coming out of my mouth). They have never stopped letting me know how proud they are of me and that means the world to me. I love you all.

Last but most definitely not least, I would like to thank my husband Mike. I could go on and on at great length regarding his massive contributions in the way of support, understanding, and patience throughout this entire process. If an award for these things existed, he would absolutely win it. Through all of the highs and lows over the past six years of graduate school, he has always been by my side. He is truly the best husband anyone could ask for and I don't think that I could have done this without him.

Table of Contents

Abstract

Acknowledgements

Table of Contents

List of Figures and Tables

Chapter 1: Introduction. 1

Influenza Virus Classification and Organization. 1

IAV Disease and Pandemics. 2

Overview of the Influenza Virus Life Cycle. 5

Influenza Virus Transmission 6

Influenza Virus Morphology 10

The M1 Matrix Protein. 11

Additional Factors that Influence Influenza Virus Morphology. 13

Project Background 15

Figure Legends 19

Figures 20

Chapter 2: Spherical Influenza Viruses Have a Fitness Advantage in Embryonated Eggs, while Filament-Producing Strains Are Selected *In Vivo*. 22

Abstract 23

Introduction. 24

Materials and Methods. 26

Results. 30

Discussion.	37
References.	41
Figure Legends.	46
Figures.	51

Chapter 3: Filament-producing mutants of influenza A/Puerto Rico/8/1934 (H1N1)

virus have a higher neuraminidase activity than the spherical wild-type. 63

Abstract.	64
Introduction.	65
Materials and Methods.	67
Results.	73
Discussion.	80
References.	84
Figure Legends.	89
Figures.	92

Chapter 4: Supplementary Data – Paired Spherical and Filamentous Viruses 98

Introduction.	98
Material and Methods.	98
Results.	101
Conclusions.	103
Figure Legends.	104
Figures.	106

Chapter 5: Discussion and Future Directions	111
Introduction of artificial mutations previously shown to affect viral morphology results in general attenuation.	111
An exclusively spherical morphology is not necessary for growth in laboratory substrates, while filament formation is selected through passaging <i>in vivo</i>	112
Filament-forming rPR8 M1 mutant viruses have a higher neuraminidase activity compared to rPR8wt virus.	114
Possible mechanisms promoting increased neuraminidase activity observed in filament-forming strains.	115
Possible benefits of increased neuraminidase activity to viral fitness.	118
Overall summary and conclusions.	121
Figure Legends.	121
Figures	123
 References	 127

List of Figures and Tables

Chapter 1: Introduction

Figure 1: Generation of paired spherical and filamentous viruses

Figure 2: Serial passage experiment set-up

Chapter 2: Spherical Influenza Viruses Have a Fitness Advantage in Embryonated Eggs, while Filament-Producing Strains Are Selected *In Vivo*

Figure 1: Low-passage human influenza virus isolates have filamentous morphology

Figure 2: Ten egg passages led to loss of filaments for M5081 but not rNL602 virus

Figure 3: EP10 Lines show improved growth in embryonated chickens eggs

Figure 4: Ten serial passages in MDCK cells led to a loss of filaments for two of six lineages

Figure 5: CKP10 Lines show improved growth in MDCK cells

Figure 6: T169I and Q198K mutations in the rNL602 M1 protein result in a predominantly spherical morphology

Figure 7: Compared to the wild-type virus, rNL602 M1 T169I and M1 Q198K mutant viruses show improved growth in eggs but inferior growth in MDCK cells and guinea pigs

Figure 8: Compared to the wild-type virus, rNL602 M1 T169I and M1 Q198K mutant viruses show delayed growth and transmission in guinea pigs

Figure 9: Serial passage in guinea pigs led to the emergence of rPR8 virus variants with filamentous morphology

Figure 10: Point mutations in the rPR8 M1 protein result in robust filament formation

Figure 11: Compared to the wild-type virus, rPR8 M1 mutant viruses show similar or inferior growth in eggs, MDCK cells, and guinea pigs

Figure 12: Compared to the rPR8wt virus, the rPR8 GP P12 virus transmits in guinea pigs while the rPR8 M1 N87S virus does not

Chapter 3: Filament-producing mutants of influenza A/Puerto Rico/8/1934 (H1N1) virus have a higher neuraminidase activity than the spherical wild-type

Figure 1: rPR8 M1 R101G and rPR8 M1 N87S viruses elute red blood cells at a faster rate than rPR8wt virus.

Table 1: 128 HAU of rPR8wt, rPR8 M1 N87S and rPR8 M1 R101G viruses comprise comparable infectious titers and genome copies

Figure 2: rPR8 M1 R101G and rPR8 M1 N87S viruses have higher neuraminidase activity than rPR8wt virus

Table 2: rPR8 M1 N87S and rPR8 M1 R101G viruses have a higher neuraminidase activity than rPR8 wt virus in a MUNANA-based assay

Figure 3: NA and M1 protein levels between rPR8wt, rPR8 M1 N87S, and rPR8 M1 R101G are similar when normalized to NP protein levels

Figure 4: rPR8wt, rPR8 M1 N87S, and rPR8 M1 R101G viruses have the same red blood cell binding avidity.

Table 3: There are no differences in hemagglutination inhibition among rPR8wt, rPR8 M1 N87S, rPR8 M1 R101G viruses

Figure 5: There is no difference in plaque reduction among rPR8wt, rPR8 M1 N87S, and rPR8 M1 R101G viruses

Figure 6: No difference in virion stability at an elevated temperature was observed between rPR8wt, rPR8 M1 N87S, and rPR8 M1 R101G viruses

Chapter 4: Supplementary Data – Paired Spherical and Filamentous Viruses

Figure 1: rPR8wt is predominantly spherical in morphology while rPR8fil produces filamentous virions

Figure 2: rPR8fil is attenuated in laboratory substrates

Figure 3: rPR8fil is attenuated in a primary cell line and in guinea pigs

Figure 4: rNL602wt produces filamentous virions while the rNL602sph mutant produces spherical virions

Figure 5: rNL602sph is attenuated in all substrates

Chapter 5: Discussion and Future Directions

Figure 1: Filtered rPR8 M1 N87S and rPR8 M1 R101G mutant viruses elute red blood cells at a similar or lower rate compared to rPR8wt

Figure 2: Filtered rPR8wt, rPR8 M1 N87S, and rPR8 M1 R101G have negligible neuraminidase activity when compared to non-filtered viruses in the MUNANA assay.

Figure 3: Mucus-based neutralization assay

Figure 4: Identification of additional mutations in N87S-containing clones using HRM analysis.

Chapter 1: Introduction

Influenza Virus Classification and Organization

Influenza A virus (IAV) is a member of the viral family *Orthomyxoviridae*. The family *Orthomyxoviridae* contains five genera: *influenzavirus A*, *influenzavirus B*, *influenzavirus C*, *Thogotovirus*, and *Isavirus*. A sixth genus, *influenzavirus D*, has been proposed following the discovery of a 7-segmented orthomyxovirus circulating in cattle (52). IAV is enveloped and contains an eight-segmented negative-sense RNA genome that encodes at least ten proteins (105). The major reservoir of IAV is wild aquatic birds. Recently, bats have also been identified as a possible reservoir of IAV; however, strains isolated in bats are highly divergent from those isolated in avian and other mammalian hosts (145, 146, 156).

Influenza A viruses are typed based on serological classification of their hemagglutinin (HA) and neuraminidase (NA) surface glycoproteins. Influenza A virus binds to sialic acid moieties located on the surface of the cells of the respiratory tract. The viral HA protein is involved both in the receptor binding and membrane fusion events. To date, eighteen HA subtypes have been identified (H1 – H18). The recently identified H17 and H18 are unique to strains isolated from bats. (145, 146) Historically, viruses of only three of these subtypes (H1, H2, and H3) have become established in the human population. Recently, viruses containing the avian H5, H7, and H9 subtypes have also been associated with zoonotic human infection. The NA protein aids in viral egress by cleaving the sialic acids on the surface of the infected cell, thus preventing virus clumping and reinfection of the same cell. Currently, eleven NA subtypes (N1 – N11)

have been identified. N10 and N11 have been identified recently in bats, however characterization of N10 indicates a lack of neuraminidase activity. Two NA subtypes (N1 and N2) have been associated with human epidemic strains. In addition, viruses with N2, N3, N7 and N9 subtype NAs have transmitted to humans from avian species (76, 105, 145, 146, 170).

Influenza A viruses are diverse. Due to the fact that the IAV polymerase lacks proofreading ability, mutations can occur frequently over the course of viral replication.

In the laboratory, the rate at which random errors in replication occur has been documented to be approximately 1×10^{-4} errors per nucleotide. Selection of viruses carrying point mutations that confer a fitness advantage (such as escape from host antibodies) results in fixation of those mutations in the viral population (genetic drift).

The rate at which mutations become fixed in the viral genome has been calculated to be higher than 1×10^{-3} mutations per site per year for avian influenza A viruses (27). The segmented nature of the IAV genome also enables the virus to undergo genetic reassortment in the event that a cell is coinfecting with two different strains. Reassortment can produce progeny viruses that contain a novel constellation of gene segments (genetic shift). Indeed, the pandemic viruses of 1957, 1968, and 2009 were generated through one or more reassortment events (159).

IAV Disease and Pandemics

IAV can infect humans, causing acute respiratory illness. Once infected, incubation times range from twenty-four hours to several days. Symptoms typically include headache, high fever, cough, nasal congestion, body aches, and malaise (159). Additionally, IAV is

the causative agent of seasonal epidemics of respiratory illness as well as occasional pandemics. Influenza A virus pandemics of the past century include those of 1918, 1957, 1968, and 2009.

Pandemics

The 1918 H1N1 influenza pandemic is estimated to have killed approximately 50 million people worldwide and remains unprecedented in its severity (62). Most influenza outbreaks exhibit a “U-shaped” pattern of mortality, with the majority of fatal cases occurring in the very young and the elderly. The 1918 pandemic exhibited a “W-shaped” pattern, with significant mortality occurring in otherwise healthy individuals aged 20-40, likely mediated by an aberrant immune response or “cytokine storm” (8, 64, 68).

Secondary bacterial infections acquired over the course of illness played a dominant role in mortality as well (17, 92, 132). A recent study using a novel, host-specific molecular clock approach has indicated that the 1918 virus likely emerged via a reassortment event that brought together a human H1 and the remaining seven genome segments from an avian virus (158).

The next pandemic occurred in 1957, and is thought to have originated in China. An H2N2 subtype strain, the pandemic virus had obtained its HA and NA segments from reassortment with an avian virus (123). Additionally, the PB1 segment was also of avian origin (65). The remaining five gene segments (PB2, PA, NP, M, and NS) were likely preserved from strains circulating in humans prior to the 1957 pandemic.

In 1968, a new pandemic virus of the H3N2 subtype, thought to have originated in Hong Kong, replaced the circulating H2N2 virus. In this case, the HA segment of the circulating H2N2 virus was replaced with that of an avian-derived H3 (123). Like the

1957 pandemic virus, it was also observed that the PB1 segment of the 1968 pandemic virus was obtained from an avian virus (65).

Between late-2008 and early 2009 a novel H1N1 influenza virus emerged in Mexico and began circulating in humans (102). The outbreak spread worldwide and was defined as a pandemic in June 2009 by the WHO. The 2009 pandemic virus was of swine origin but contained genes from five different lineages, including those of both North American and Eurasian swine influenza viruses (44, 136). The six gene segments contributed from the North American swine lineages were derived from a triple-reassortant virus that had been circulating in swine since 1998 (15, 154). This triple-reassortant virus acquired its PB2 and PA segments from an avian virus, its PB1 segment from a human H3N2 subtype influenza virus, and the remaining gene segments from the classical swine H1N1 lineage (153). The remaining two gene segments (NA and M) of the 2009 pandemic strain were derived from the Eurasian avian-like swine lineage (44, 136).

Seasonal epidemics

IAV infection exhibits a seasonal pattern in temperate climates (140). The highest infection rates are observed during the winter months, which is thought to be due to improved transmission under conditions of lower temperature and humidity (78). On average, 10-20% of the United States population is infected each year. The attack rate of the virus is observed to be highest in children (90). The rate at which the virus spreads has been shown to relate to the level of pre-existing immunity within the population and the virulence of the virus (159). Influenza is estimated to cause between 50,000-100,000 hospitalizations each year, with the most hospitalizations occurring in young children and the elderly. Additionally, seasonal IAV epidemics can have a significant economic

impact as a result of losses in overall productivity due to absenteeism from work or school (159).

Overview of the Influenza Virus Life Cycle

The site of IAV infection in mammalian hosts is the epithelium of the upper respiratory tract. The viral NA protein appears to play a role early in infection, most likely through the cleavage of sialic acids present in the surrounding mucins, thus providing access to the surface of the target cell (86). Following binding of the HA to sialic acids present on the cell surface, the virus is endocytosed. IAV can enter the cell using both clatherin and non-clatherin mediated pathways as well as macropinocytosis (35, 37, 84, 119, 133). Lowering of the pH mediated by acidification of the endosome promotes changes in the structure of the HA protein leading to membrane fusion (reviewed in detail in (50)). The M2 proton channel, a small IAV transmembrane protein, allows protons to pass through to the interior of the virion, thus leading to the dissociation of the ribonucleoprotein (RNP) complex from the M1 matrix protein (19, 107). Nuclear localization sequences on the viral nucleoprotein (NP) and polymerase subunits (PB1, PB2, and PA) facilitate the transport of the RNPs to the nucleus following uncoating of the virion (34, 66, 95, 98, 100, 103, 142, 155, 160). IAV transcription and replication occurs within the host cell nucleus with the genomic RNA serving as a template for production of both the mRNA and the complementary RNA (cRNA) needed as a genome replication intermediate (54, 58, 129). The proteins PB1, PB2, and PA comprise the viral polymerase and are associated with the viral RNP complexes. The PB1 protein contains the RNA-dependent RNA polymerase activity (109). IAV primes transcription by “snatching” caps from host

pre-mRNAs (108). The PB2 protein binds the pre-mRNA cap while the PA protein contains the endonuclease activity needed to remove the cap from its pre-mRNA (36, 49, 165). Following transcription, IAV mRNAs are transported from the nucleus and translated by the host cell machinery to produce viral proteins. In the later phases of replication, M1 enters the nucleus and, along with NEP (NS2), and the cellular protein CRM1, mediates the export of the newly-synthesized RNP complexes through nuclear pore complexes (2, 18, 83, 151, 157, 162). The RNPs of IAV are assembled on recycling endosomes containing the Rab11 protein and are transported to the membrane via the host cell microtubule network (4, 6, 61, 91). Binding to the cytoplasmic tails of the HA and NA proteins, which associate with lipid rafts rich in cholesterol and sphingolipids, mediates recruitment of M1 to the cell membrane. M1 is also involved in drawing M2 closer to the lipid raft domains (3, 25, 40, 57, 75, 87, 115, 120). The HA, NA, and M1 proteins have all been associated with initiation of budding; however the exact details regarding the involvement of each protein remains unclear (26, 47, 71). The M2 protein promotes membrane scission of the budding virion (110, 116, 121). The viral NA surface glycoprotein is the receptor-destroying enzyme, cleaving the sialic acids on the surface of the virus and infected cells and thus aiding in release of the progeny virion. The NA protein has been shown to cluster on the surface of the budding virion and it is thought that this clustering increases the efficiency of release (22, 96, 101).

Influenza Virus Transmission

Influenza virus can be transmitted from person to person both by contact and aerosol.

Contact transmission can be mediated through direct interaction with an infected

individual or through indirect contact involving contaminated fomites. Aerosol transmission occurs when an infected individual releases infectious respiratory droplets through breathing, coughs or sneezes and an uninfected individual then inhales the droplets. Respiratory droplets expelled by an infected individual can be suspended in the surrounding air for variable lengths of time, depending on the size of the droplets. Smaller droplets remain airborne for a longer period of time, which allows their spread over greater distances and increases the opportunity for transmission to occur (reviewed in (106, 143)). The size of respiratory droplets also impacts the site of initial infection in recipient hosts: larger aerosol droplets tend to get stuck in the upper respiratory tract while smaller aerosols, or droplet nuclei ($<10\ \mu\text{m}$ in diameter), can be deposited in both the upper respiratory tract and the lower respiratory tract (reviewed in (14)). It is important to note that environmental factors such as the ambient temperature and the relative humidity have also been shown to affect the IAV transmission ((78) and reviewed in (106)).

Viral Factors Affecting Transmission

The receptor binding specificity of the influenza virus HA protein has been shown to affect transmission efficiency. The HA proteins of human IAVs canonically bind to α -2,6 linked sialic acids while avian HAs bind to α -2,3 linked sialic acids (33, 85, 113). Avian HAs have poor binding avidity to the sialic acids found in the human upper respiratory tract, as most of the sialic acids found at this location are of the α -2,6 linkage. This is thought to be a major reason why avian influenza viruses do not transmit from human to human. However, α -2,3 linked sialic acids can be found in the human lower respiratory tract and this binding specificity has been associated with the severe viral pneumonia

observed in human infection with certain avian influenza strains. Many mutations in HA that promote receptor binding to α -2,6 linkages as opposed to α -2,3 linkages and vice versa have been identified (9, 32, 42, 45, 114, 139, 161). Specificity altering mutations within or near the HA receptor binding site and within glycosylation sites in the globular head domain that increase binding to α 2,6-linked sialic acids also increase the efficiency of influenza virus transmission in the ferret model (42, 53, 55, 137, 147).

The acid stability of the HA protein also has an impact on transmission, as the structural changes that occur in HA at low pH are irreversible (82). Highly pathogenic avian influenza (HPAI) viruses have a lower acid stability than avian strains of low pathogenicity (82). Growth in the mammalian upper respiratory tract, which is an acidic environment, requires a more stable HA (82). Stabilizing mutations in the HA of avian IAV strains lead to improved growth within the mammalian upper respiratory tract (69, 166, 167). Coupled with mutations that increase α -2,6 binding, stabilizing mutations have been shown to promote transmission of avian strains in mammalian hosts (53, 55, 131). Amino acid positions 627 and 701 in the viral polymerase protein PB2 have been shown to affect transmission as well. Most human viruses contain a lysine residue at position 627 while avian strains predominantly have a glutamic acid. Encoding a lysine at position 627 has been shown to not only promote transmission in mammals, but also higher rates of replication and better viral growth at 33°C (the temperature of the human upper respiratory tract). Similar observations have been made for viruses encoding an asparagine at position 701 as opposed to an aspartic acid (21, 41, 81, 88, 138, 149). Additionally, the viral NA has been shown to affect transmission (72, 80, 164). The enzymatic activity of the NA affects transmission, as viruses that have acquired

mutations conferring resistance to NA inhibitors (which lower the NA activity) have been shown to transmit more poorly via the aerosol route in the guinea pig model. This defect was not found to be due to lower growth kinetics of the inhibitor-resistant viruses, as the mutant viruses grew similarly to wild-type in eggs, cell culture, and guinea pigs; but is likely due to inefficient release from the infected cell thus lowering the amount of virions present in respiratory droplets (13, 63).

Lastly, several studies have also indicated that the M segment plays a role in IAV transmission (23, 24, 30, 72, 80). The mechanism behind this observation and whether it is directly linked to viral morphology has yet to be determined.

Animal Models for IAV Transmission

Mice are a convenient model for the study of many infectious diseases due to their small size, low cost, ease of genetic manipulation, and the breadth immunologic reagents available. For these reasons, mice are the most commonly used animal model for influenza. IAV does not, however, transmit efficiently between mice and prior adaption of primary IAV strains to mice is usually required to see virulence (79, 124, 125). As such, other animal models have been developed to more effectively study transmission of IAV. These models are the ferret model and the guinea pig model.

Ferrets have long been the gold standard for studying IAV transmission (reviewed in (143)). When infected with IAV, the ferret displays clinical symptoms similar to those observed in humans. Additionally, ferrets can be infected with and transmit primary isolates of IAV without prior adaptation. However, the drawbacks to the ferret model include the limited availability of reagents for studying the immune response to infection as well greater cost and housing requirements relative to those of mice and guinea pigs.

The guinea pig is a more recently developed animal model for the study of IAV transmission. Like the ferret, the guinea pig can be infected with and transmit primary isolates of IAV without prior adaptation. The guinea pig model also has some practical advantages over the ferret model due to the guinea pig's lower cost and smaller size. Unlike the ferret model, there are no detectable signs of clinical disease in the guinea pig; however histological analyses reveal pathology in the guinea pig upper and lower respiratory tracts following influenza virus infection (7, 70, 79, 141, 148).

Influenza Virus Morphology

IAV is a pleomorphic virus, producing virions of two different morphologies (28, 29, 31, 93). The first of these two morphologies are spheres. Spherical virions are about 100 nm in diameter. Most strains that have been grown extensively in laboratory substrates such as embryonated chicken eggs (ECE's) or Madin-Darby canine kidney (MDCK) cells have been shown to form virions of almost exclusively spherical and ovoid morphology. The second of the two morphologies are filaments. Filament-producing viruses are generally found in low-passage or clinical isolates (46, 56, 97, 127). IAV filaments are of variable length and have been observed to be up to 30 μm long (94). It is important to note that filament-producing viruses always coexist with a population of spherical and ovoid virions.

The M1 Matrix Protein

M1 Protein Structure

The M1 matrix protein is the most abundant protein found in the IAV virion. M1 is a 252 amino acid protein encoded on segment 7 of the IAV genome along with the proton channel protein M2, which is generated from an alternatively spliced mRNA (73). The M1 protein is comprised of α -helices that are separated by linker sequences. The crystal structure of the N-terminal domain (comprising amino acids 2 through 158) of M1 has been solved at both acidic (pH = 4) and neutral pH and is composed of two bundles of four α -helices separated by an α -helix-containing linker. The structure of the C-terminal domain has not been solved, as it is particularly sensitive to protease degradation (5, 51, 128).

M1 Protein Function

The M1 matrix protein can oligomerize to form a helical structure under the surface of the viral membrane, providing rigidity to the virion (22, 51, 126) and acting as a bridge between the cytoplasmic tails of the viral membrane proteins and the viral RNP's (73). Early studies indicated that M1 also has an inhibitory effect on viral gene transcription through association with the viral RNP's (152, 171). The C-terminal domain of the M1 protein mediates this interaction (10). M1 also contains a nuclear localization sequence (RKLKR) between amino acid residues 101 and 105 (77, 163). Upon entering the nucleus, M1 is required for the movement of the viral RNP's from the nucleus to the cytoplasm (18, 83, 157). Additionally, NEP (also called NS2) has been shown to bind M1 at this localization sequence (2, 151, 162). NEP is required for export of viral RNP's from the nucleus, contains a nuclear export sequence, and interacts with the cellular

protein Crm1 (a nuclear transport receptor) (99, 104). Masking of the M1 nuclear localization sequence by NEP binding is thought to promote nuclear export of the M1/RNP complex to the cytoplasm.

During virion assembly, M1 associates with the cell membrane (48, 118, 169), interacting with the cytoplasmic tails of the viral proteins HA, NA, and M2 (3, 25, 40, 57, 87).

Deletions or mutations of the cytoplasmic tail regions of HA, NA, and M2 have been shown to affect their association with M1 as well as budding, infectivity, and morphology of the progeny virions (40, 43, 59, 60, 89, 168). Despite the fact that expression of M1 alone has been shown to mediate virus-like particle (VLP) formation in both vaccinia and baculovirus systems, this observation could not be replicated using a transfection model, indicating that other viral proteins are necessary for budding initiation (26, 47, 74).

Expression of the HA and/or NA proteins in a transfection model is sufficient to generate VLPs, suggesting that one or both of these proteins initiates budding (26, 71). The precise role of M1 in viral budding initiation is still unclear, although it has been suggested that the helical structure of the M1 protein could alter membrane curvature, thus increasing the efficiency of budding initiation mediated by the viral glycoproteins (117).

M1 and IAV Morphology

The M1 matrix protein has been shown to be the major genetic determinant of IAV morphology (12, 39, 112). Early studies using reverse genetics indicated that spherical viruses containing the M segment of the filament-producing strain A/Udorn/301/1972 (H3N2) [Udorn] produced filamentous virions (12, 39). Furthermore, spherical viruses containing only the M1 coding region of segment 7 of the Udorn strain also produced filaments (12, 39). Through comparison of the amino acid sequences of the M1 protein

between the spherical strain A/WSN/1933 (H1N1) [WSN] and Udorn, several amino acid differences were identified. Using reverse genetics to introduce single point mutations in WSN M1 corresponding to those found in Udorn indicated that specific residues of M1 were important for filament-formation (12, 20, 39, 112). More recently, cryotomography studies comparing the structure of filamentous and spherical virions showed that the pitch of the helical turn in filamentous virions is different from that of spherical virions (22). This observation supports the idea that the formation of the M1 matrix layer could affect the production of spheres versus filaments.

Additional Factors that Influence Influenza Virus Morphology

Several other viral proteins have also been shown to affect IAV morphology. These proteins include the HA and NA surface glycoproteins, the M2 proton channel, and NP. Additionally, several host cell factors that affect the formation of filamentous virions have also been identified.

Viral proteins

The cytoplasmic tails of HA and NA are highly conserved, containing 10-11 and 6 amino acid residues, respectively. In studies using the spherical laboratory strain WSN, deletion of the HA cytoplasmic tail region still yielded virions predominantly spherical in morphology. However, deleting the cytoplasmic tail region of the NA protein yielded progeny virions with a filamentous morphology (60, 89). Deletion of the cytoplasmic tails of both HA and NA proteins produced progeny virions of a greatly exaggerated filamentous morphology (60).

The M2 proton channel contains a long (54 amino acid residues) cytoplasmic tail region that has been shown to influence virion morphology as well. In a WSN virus containing the M segment of the filament-producing Udorn strain, truncation of the M2 cytoplasmic tail at amino acid position 70 was shown to lead to production of spherical virions (87). Conversely, viruses containing a deletion of the WSN M2 cytoplasmic tail greater than 22 amino acid residues were found to be more filamentous than the wild-type (57). The M2 cytoplasmic tail contains a membrane proximal amphipathic helix (amino acid residues 45-62), which is necessary for membrane association, efficient membrane scission, and also viral filament formation (87, 110, 115, 122, 144). In the Udorn strain, mutation of five hydrophobic residues of the M2 amphipathic helix to alanine has been shown to ablate viral filament formation, resulting in the formation of predominantly spherical and ovoid virions (110, 115).

Through electron microscopy imaging, both WSN and A/Aichi/2/1968 (H3N2) were observed to be spherical despite the fact that the Aichi strain M1 encodes amino acid residues associated with filament formation. When the Aichi M1 segment was placed into the WSN background, filament formation was observed; indicating that another protein besides M1 was influencing the morphology of Aichi. Through the generation of chimeric WSN/Aichi NP proteins on a WSN background, it was observed that the N-terminal region of Aichi NP inhibited the formation of filaments. Several amino acid positions (specifically 214, 217, and 253) of Aichi NP were shown to affect virion morphology. The mechanism behind this effect was suggested to be an altered interaction between M1 and NP, resulting in a conformational change in the M1 matrix layer that in turn affects virion morphology (11).

Host cell factors

Several host factors are important for IAV filament formation. The host cell actin network has been shown to be necessary for the formation of filamentous virions. Treatment of infected MDCK cells with the actin polymerization inhibitor cytochalasin D was shown to ablate filament formation (but not sphere formation) of the Udorn strain (111). Additionally, treatment of infected MDCK cells with inhibitors of actin depolymerization (specifically, jasplakinolide and latrunculin A) was shown to inhibit filament formation but not sphere formation (134). It was proposed that a single lipid raft domain was required for budding of the smaller spherical virions while the larger filamentous virions required several lipid raft domains, perhaps coordinated together by the host cell actin network. Thus, filament formation would be reduced by inhibited actin polymerization and/or depolymerization (134).

Recently, the Rab11 and FIP3 proteins (both involved in membrane trafficking and actin regulation) have been shown to be important for IAV filament budding. Cells depleted for Rab11 and FIP3 were shown to be deficient in filament formation (16).

Project Background

Early studies indicated that the filamentous morphology can be lost in favor of a spherical morphology through repeated passages in ECE's (29, 67). The observation that the filamentous morphology is maintained in nature but is dispensable for growth in laboratory substrates suggests that filaments confer a selective advantage to the virus within the infected host that is not necessary for growth in the laboratory.

Initially, in order to evaluate the hypothesis that filaments confer a fitness advantage *in vivo* while spherical virions are more fit in laboratory substrates, we used reverse genetics to generate paired spherical and filamentous viruses. We used two viruses for this effort – the spherical laboratory strain, A/Puerto Rico/8/1934 (H1N1) [rPR8], and the filament-producing 2009 pandemic strain, A/Netherlands/602/2009 (H1N1) [rNL602]. The mutation K102A was introduced into the M1 protein of rPR8wt to yield a filamentous mutant [rPR8fil]. This mutation was previously shown to confer a filamentous morphology to the spherical laboratory strain WSN (20). The mutations A41V, R95K, and E204D were introduced into the M1 protein of rNL602wt to yield a spherical mutant [rNL602sph]. These three mutations were previously shown to individually confer a spherical morphology to Udorn strain (12, 39, 112). (Figure 1)

Growth curves were performed in four different substrates – ECE's, MDCK cells, human tracheobronchial epithelial (HTBE) primary cells, and guinea pigs – under the expectation that spherical viruses would have a fitness advantage over filament-producing viruses in the common laboratory substrates (ECE's, MDCK cells) while filament-producing viruses would have a fitness advantage over spheres in the primary cells and in the guinea pig. After performing the growth curves, we observed that both mutant viruses (rPR8fil and rNL602sph) were generally attenuated in all substrates.

As the mutations used to generate the paired spherical and filamentous viruses were introduced artificially and were found to attenuate the resulting mutant viruses, we set up a group of serial passage experiments in three different substrates – ECE's, MDCK cells, and an animal host (the guinea pig) – in order to identify naturally-occurring mutations that affect virion morphology. We reasoned that mutations arising naturally over the

course of serial passage are less likely to be attenuating than artificial mutations. The first two substrates – ECE's and MDCK cells – are common laboratory substrates believed to select for spherical virions. We chose to passage two filament-producing viruses in these substrates with the aim of selecting for a variant that produces predominantly spherical and ovoid virions. The two viruses we chose were a recombinant 2009 pandemic strain rNL602 and a clinical isolate, A/Georgia/M5081/2012 (H1N1) [M5081]. Conversely, we passaged the spherical laboratory strain rPR8 in guinea pigs aiming to select for a variant that produces filaments (Figure 2).

We found that a predominantly spherical morphology is not necessary for improved growth in either laboratory substrate, as rNL602 exhibited improved growth but maintained its highly filamentous morphology after ten passages in ECE's and in MDCK cells. We did, however, identify two separate point mutations within the M1 protein of rNL602 egg passage ten (EP10) lineages that, when introduced individually, conferred both a spherical morphology and a growth advantage in ECE's, indicating that a spherical morphology can be advantageous in this substrate (127).

Through passaging of rPR8 twelve times in guinea pigs, we observed the emergence of filamentous virions, indicating a selection for this morphology *in vivo*. Additionally, we identified several point mutations within M1 through sequencing of the M segment of the guinea pig passage twelve (P12) virus pool. When introduced individually using reverse genetics, the resulting mutant viruses produced filaments very robustly when compared to rPR8wt (127).

The fact that filament formation is selected for through passaging in an animal host confirms that there is an advantage to the filamentous morphology *in vivo*, however the

nature of this advantage remained unclear. In an effort to further investigate the nature of this selective advantage, we compared rPR8wt to two of the previously described filament-producing mutants – rPR8 M1 N87S [N87S] and rPR8 M1 R101G [R101G] – in several *in vitro* assays. N87S is the most fit of the mutant viruses and produces very long filaments observed by thin-section transmission electron microscopy (TEM). In terms of the number of filaments produced rather than length, R101G is the most filamentous of the mutant viruses compared to rPR8wt. These mutant viruses represent an ideal system for the identification of functional differences between spherical and filamentous IAV in that i) they are highly similar to rPR8wt – differing only by a single point mutation in M1, ii) they are naturally-occurring, and iii) they produce significantly more filaments in comparison to rPR8wt (N87S – 16%, R101G – 41%).

Due to the differing surface area of filamentous and spherical particles, we focused on assessing possible differences between them on the functions of the HA and NA surface proteins. We found that the filament-producing mutants had a higher NA activity than rPR8wt in two independent NA activity assays. No difference in HAU:PFU ratio, red blood cell binding avidity, hemagglutination inhibition (HI), plaque reduction, or thermostability were observed between the two morphologies. Taken together, it appears that the selective advantage conferred by the filamentous morphology may lie with increased NA activity. Through this work, we have shown that not only in the filamentous morphology is selected for within an animal host, and that filament-producing virions have a higher NA activity than spheres – a functional difference that could be advantageous to the virus for penetration of respiratory mucus, release from host cells and/or release from the host upon transmission.

Figure Legends

Figure 1: Generation of paired spherical and filamentous viruses. A) Reverse genetics was used to introduce the M1 K102A point mutation into the spherical A/Puerto Rico/8/1934 (H1N1) strain, yielding a filament-producing mutant virus. B) Reverse genetics was used to introduce the M1 A41V, M1 R95K, and M1 E204D mutations together into the filament-producing A/Netherlands/602/2009 (H1N1) strain, yielding a spherical mutant virus.

Figure 2: Serial passage experiment set-up. Two filament producing viruses, A/Netherlands/602/2009 (H1N1) and A/Georgia/M5081/2012 (H1N1), were passaged blindly ten times in two common laboratory substrates, embryonated chicken eggs and MDCK cells. The spherical laboratory strain, A/Puerto Rico/8/1934 (H1N1), was passaged twelve times in an animal host, the guinea pig.

Figure 1.

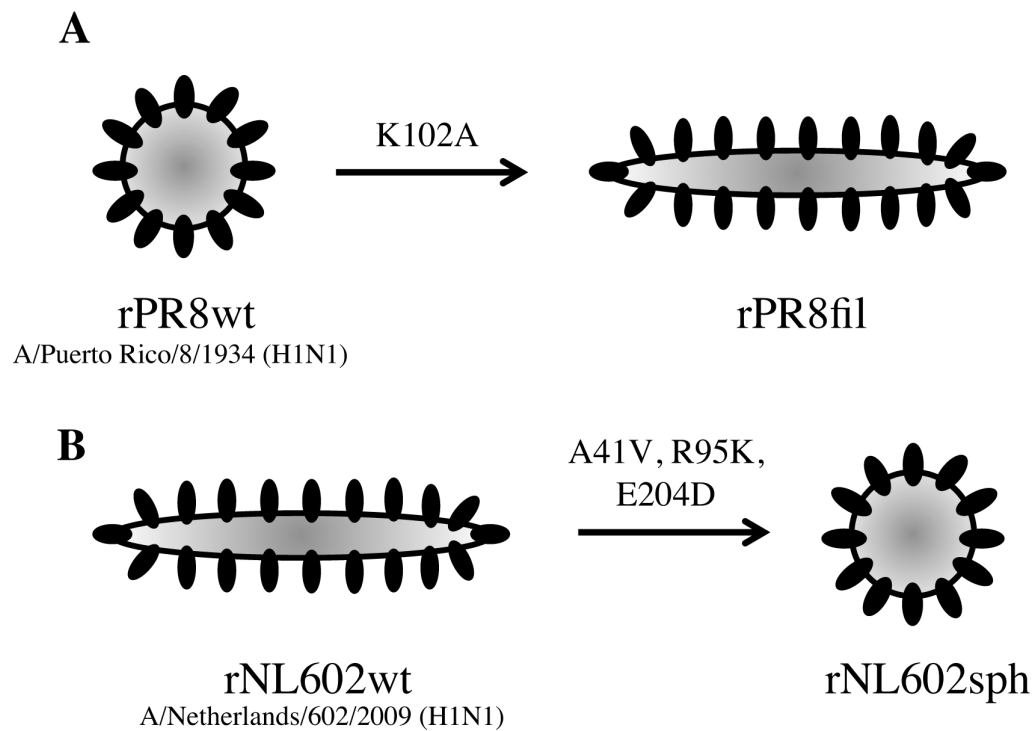
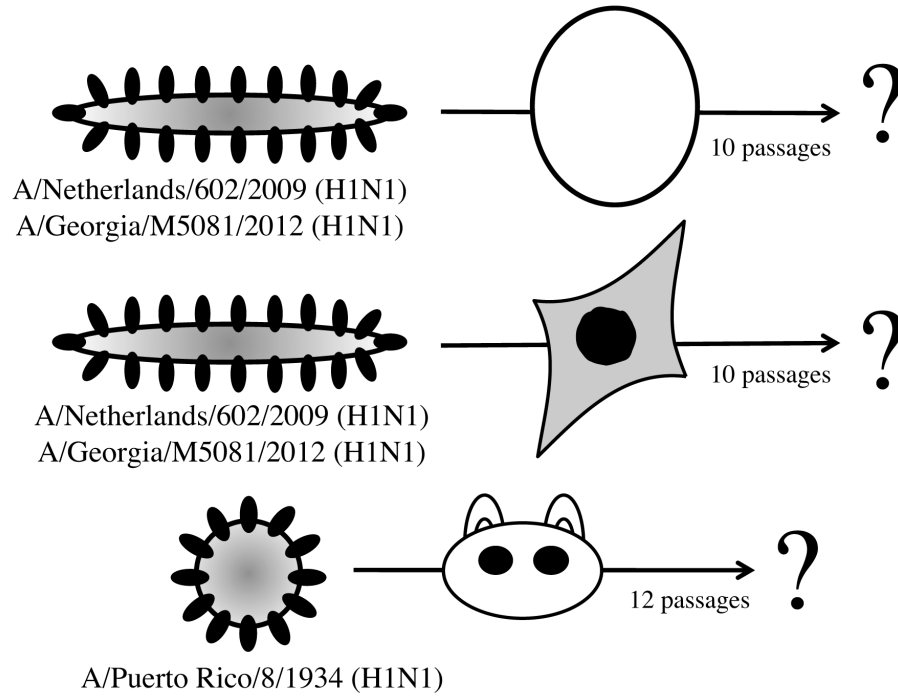


Figure 2.



Chapter 2: Spherical influenza viruses have a fitness advantage in embryonated eggs, while filament-producing strains are selected *in vivo*

Jill Seladi-Schulman, John Steel, Anice C. Lowen#

The work of this chapter was published in 2013 in the *Journal of Virology*.

Article citation:

Seladi-Schulman J, Steel J, Lowen AC. 2013. Spherical influenza viruses have a fitness advantage in embryonated eggs, while filament-producing strains are selected *in vivo*. *Journal of Virology* **87**: 13343-13353

Abstract

Influenza viruses can take on two distinct morphologies: filamentous or spherical. While the functional significance of each virion type is unclear, filaments are generally observed in low-passage isolates while an exclusively spherical morphology is seen in strains grown extensively in laboratory substrates. Previous studies have shown that filamentous morphology is lost upon passage in eggs. The fact that the filamentous morphology is maintained in nature but not in the laboratory suggests that filaments may provide an advantage in the host that is not necessary for growth in laboratory substrates. To test this hypothesis and identify naturally occurring mutations that alter morphology, we examined the effect of serial adaptation in eggs, MDCK cells, and guinea pigs. Two filamentous strains, A/Netherlands/602/2009 (H1N1) and A/Georgia/M5081/2012 (H1N1), were passaged in eggs and MDCK cells. Conversely, the spherical laboratory strain A/Puerto Rico/8/1934 (H1N1) was passaged in guinea pigs. We found that, although passage in eggs and MDCK cells can lead to a loss of filaments, an exclusively spherical morphology is not required for highly efficient growth in either substrate. We did, however, identify two point mutations in the matrix of egg passage 10 isolates that confer spherical morphology and increased growth in eggs. In contrast, serial passage in guinea pigs resulted in the selection of filament-forming variants. Sequencing revealed point mutations to the PR8 matrix that, when introduced individually, yielded filaments. These findings suggest a functional role for filaments in the infected host and expand the breadth of mutations known to affect influenza virus shape.

Introduction

Influenza A virus is an enveloped, negative sense, RNA virus with an eight segmented genome (1). In humans, these viruses cause widespread seasonal epidemics of respiratory disease, as well as occasional pandemics, the most recent of which occurred in 2009 (2). Early research found that influenza virus is pleomorphic, forming both filamentous and spherical virions (3). Filaments are generally found in primary or low-passage isolates and their formation by influenza viruses of both avian and human origin has been reported (4-6). These filaments are of variable length, but can reach up to 30 μm in size (7). While populations of spherical virions measuring about 100 nm in diameter are also observed in primary isolates, laboratory adapted strains such as A/Puerto Rico/8/1934 (H1N1) [PR8] and A/WSN/1933 (H1N1) [WSN] are made up exclusively of spherical and ovoid particles (7).

Early studies revealed that filamentous strains gradually become spherical following repeated passage in embryonated chicken eggs (ECEs) (8, 9). Whether this conversion also occurs upon passage in MDCK cells is unclear, as we were unable to find data on this point reported in the literature. More recently, reverse genetics based mapping studies demonstrated that the M1 protein is a major genetic determinant of virion morphology (10, 11). Additionally, it has been shown that the cytoplasmic tails of the M2 proton channel, hemagglutinin (HA), and neuraminidase (NA) proteins influence the morphology of influenza virus (12, 13).

The fact that filaments are maintained in nature, but lost upon passage in ECEs, implies that filaments confer a selective advantage in the infected host that is not necessary for growth in the laboratory. While several studies have identified amino acid changes that

mediate the switch from a filamentous to spherical morphology and vice versa, these mutations were identified via the artificial methods of alanine-scanning (14) and substitution of differing amino acids from strains of the opposite morphology (10, 11). To our knowledge, naturally arising mutations that impact virion morphology have not been reported.

We aimed to evaluate the hypothesis that filamentous virion morphology confers a selective advantage *in vivo*, while viruses with exclusively spherical morphology are more fit in laboratory substrates. Since introduction of artificial mutations that are known to change virion morphology (10, 11, 14) was found to lead to general attenuation (data not shown), we undertook serial passage experiments aimed at identifying naturally occurring mutations that alter morphology. The passage experiments themselves offered insight into the interplay between virion morphology and viral fitness, by revealing which morphologies are selected for in ECEs, MDCK cells, and guinea pigs. When two human strains with mixed filamentous and spherical morphology were passaged in ECEs or MDCK cells, we found that, while filaments were not always maintained, an exclusively spherical morphology was not necessary for increased growth in laboratory substrates. Conversely, serial passage of the spherical PR8 virus in guinea pigs led to the emergence of filamentous virions, suggesting that filaments confer a selective advantage in the infected animal host. Through sequencing of egg- and guinea pig-passaged viruses, respectively, we identified point mutations in the M1 matrix protein that convert the NL602 virus to a spherical morphology or cause the PR8 virus to form filaments. The resultant mutant viruses were then characterized in ECEs, MDCK cells and guinea pigs.

Material and Methods

Viruses:

rNL602wt, rPR8wt, rNL602 M1 T169I, rNL602 M1 Q198K, rPR8 M1 N87S, rPR8 M1 N92S, rPR8 M1 R101G, and rPR8 M1 S157C viruses were generated using reverse genetics essentially as previously described (15, 16). In brief, rNL602-based viruses were recovered by 8 (pHW) plasmid transfection of 293T cells and subsequent co-culture with MDCK cells. rPR8-based viruses were recovered by 8 (pDZ) plasmid transfection of 293T cells and subsequent injection of transfected cells and culture medium into 9-11 day old embryonated chicken's eggs. rNL602 virus and mutants thereof were grown in MDCK cells and rPR8 virus and mutants were grown in 9-11 day old embryonated chicken's eggs. A/Georgia/M5081/2012 (H1N1) [M5081], A/Georgia/F32551/2012 (H1N1) [F32551] and A/Georgia/T51700/2012 (H1N1) [T51700] viruses were isolated from distinct clinical specimens obtained from the microbiology laboratory of Children's Healthcare of Atlanta. F32551 and T51700 viruses were isolated through direct inoculation of differentiated human tracheobronchial epithelial (HTBE) cells. In the case of M5081 virus, a plaque assay in MDCK cells was performed with the nasal swab material, a single plaque was isolated and this plaque material was amplified in HTBE cells to generate a working stock.

Serial Passage:

Both rNL602wt and M5081wt viruses were passaged blindly ten times in embryonated chicken eggs and in MDCK cells. For the egg passages, six replicate passages were run

for each virus. The initial inoculum was 250 PFU/egg. In subsequent passages, eggs were inoculated with 100 μ l undiluted allantoic fluid from the previous passage. Inoculated eggs were incubated at 37°C for 48 hours and then 4°C overnight prior to collection of allantoic fluid.

For the MDCK cell passage, three replicate passages were run for each virus. Initially, cells were infected at a multiplicity of infection (MOI) of 0.05 PFU/cell. In subsequent passages, cells were inoculated with a 1:10 dilution of cell culture supernatant from the previous passage. Cells were incubated for 48 hours at 33°C, after which the cell culture supernatant was collected. To test whether the use of undiluted allantoic fluid or culture supernatant obscured the emergence of spherical variants at low levels, we performed an additional three passages in each substrate, with each virus lineage, performing a 10^{-3} dilution prior to passage. The resultant P13 populations of virus showed similar morphology to their P10 counterparts (data not shown).

rPR8wt virus was passaged twelve times in guinea pigs. At each passage, a single guinea pig was infected intranasally with 10^4 PFU of virus in 300 μ l of PBS. Nasal wash samples were collected in PBS at four days post-infection, titered via plaque assay in MDCK cells and then used as the inoculum for the next passage. If titer was too low to permit inoculation with 10^4 PFU, undiluted nasal wash was used.

M segment sequencing

Viral RNA was extracted from rNL602 EP10 plaque clones or rPR8 guinea pig P12 nasal wash fluid using the QIAamp Viral RNA Mini Kit (QIAGEN) according to the manufacturer's instructions. cDNA of the M segment was generated using Transcriptor

reverse transcriptase (Roche) and a universal forward primer for the M segment (17). The resulting product was then amplified using the Expand High Fidelity PCR system (Roche) and universal forward and reverse primers for the M segment (17). PCR products were then extracted from agarose gel slices using the QIAquick Gel Extraction Kit (QIAGEN) and sequenced directly (Genewiz).

Transmission electron microscopy (TEM):

For imaging of virions, MDCK cells were infected at MOI = 5 PFU/cell. At 16 hours post-infection, cells were fixed with 2.5% glutaraldehyde in 0.1 M cacodylate buffer for 2-3 h at room temperature or overnight at 4°C. If, due to low stock titers, an MOI of 5 PFU/cell could not be achieved, cells were infected at the highest possible MOI and incubated for 24 hours prior to fixing. Cells were then embedded in Eponate 12 resin, cut into 80 nm sections, and stained with 5% uranyl acetate and 2% lead citrate at the Emory Robert P. Apkarian Integrated Electron Microscopy Core. After sample preparation, grids were imaged at 75 kV using a Hitachi H-7500 transmission electron microscope.

TEM particle counts:

Virions within TEM fields were counted at magnification = 40 KX. For each virus between 47 and 207 virions were counted. Filaments were defined as being equal to or greater than 300 nm in length. Virions shorter than 300 nm in length were defined as spheres. Empty virions were additionally counted as spheres, although such particles could represent a cross-section through a filamentous virion. From these counts, the percentage of spherical and filamentous virions was calculated. The difference in

proportions test was used to determine if the proportion of virions that were filamentous was significantly different than that of the wild-type. Results were considered significant if $p < 0.05$.

Growth curves:

Growth curves in MDCK cells were performed in triplicate using an MOI of 0.001 PFU/cell. Tissue culture supernatant was collected at 1, 6, 12, 24, 48, and 72 hours post-infection. Virus titer was determined via plaque assay in MDCK cells. Growth curves in 9-11 day old embryonated chicken eggs were performed using three eggs/virus/time point. Each egg was infected with 250 PFU of virus. At each time point (1, 12, 24, 48, and 72 hours post-infection), eggs were placed at 4°C to halt virus growth. Allantoic fluid was collected the next day from chilled eggs and virus titer was quantified via plaque assay in MDCK cells.

Growth experiments in guinea pigs:

Female Hartley strain guinea pigs weighing 300-350 g were obtained from Charles River Laboratories. Four animals were infected intranasally with 1000 PFU of each virus in 300 μ l of PBS. Nasal washes were collected in PBS at days 2, 4, 6, and 8 post-infection and virus titer was quantified via plaque assay in MDCK cells.

Transmission experiments in guinea pigs:

Four guinea pigs were infected intranasally with 1000 PFU of each virus in 300 ml of PBS. Animals were then housed in environmental chambers (Caron model # 6040) kept

at constant temperature (10°C) and relative humidity (20%). Twenty-four hours post-infection, an uninfected guinea pig was co-housed with each infected guinea pig. Nasal washes were collected in PBS at days 2, 4, 6, and 8 post-infection and virus titer was quantified via plaque assay in MDCK cells.

Results

Human clinical influenza virus isolates produce filamentous virions.

To confirm that low passage human influenza viruses, and particularly the strains that we were working with, have a filamentous morphology, thin section transmission electron microscopy (TEM) was performed. MDCK cells infected with each of the following five strains were examined: i) the A/Netherlands/602/2009 (H1N1) [NL602] virus biological isolate, grown in MDCK cells (passage 3); ii) the recombinant A/Netherlands/602/2009 (H1N1) [rNL602] virus generated by reverse genetics and amplified in MDCK cells (18); iii) A/Georgia/M5081/2012 (H1N1) [M5081] virus, which was isolated from a nasal swab specimen passaged once in MDCK cells and again in differentiated human tracheobronchial epithelial (HTBE) cells; iv) A/Georgia/T51700/2012 (H1N1) [T51700] virus, isolated through direct inoculation of HTBE cells; and v) A/Georgia/F32551/2012 (H1N1) [F32551] virus, also isolated in HTBE cells. Our results (Figure 1A-E) indicate that each of these human viruses produced virions of filamentous morphology, confirming that this property of clinical isolates is not unique to those strains previously described by others (6, 19).

Spherical morphology is not required for increased growth in embryonated chicken eggs.

To investigate the effect of adaptation to ECEs on the morphology of low passage human influenza isolates, we passaged rNL602wt virus blindly a total of ten times in this substrate. Passage was performed in six parallel replicates, which will be referred to as “lines” throughout the manuscript. Provided all six lines persisted after passage 10 (P10), only three were picked for further analysis. For the purposes of this analysis, we defined spheres as being virions less than 300 nm in length. Filaments were defined as being equal to or greater than 300 nm in length.

In the case of rNL602, virus was recovered from all six lines after P10. Those with the highest viral titers, lines 2, 5, and 6, were chosen for further analysis. Virion morphology compared to the NL602wt virus was assessed using thin-section TEM of MDCK cells infected at high MOI. We found that all three of the P10 lines were comparable in morphology to the wild-type virus, showing both short and long filaments, with a small population of spheres (Figure 2A-H, 2Q). This result was surprising, as previous studies have reported conversion to a predominantly spherical morphology in some strains in ten passages or fewer (9).

To investigate the possibility that the passage number required for morphology change is strain-dependent, we also passaged a clinical strain, M5081, ten times in ECEs. Prior to passage, M5081 virus was confirmed to be filamentous in nature by TEM, with many short filaments and occasional long filaments (Figure 1C). Only 3/6 lines were recovered after P10 – lines 2, 4, and 5. Upon thin-section TEM analysis, we found that, within all three EP10 populations, most virions were spherical in morphology (Figure 2I-P, 2R).

Thus, in the case of M5081 virus, serial passage in ECEs did appear to have an effect on virion morphology, suggesting that the rate of morphology change in response to passage may be strain-specific.

Next, we compared the growth of the wild-type and passaged strains of both rNL602 and M5081 viruses in ECEs. We found that both rNL602 and M5081 passaged viruses had marked growth advantages when compared to the corresponding wild-type viruses, showing more rapid growth kinetics and higher viral titers (Figure 3). These results show that conversion to a spherical morphology is not required for increased growth in ECEs since, although the morphology of M5081 virus appeared to be affected by passage, the rNL602 passaged lines still remained highly filamentous in morphology.

Spherical morphology is not required for increased growth in MDCK cells

We also wanted to assess the effect of virus passage in MDCK cells, another common laboratory substrate for influenza virus. As with the ECEs, we passaged both rNL602wt and M5081wt viruses blindly ten times in MDCK cells. Passage was done in 6-well plates with three parallel replicates (“lines”) for each virus.

Following ten passages, the morphology of each virus line was compared to that of the wild-type using thin-section TEM of infected MDCK cells. We found that, in the case of the rNL602 strains, 2/3 P10 lines remained highly filamentous in morphology, with filaments of varying lengths present on the surface of infected cells (Figure 4A-H, 4Q). In the case of M5081 virus, we found that Line 3 consisted of virions that were mostly spheres or short filaments. No long filaments were observed. Lines 1 and 2, however, retained a morphology that was very similar to the wild-type (Figure 4I-P, 4R).

Next, we compared the growth of the P10 lines versus the wild-type in MDCK cells for both rNL602 and M5081 viruses. We found that, in the case of the rNL602 strain, the P10 lines displayed a modest growth advantage compared to the wild-type, showing an approximately 10-fold increase at 48 hours (Figure 5A). The M5081 virus P10 lines exhibited a larger growth advantage (~1000-fold increase at 48 hours) in comparison to the M5081wt virus (Figure 5B). The differences between the rNL602 and the M5081 growth comparisons appear to be due to the more efficient growth in MDCK cells of the rNL602wt virus compared to the M5081wt virus. The rNL602wt virus may exhibit some adaptation to MDCK cells due to the fact that this stock was generated in MDCK cells, while the M5081 virus was grown in HTBE cells. As passaging only appeared to have an effect on the virion morphology of 2/6 P10 lines, the results show that, as was found in ECEs, a conversion to a spherical morphology is not necessary for increased growth in MDCK cells.

rNL602 M1 T169I and Q198K confer a spherical morphology and a growth advantage in ECEs

Partial genome sequencing of plaque clones isolated from rNL602 EP10 lines revealed three mutations – two in the M1 matrix protein (T169I and Q198K) and one in the M2 ion channel protein (E70K). The M segments of six plaque clones were sequenced per line and each mutation was identified in a single clone. The M1 T169I and M1 Q198K mutations were identified in separate clones of rNL602 EP10 Line 2. The M2 E70K mutation was identified in a clone of Line 6. Since the M segment gene products have been implicated previously in determining morphology, we wished to test whether these

three amino acid changes would alter virion morphology. We therefore introduced each mutation into the M segment of rNL602wt virus using reverse genetics to generate three mutant viruses. When we examined these viruses using thin-section TEM of infected MDCK cells, we found that the M1 T169I virus produced spherical virions as well as short filaments. The majority of virions produced by the M1 Q198K mutant were also spherical, with very few filaments present. Lastly, the E70K mutant was found to be highly filamentous in morphology, similar to the rNL602wt virus, and was thus excluded from further study (Figure 6).

Next, we compared the growth of the M1 T169I and Q198K mutants to rNL602wt virus in ECEs, MDCK cells, and guinea pigs. We found that both mutant viruses had a growth advantage in ECEs compared to rNL602wt virus. In addition to higher peak titers, the mutant viruses displayed kinetics of growth similar to those of the EP10 lines (Figure 7A). However, when growth of the wild-type and mutant viruses were compared in MDCK cells it was observed that both the M1 T169I and Q198K mutant had a mild growth defect in this substrate (Figure 7B). A growth defect was also observed when the growth of the mutant viruses was compared to the wild-type in guinea pigs (Figure 7C). These observations suggest that both mutations are egg-specific adaptations. Thus, despite the finding that a spherical morphology is not necessary for increased growth in laboratory substrates, mutations arising naturally over the course of passage were found to both convert the virus to the spherical phenotype and lead to a growth advantage in ECEs.

Additionally, we wished to compare the transmission of the rNL602 mutant viruses to that of the wild-type using a guinea pig contact transmission model. We found that the

wild-type virus showed transmission to 3/4 contacts by day 4 and all contacts by day 6. In contrast, transmission of the mutant viruses was not detected until day 6. By day 8, all three viruses had reached 100% transmission (Figure 8). The observed delay in transmission of the mutant viruses correlated with their delayed growth in guinea pigs, suggesting that the M1 T169I and Q198K mutations altered growth kinetics and this effect, in turn, influenced the rate of transmission.

Serial passage in guinea pigs leads to emergence of filamentous virions

In order to investigate the effects of serial passage *in vivo* on the morphology of a laboratory-adapted strain, we passaged rPR8wt virus twelve times in guinea pigs. Briefly, female Hartley guinea pigs were inoculated intranasally with 1×10^4 PFU of rPR8wt virus. At 4 days post-infection, nasal washes were collected. Following titration, 1×10^4 PFU of nasal wash was used for the next passage. In the event that this inoculum titer could not be attained, undiluted nasal wash was used instead.

After twelve passages, we assessed the morphology of the passage 12 (P12) virus using thin-section TEM of infected MDCK cells. While the rPR8wt-infected samples showed uniformly spherical virions (Figure 9A), we observed the emergence of filamentous virions in the P12-infected samples (Figure 9B-D). This emergence of filaments upon serial passage in guinea pigs indicates that a filamentous morphology is selected within an animal host, supporting our hypothesis that filaments play a functional role *in vivo*. Next, we compared the growth of the P12 virus to that of the wild-type rPR8wt virus. We inoculated four guinea pigs intranasally with 1000 PFU of either rPR8wt or P12 in 300 ml PBS. Nasal washes were taken at days 2, 4, 6, and 8 post-infection and viral titer was

determined via plaque assay on MDCK cells. We found that the P12 virus had a mild, but statistically significant, growth advantage at day 2 in guinea pigs when compared to rPR8wt (Figure 9E). These results, coupled with the emergence of filamentous virions in the P12 samples, suggest that filaments play a functional role within the infected host.

Mutations identified in the guinea pig P12 virus matrix protein result in robust filament formation

Through sequencing of the M segment of the guinea pig P12 virus pool we identified seven nucleotide positions with two overlapping peaks, suggesting heterogeneity within the virus population at these sites. All seven were in the M1 matrix protein. We introduced each mutation individually into the cDNA of the PR8 M segment and, using reverse genetics, we were able to rescue mutant viruses from four of these plasmids. Examination of the four mutant viruses using thin-section TEM revealed that, compared to the wild-type, all showed robust filament formation, producing significantly more filaments than rPR8wt (Figure 10).

Next, we compared the growth of the mutant viruses to the wild-type in embryonated chicken eggs, MDCK cells, and guinea pigs. We found that in all three substrates rPR8wt retained a growth advantage over most of the mutant viruses. The exception was the M1 N87S mutant, which grew comparably to rPR8wt in all three substrates (Figure 11). As such, the N87S mutant was used in a contact transmission experiment in guinea pigs with rPR8wt and the PR8 GP P12 virus to determine if increased filament formation had an effect on virus transmission. Consistent with previously reported data, the rPR8wt virus did not transmit between contact guinea pigs (20). In contrast, the PR8 P12 virus

transmitted to two of four contact guinea pigs (Figure 12), indicating that mutations accumulated over the course of serial passage that promote transmission. Introduction of the N87S mutation alone, however, did not improve the transmissibility of the rPR8wt virus.

Discussion

After the initial observation that serial passaging in ECEs had an effect on the morphology of influenza virus, little work has been done to elucidate why this phenomenon occurs or the mechanism behind it. Published observations showed the conversion of several strains of influenza virus to a predominantly spherical morphology by ten passages in ECEs (9). Likewise, our results showed a shift in morphology favoring more spherical virions in all three EP10 lines of M5081. However, the rNL602 EP10 lines maintained a predominantly filamentous phenotype; this difference may be due to strain specific requirements or the precise conditions of passaging. The idea of strain specificity is supported by the fact that some laboratory strains such as A/Udorn/301/1972 (H3N2) and A/Victoria/3/1975 (H3N2) have retained their filamentous morphology despite being grown extensively in laboratory substrates (10, 11). To our knowledge, the effect of serial passage in MDCK cells on virion morphology has not been assessed. We found that 4 out of 6 of the CKP10 lines that were tested for both rNL602 and M5081 strains retained a highly filamentous morphology. The fact that all of the EP10 and CKP10 lines have a considerable growth advantage in comparison to their corresponding wild-type viruses, regardless of changes in morphology, indicates that a spherical morphology is not required for increased growth in laboratory substrates.

The presence of mutations that mediate a conversion to a spherical morphology within the populations of rNL602 EP10 strains suggests that some morphology transition took place, although the spherical variants were not readily detected by TEM. However, the fact that these mutant viruses retained a growth advantage in ECEs while showing attenuation in MDCK cells suggests that these mutations are adaptive specifically in eggs and not more generally in laboratory substrates. This finding agrees with our data indicating that ten passages in MDCK cells brought about only a marginal change in morphology and only in one of the three rNL602 virus lineages. It should be noted, however, that although both the T169I and Q198K mutations confer a spherical morphology on the rNL602 virus and both improve growth in eggs, we have not demonstrated that these two effects are causally linked.

In contrast to the conversion from filamentous to spherical morphology through egg passage, we found that passage of a spherical, laboratory-adapted strain (rPR8) in an animal host led to the emergence of filamentous virions. The selection of filamentous variants in guinea pigs suggests that an elongated virion morphology confers a fitness advantage *in vivo*. Nevertheless, when point mutations identified within the rPR8 GP P12 virus population and leading to filament formation were introduced individually into the rPR8 virus, these mutations were found to attenuate the growth of the virus in guinea pigs. This result suggests that, to be advantageous, the individual changes to the M1 protein that we identified need to be coupled with complimentary changes elsewhere in the genome. Similarly, although the rPR8 P12 virus population was observed to transmit to 2/4 contact guinea pigs, the filamentous mutant rPR8 M1 N87S did not transmit. This lack of transmission indicates that a filamentous morphology is not sufficient to confer a

transmissible phenotype on the rPR8 virus, a finding that is not unexpected based on the multi-genic nature of influenza virus transmission determinants (16, 20-28).

The amino acids within M1 that we found to affect virion morphology differ, in most cases, from those described previously by others. For example, both Roberts and Compans as well as Elleman and Barclay found position 41 to be important; Bourmakina and Garcia-Sastre found positions 95 and 204 to determine morphology; and Burleigh et al. found position 102 to affect virion shape (10-12, 14). That the amino acids described herein differ is most likely due to our approach: we have identified mutations arising naturally during serial passage, whereas previous research focused on amino acids differing between selected spherical (e.g. WSN and PR8) and filamentous (e.g. A/Udorn/301/1972 and A/Victoria/3/75) strains. Taken together, it appears that a number of different elements within the M1 protein can alter virion morphology, an observation that will most likely not be explained until the mechanism by which M1 directs the formation of filaments or spheres is revealed.

Overall, the mutations identified herein occur at highly conserved sites within the M1 protein; nevertheless, a small number of natural isolates carrying the same or similar mutations were found in the NCBI database. Through M1 protein sequence alignment we found that, amongst human H1N1 strains isolated in the United States between 2008-2013, two isolates contained the Q198K mutation (A/Boston/685/2009 and A/Hawaii/07/2010). None of the mutations described herein were identified in pre-2008 human H1N1 isolates or in avian H1N1 isolates for which M1 protein sequence data is available in the NCBI database. Interestingly, through alignment the M1 sequence of swine H1N1 strains, we found some isolates containing the N87S

(A/swine/Iowa/46519_1/2007), R101G (A/swine/Iowa/15/1930), S157C (A/swine/Iowa/H04YS2/2004, A/swine/Iowa/H03G1/2003, and A/swine/Iowa/H03LJ10/2003), and T169I (A/swine/Ontario/53518/03) mutations.

Whether the mutations identified in the NCBI database affect morphology in the context of the particular strains carrying them is, of course, unknown.

Through characterization of paired spherical and filamentous viruses differing at a single amino acid (rPR8wt vs. rPR8 M1 N87S and rNL602wt vs. rNL602 M1 I169T or Q198K) in a guinea pig transmission model, we hoped to test whether filamentous morphology improves influenza virus transmission. While the spherical rNL602 viruses showed delayed transmission relative to rNL602wt, the kinetics of transmission mirrored the kinetics of shedding, suggesting that the M1 mutations affected viral growth rather than transmission directly. Similarly, the rPR8 M1 N87S mutation, when introduced individually, led to attenuated growth *in vivo* and no transmission was seen with this filament-producing variant. Taken together, our data do not suggest a role for virion morphology in determining transmission phenotype; our data do not, however, exclude this possibility. The virus strains we are working with are highly transmissible (rNL602) and completely non-transmissible (rPR8) in the guinea pig model; thus, while changes in morphology are not sufficient to alter their respective transmission phenotypes, in the appropriate context, morphology may contribute to transmission. Our finding that filaments are selected in guinea pigs (even in the absence of transmission between hosts) clearly suggests that filamentous virions are functionally significant *in vivo*. The precise function(s) of filament production by influenza viruses will be pursued further in subsequent work.

Acknowledgements

We are grateful to Ron Fouchier for the A/Netherlands/602/2009 (H1N1) virus and reverse genetics system. We would also like to thank Hong Yi and Jeannette Taylor of the Robert P. Apkarian Integrated Electron Microscopy Core for TEM sample processing and Anshante Jones and Shamika Danzy for technical assistance. This work was funded by the Centers for Excellence in Influenza Research and Surveillance (CEIRS) contract number HHSN266200700006C.

References

1. **Palese P, Shaw ML.** 2007. Orthomyxoviridae: the viruses and their replication, p 1647-1689. *In* Knipe DM, Howley PM, (ed). *Fields Virology*. 5th edition. Lippincott Williams & Wilkins, Philadelphia,PA.
2. **Novel Swine-Origin Influenza A (H1N1) Virus Investigation Team, Dawood FS, Jain S, Finelli L, Shaw MW, Lindstrom S, Garten RJ, Gubareva LV, Xu X, Bridges CB, Uyeki TM.** 2009. Emergence of a novel swine-origin influenza A (H1N1) virus in humans. *N Engl J Med*. **360**:2605-2615.
3. **Chu CM, Dawson IM, Elford WJ.** 1949. Filamentous forms associated with newly isolated influenza virus. *Lancet*. **1**:602.
4. **Gubareva LV, Bethell R, Hart GJ, Murti KG, Penn CR, Webster RG.** 1996. Characterization of Mutants of Influenza A Virus Selected with the Neuraminidase Inhibitor 4-Guanidino-Neu5Ac2en. *J Virol*. **70**:1818-1827.
5. **Shortridge KF, Zhou NN, Guan Y, Gao P, Ito T, Kawaoka Y, Kodihalli**

- S, Krauss S, Markwell D, Murti KG, Norwood M, Senne D, Sims L, Takada A, Webster RG.** 1998. Characterization of Avian H5N1 Influenza Viruses from Poultry in Hong Kong. *Virology*. **252**:331-342.
6. **Itoh Y, Shinya K, Kiso M, Watanabe T, Sakoda Y, Hatta M, Muramoto Y, Tamura D, Sakai-Tagawa Y, Noda T, Sakabe S, Imai M, Hatta Y, Watanabe S, Li C, Yamada S, Fujii K, Murakami S, Imai H, Kakugawa S, Ito M, Takano R, Iwatsuki-Horimoto K, Shimojima M, Horimoto T, Goto H, Takahashi K, Makino A, Ishigaki H, Nakayama M, Okamatsu M, Takahashi K, Warshauer D, Shult PA, Saito R, Suzuki H, Furuta Y, Yamashita M, Mitamura K, Nakano K, Nakamura M, Brockman-Schneider R, Mitamura H, Yamazaki M, Sugaya N, Suresh M, Ozawa M, Neumann G, Gern J, Kida H, Ogasawara K, Kawaoka Y.** 2009. In vitro and in vivo characterization of new swine-origin H1N1 influenza viruses. *Nature*. **460**:1021-1025.
7. **Mosley VM, Wyckoff RW.** 1946. Electron micrography of the virus of influenza. *Nature*. **157**:263.
8. **Kilbourne ED, Murphy JS.** 1960. Genetic studies of influenza viruses. I. Viral morphology and growth capacity as exchangeable genetic traits. Rapid in ovo adaptation of early passage Asian strain isolates by combination with PR8. *J Exp Med*. **111**:387-406.
9. **Choppin PW, Murphy JS, Tamm I.** 1960. Studies of two kinds of virus particles which comprise influenza A2 virus strains. III. Morphological characteristics: independence to morphological and functional traits. *J*

- Exp Med. **112**:945-952.
10. **Bourmakina SV, Garcia-Sastre A.** 2003. Reverse genetics studies on the filamentous morphology of influenza A virus. *J Gen Virol.* **84**:517-527.
 11. **Elleman CJ, Barclay WS.** 2004. The M1 matrix protein controls the filamentous phenotype of influenza A virus. *Virology.* **321**:144-153.
 12. **Roberts PC, Lamb RA, Compans RW.** 1998. The M1 and M2 proteins of influenza A virus are important determinants in filamentous particle formation. *Virology.* **240**:127-137.
 13. **Jin H, Leser GP, Zhang J, Lamb RA.** 1997. Influenza virus hemagglutinin and neuraminidase cytoplasmic tails control particle shape. *EMBO J.* **16**:1236-1247.
 14. **Burleigh LM, Calder LJ, Skehel JJ, Steinhauer DA.** 2005. Influenza A viruses with mutations in the M1 helix six domain display a wide variety of morphological phenotypes. *J Virol.* **79**:1262-1270.
 15. **Fodor E, Devenish L, Engelhardt OG, Palese P, Brownlee GG, Garcia-Sastre A.** 1999. Rescue of influenza A virus from recombinant DNA. *J Virol* **73**:9679-9682.
 16. **Steel J, Lowen AC, Mubareka S, Palese P.** 2009. Transmission of influenza virus in a mammalian host is increased by PB2 amino acids 627K or 627E/701N. *PLoS Pathog.* **5**:e1000252.
 17. **Hoffmann E, Stech J, Guan Y, Webster RG, Perez DR.** 2001. Universal primer set for the full-length amplification of all influenza A viruses. *Arch Virol.* **146**:2275-2289.

18. **Herfst S, Chutinimitjul S, Ye J, de Wit E, Munster VJ, Schrauwen EJ, Bestebroer TM, Jonges M, Meijer A, Koopmans M, Rimmelzwaan GF, Osterhaus AD, Perez DR, Fouchier RA.** 2010. Introduction of virulence markers in PB2 of pandemic swine-origin influenza virus does not result in enhanced virulence or transmission. *J Virol.* **84**:3752-3758.
19. **Goldsmith CS, Metcalfe MG, Rollin DC, Shieh WJ, Paddock CD, Xu X, Zaki SR.** 2011. Ultrastructural characterization of pandemic (H1N1) 2009 virus. *Emerg Infect Dis.* **17**:2056-2059.
20. **Chou YY, Albrecht RA, Pica N, Lowen AC, Richt JA, Garcia-Sastre A, Palese P, Hai R.** 2011. The M segment of the 2009 new pandemic H1N1 influenza virus is critical for its high transmission efficiency in the guinea pig model. *J Virol.* **85**:11235-11241.
21. **Gao Y, Zhang Y, Shinya K, Deng G, Jiang Y, Li Z, Guan Y, Tian G, Li Y, Shi J, Liu L, Zeng X, Bu Z, Xia X, Kawaoka Y, Chen H.** 2009. Identification of amino acids in HA and PB2 critical for the transmission of H5N1 avian influenza viruses in a mammalian host. *PLoS Pathog.* **5**:e1000709.
22. **Lakdawala SS, Lamirande EW, Suguitan AL, Wang W, Santos CP, Vogel L, Matsuoka Y, Lindsley WG, Jin H, Subbarao K.** 2011. Eurasian-origin gene segments contribute to the transmissibility, aerosol release, and morphology of the 2009 pandemic H1N1 influenza virus. *PLoS Pathog.* **7**:e1002443.
23. **Yen HL, Liang CH, Wu CY, Forrest HL, Ferguson A, Choy KT, Jones J,**

- Wong DD, Cheung PP, Hsu CH, Li OT, Yuen KM, Chan RW, Poon LL, Chan MC, Nicholls JM, Krauss S, Wong CH, Guan Y, Webster RG, Webby RJ, Peiris M.** 2011. Hemagglutinin-neuraminidase balance confers respiratory-droplet transmissibility of the pandemic H1N1 influenza virus in ferrets. *Proc Natl Acad Sci USA*. **108**:14264-14269.
24. **Tumpey TM, Maines TR, Van Hoeven N, Glaser L, Solorzano A, Pappas C, Cox NJ, Swayne DE, Palese P, Katz JM, Garcia-Sastre A.** 2007. A two-amino acid change in the hemagglutinin of the 1918 influenza virus abolishes transmission. *Science*. **315**:655-659.
25. **Imai M, Watanabe T, Masato H, Das SC, Ozawa M, Shinya K, Zhong G, Hanson A, Katsura H, Watanabe S, Li C, Kawakami E, Yamada S, Kiso M, Suzuki Y, Maher EA, Neumann G, Kawaoka Y.** 2012. Experimental adaptation of an influenza H5 HA confers respiratory droplet transmission to a reassortant H5 HA / H1N1 virus in ferrets. *Nature*. **486**:420-428.
26. **Herfst S, Schrauwen EJ, Linster M, Chutinimitkul S, de Wit E, Munster VJ, Sorrell EM, Bestebroer TM, Burke DF, Smith DJ, Rimmelzwaan GF, Osterhaus AD, Fouchier RA.** 2012. Airborne transmission of influenza A/H5N1 virus between ferrets. *Science*. **336**:1534-1541.
27. **Van Hoeven N, Pappas C, Belser JA, Maines TR, Zeng H, Garcia-Sastre A, Sasisekharan R, Katz JM, Tumpey TM.** 2009. Human HA and polymerase subunit PB2 proteins confer transmission of an avian

influenza virus through the air. Proc Natl Acad Sci USA. **106**:3366-3371.

28. **Maines TR, Chen LM, Matsuoka Y, Chen H, Rowe T, Ortin J, Falcon A, Nguyen TH, Mai le Q, Sedyaningsih ER, Harun S, Tumpey TM, Donis RO, Cox NJ, Subbarao K, Katz JM.** 2006. Lack of transmission of H5N1 avian-human reassortant influenza viruses in a ferret model. Proc Natl Acad Sci USA. **103**:12121-12126.

Figure Legends

Figure 1. Low-passage human influenza virus isolates have filamentous morphology.

Transmission electron micrographs are shown at a magnification of 60KX. A) NL602wt (biological isolate), B) rNL602wt (recombinant), C) M5081wt, D) T51700wt, E) F32551wt

Figure 2. Ten egg passages led to loss of filaments for M5081 but not rNL602 virus.

Transmission electron micrographs are shown of rNL602wt and M5081wt viruses compared to egg passage 10 (EP10) Lines. All images at magnification = 40KX. A-B) rNL602wt, C-D) rNL602 EP10 Line 2, E-F) rNL602 EP10 Line 5, G-H) rNL602 EP10 Line 6, I-J) M5081wt, K-L) M5081 EP10 Line 2, M-N) M5081 EP10 Line 4, O-P) M5081 EP10 Line 5, Q) Particle count of rNL602wt compared to EP10 Lines, R) Particle counts of M5081wt compared to EP10 Lines. * indicates that the proportion of

filamentous virions was significantly different from that of the wt virus ($p < 0.05$; difference in proportions test).

Figure 3: EP10 Lines show improved growth in embryonated chickens eggs. Eggs were infected with 250 PFU of the indicated viruses. A) rNL602wt versus rNL602 EP10 lines; B) M5081wt versus M5081 EP10 lines.

Figure 4: Ten serial passages in MDCK cells led to a loss of filaments for two of six lineages. Transmission electron micrographs are shown of rNL602wt and M5081wt viruses compared to MDCK passage 10 (CKP10) Lines. All images at magnification = 40 KX. A-B) rNL602wt, C-D) rNL602 CKP10 Line 1, E-F) rNL602 CKP10 Line 2, G-H) rNL602 CKP10 Line 3, I-J) M5081wt, K-L) M5081 CKP10 Line 1, M-N) M5081 CKP10 Line 2, O-P) M5081 CKP10 Line 3, Q) Particle count of rNL602wt compared to CKP10 Lines, R) Particle counts of M5081wt compared to CKP10 Lines. * indicates that the proportion of filamentous virions was significantly different from that of the wt virus ($p < 0.05$; difference in proportions test).

Figure 5: CKP10 Lines show improved growth in MDCK cells. Cells were infected at an MOI of 0.001 PFU/cell. A) rNL602wt versus rNL602 CKP10 Lines, B) M5081wt versus M5081 CKP10 Lines.

Figure 6: T169I and Q198K mutations in the rNL602 M1 protein result in a

predominantly spherical morphology. Transmission electron micrographs are shown of rNL602wt and mutant viruses. All images are at magnification = 60KX. A-B) rNL602wt, C-D) rNL602 M1 T169I, E-F) rNL602 M1 Q198K, G-H) rNL602 M2 E70K, I) Particle counts of rNL602wt compared to mutant viruses. * indicates that the proportion of filamentous virions was significantly different from that of the wt virus ($p < 0.05$; difference in proportions test).

Figure 7: Compared to the wild type virus, rNL602 M1 T169I and M1 Q198K mutant viruses show improved growth in eggs but inferior growth in MDCK cells and guinea pigs. A) Growth in eggs. Eggs were infected with 250 PFU of the indicated viruses. B) Growth in MDCK cells. Cells were infected at an MOI of 0.001 PFU/cell. C) Shedding from guinea pig nasal passages. Guinea pigs were infected intranasally with 1000 PFU of the indicated viruses. Nasal washes were taken on days 2, 4, 6, and 8 and virus titer was quantified via plaque assay in MDCK cells.

Figure 8: Compared to the wild type virus, rNL602 M1 T169I and M1 Q198K mutant viruses show delayed growth and transmission in guinea pigs. Contact transmission of A) rNL602wt, B) rNL602 M1 T169I, and C) rNL602 M1 Q198K. Guinea pigs were infected intranasally with 1000 PFU of the indicated viruses. At 24 hours post-infection, an uninfected guinea pig was housed with an infected guinea pig. Guinea pigs were housed in environmental chambers at constant temperature (10°C) and relative humidity (20%). Nasal washes were taken on days 2, 4, 6, and 8 and virus titer was

quantified via plaque assay in MDCK cells. Dashed lines represent initially Infected animals. Solid lines represent exposed animals.

Figure 9: Serial passage in guinea pigs led to the emergence of rPR8 virus variants with filamentous morphology. Transmission electron micrographs and growth of rPR8wt and rPR8 guinea pig passage 12 (P12) viruses. All TEM images are at magnification = 60KX. A) rPR8wt virus, B-D) rPR8 GP P12 virus. E) Growth analysis *in vivo*, guinea pigs were infected intranasally with 1000 PFU of each virus. Nasal washes were taken on days 2, 4, 6, and 8 and virus titer was quantified via plaque assay in MDCK cells. * T-tests indicated that titers of the P12 virus were significantly greater than those of rPR8wt on day 2 ($p = 0.022$) while titers of rPR8wt were greater than those of P12 on day 4 ($p = 0.035$).

Figure 10: Point mutations in the PR8 M1 protein result in robust filament formation. Transmission electron micrographs are shown of rPR8wt and mutant viruses. All images are at magnification = 60KX. A-B) rPR8wt, C-D) rPR8 M1 N87S, E-F) rPR8 M1 N92S, G-H) rPR8wt M1 R101G, I-J) rPR8wt M1 S157C, K) Particle counts of rPR8wt compared to mutant viruses. * indicates that the proportion of filamentous virions was significantly different from that of the wt virus ($p < 0.05$; difference in proportions test).

Figure 11: Compared to the wild type virus, rPR8 M1 mutant viruses show similar or inferior growth in eggs, MDCK cells, and guinea pigs. A) Growth in eggs. Eggs

were infected with 250 PFU of the indicated viruses. B) Growth in MDCK cells. Cells were infected at an MOI of 0.001 PFU/cell. C) Shedding from guinea pig nasal passages. Guinea pigs were infected intranasally with 1000 PFU of the indicated viruses. Nasal washes were taken on days 2, 4, 6, and 8 and virus titer was quantified via plaque assay in MDCK cells.

Figure 12: Compared to the rPR8wt virus, the rPR8 GP P12 virus transmits in guinea pigs while the rPR8 M1 N87S virus does not. Contact transmission results are shown for A) rPR8wt, B) rPR8 GP P12, and C) rPR8 M1 N87S. Guinea pigs were infected intranasally with 1000 PFU of the indicated viruses. At 24 hours post-infection, an uninfected guinea pig was housed with an infected guinea pig. Animals were housed under controlled environmental conditions of 20% relative humidity and 10°C. Dashed lines represent initially infected animals. Solid lines represent exposed animals. Experiments shown in A and C were performed concurrently; the experiment shown in B was performed separately.

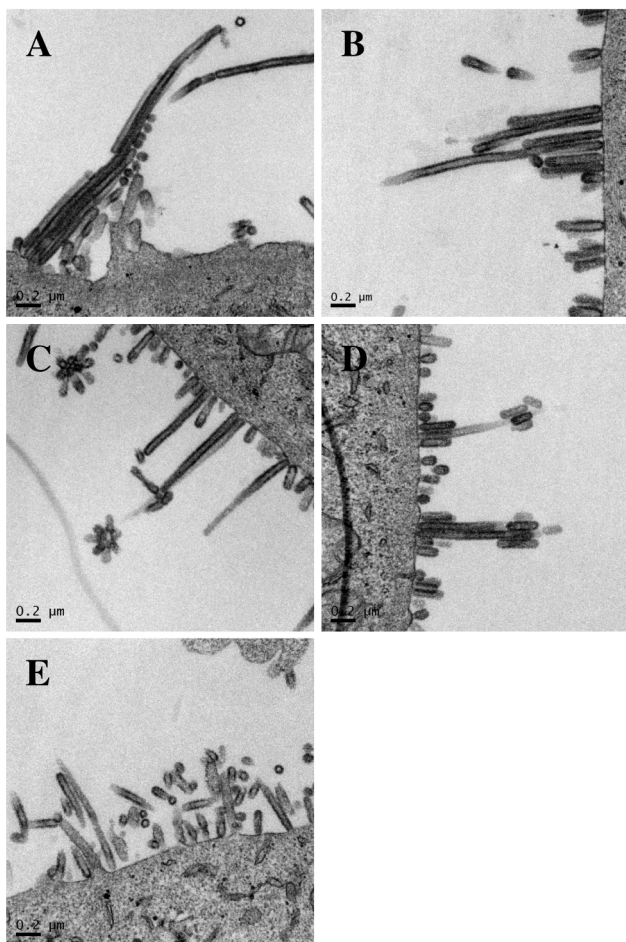
Figure 1

Figure 2

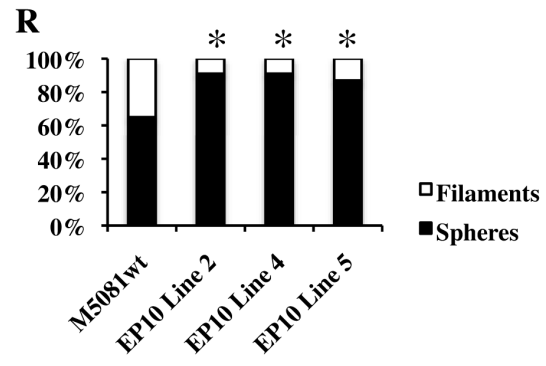
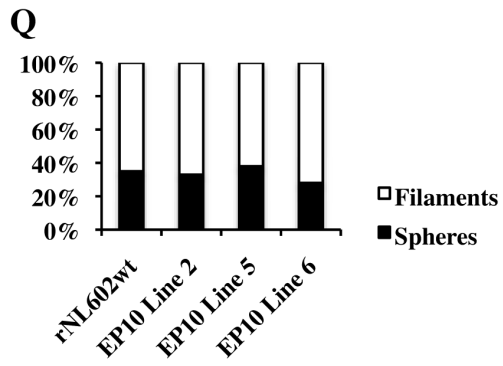
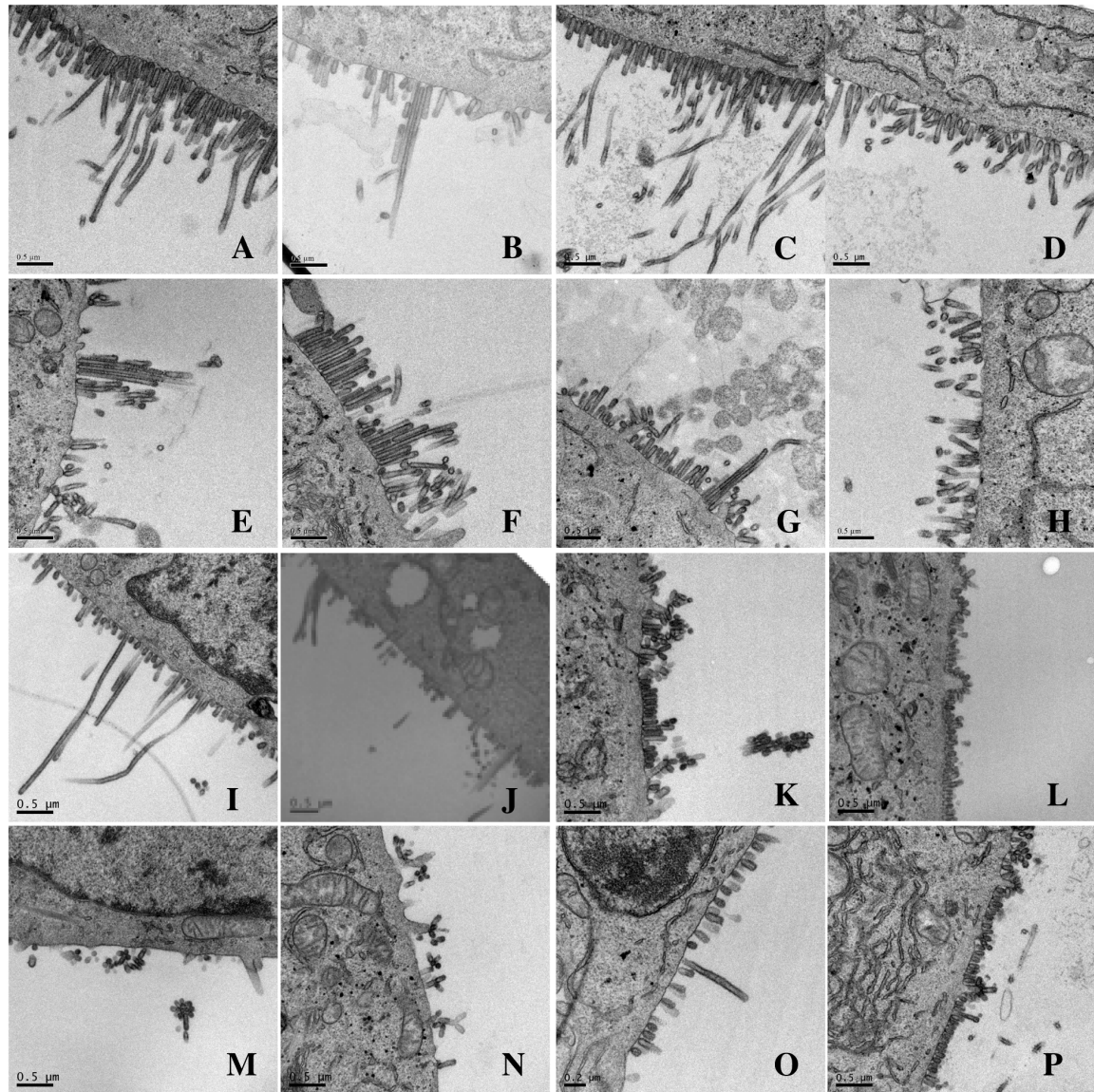
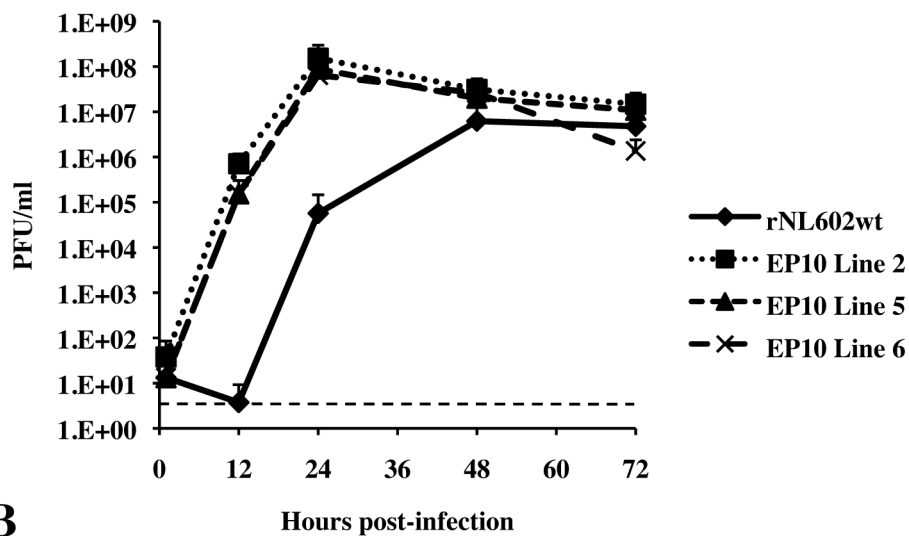


Figure 3

A



B

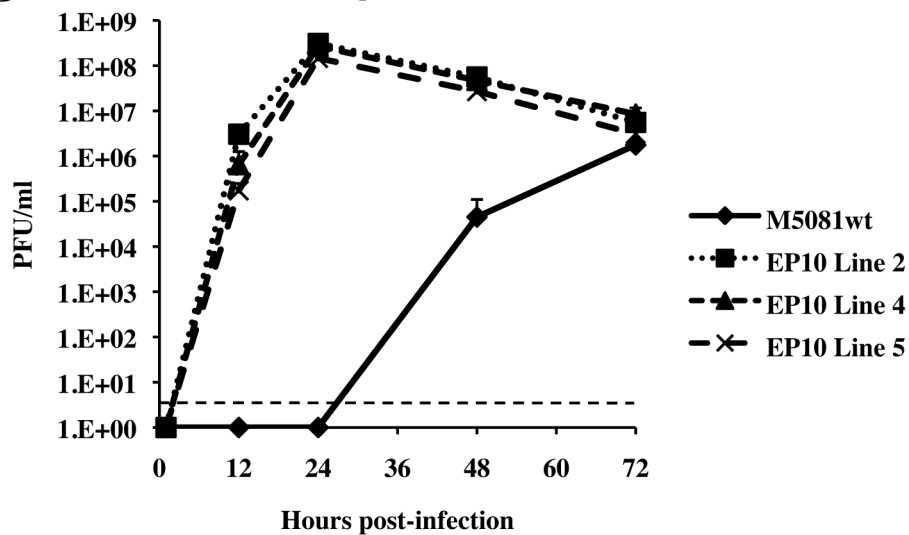


Figure 4

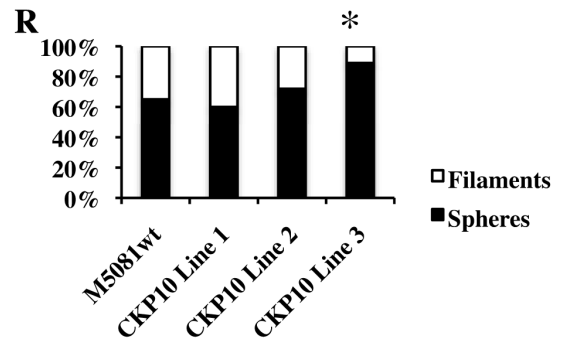
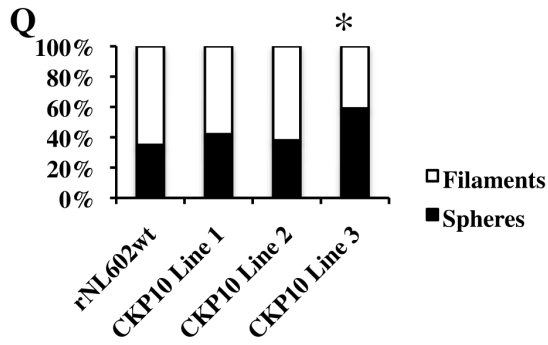
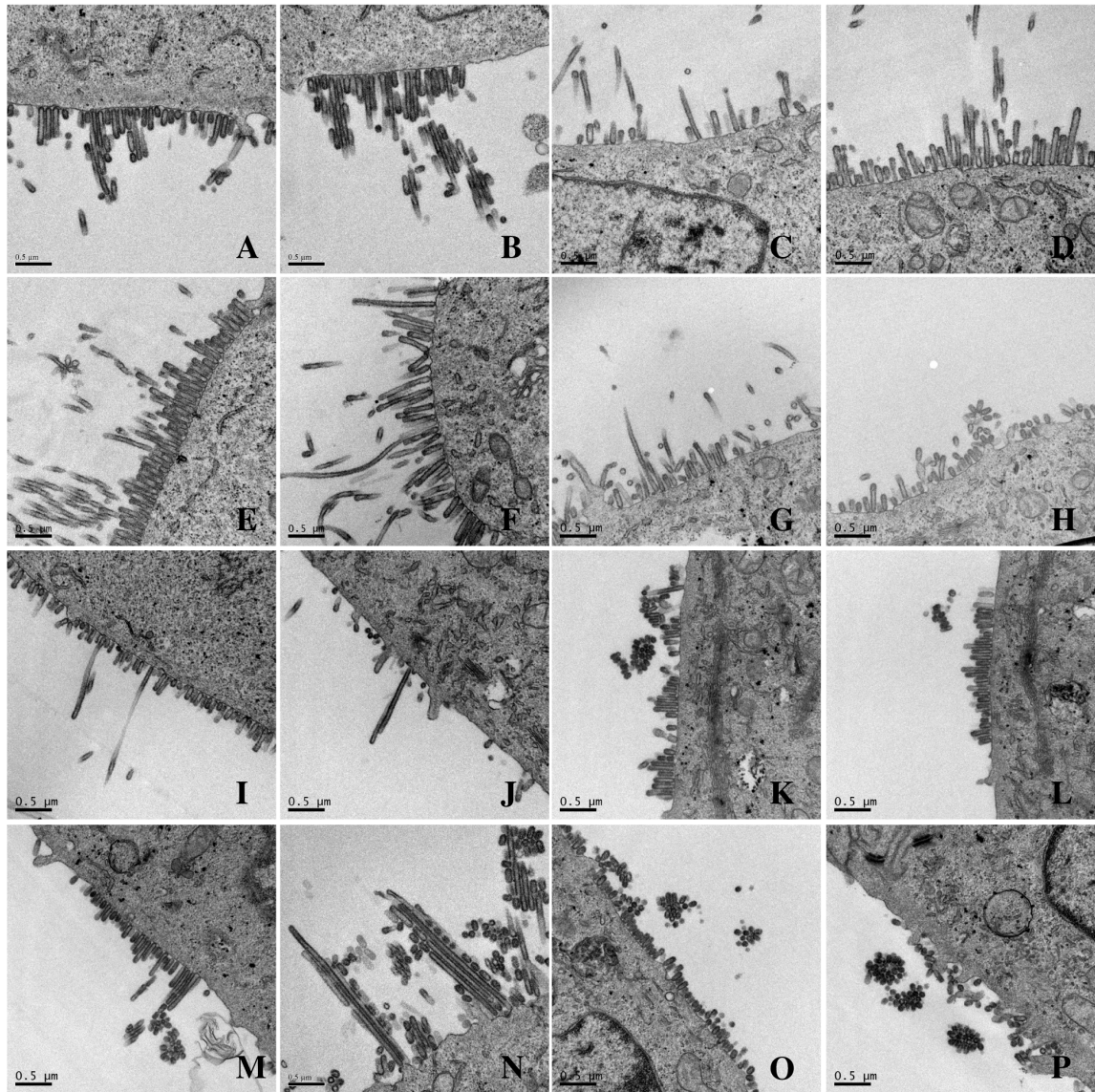
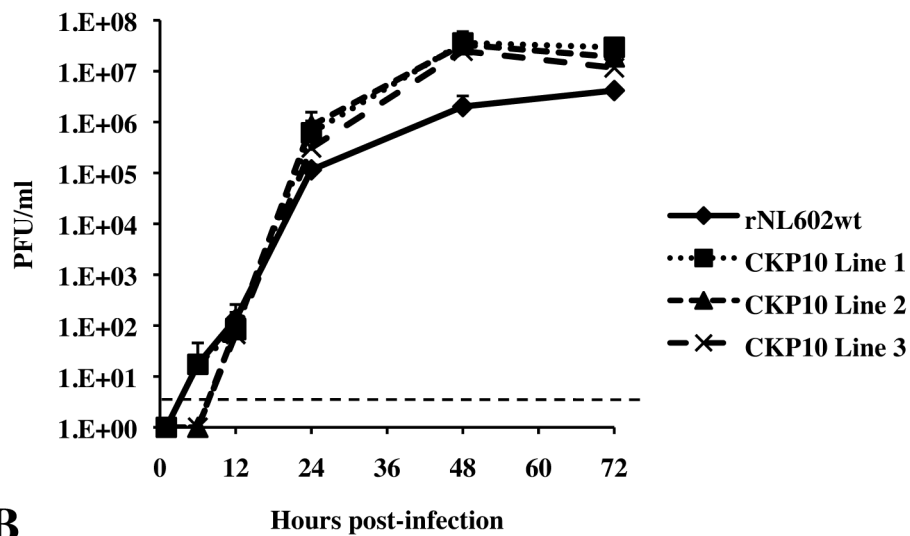


Figure 5

A



B

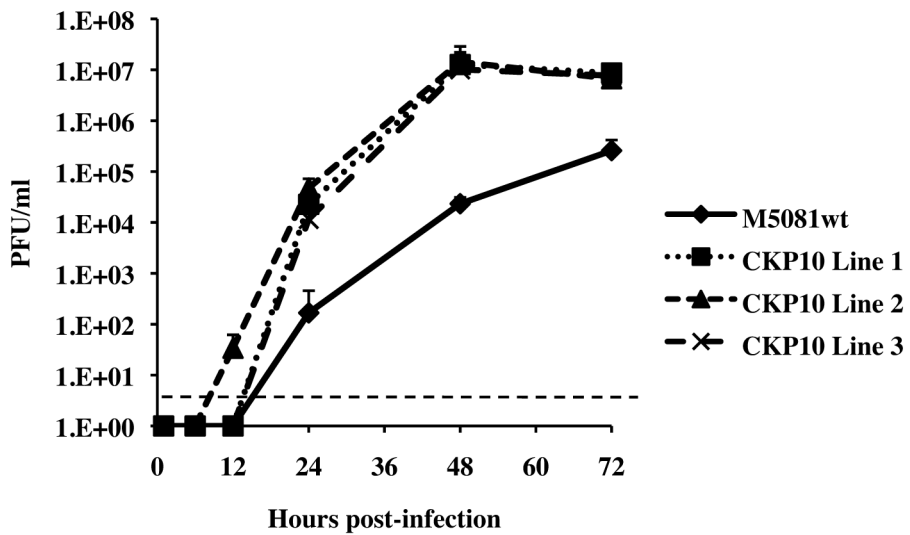


Figure 6

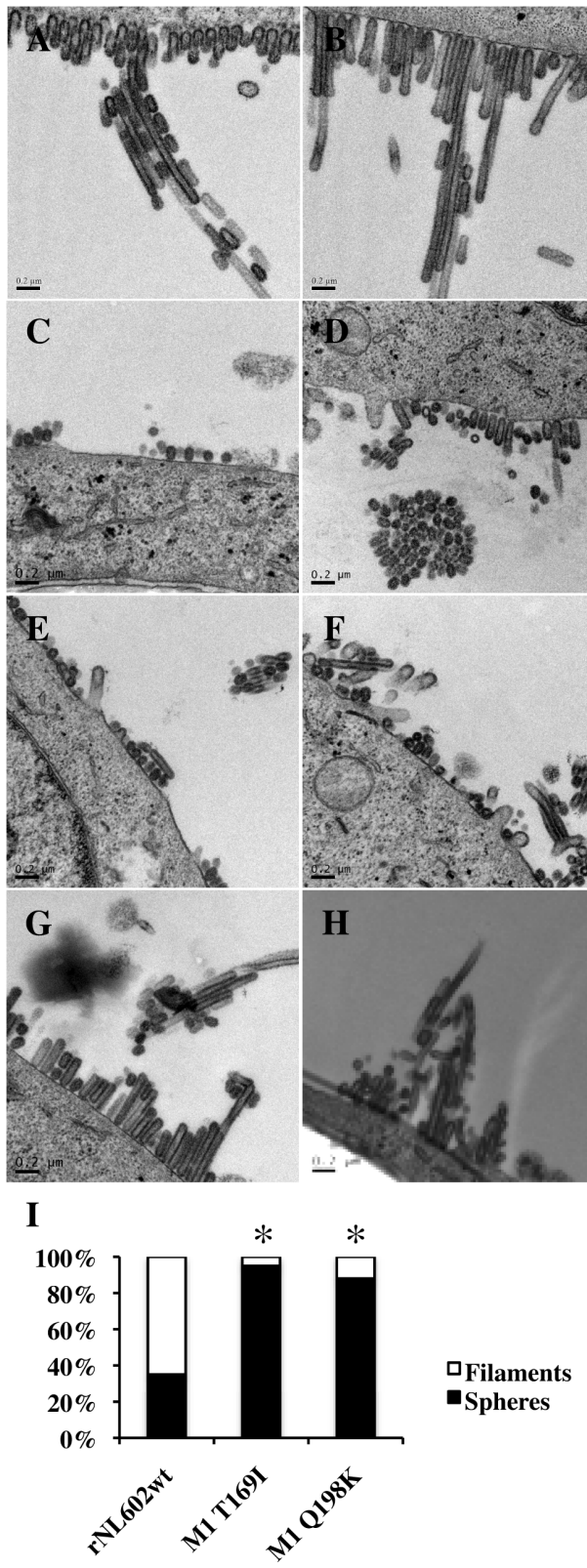


Figure 7

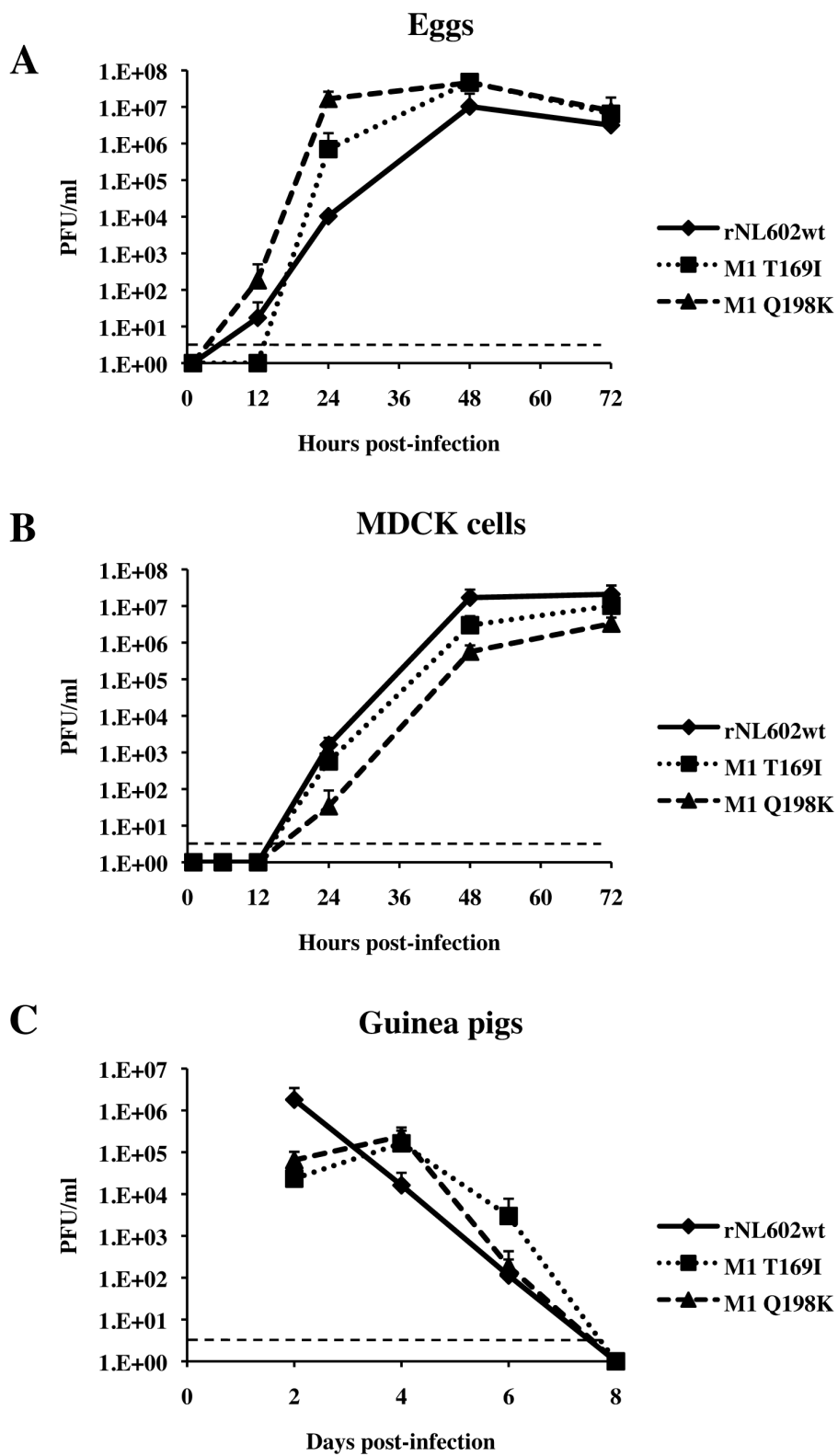


Figure 8.

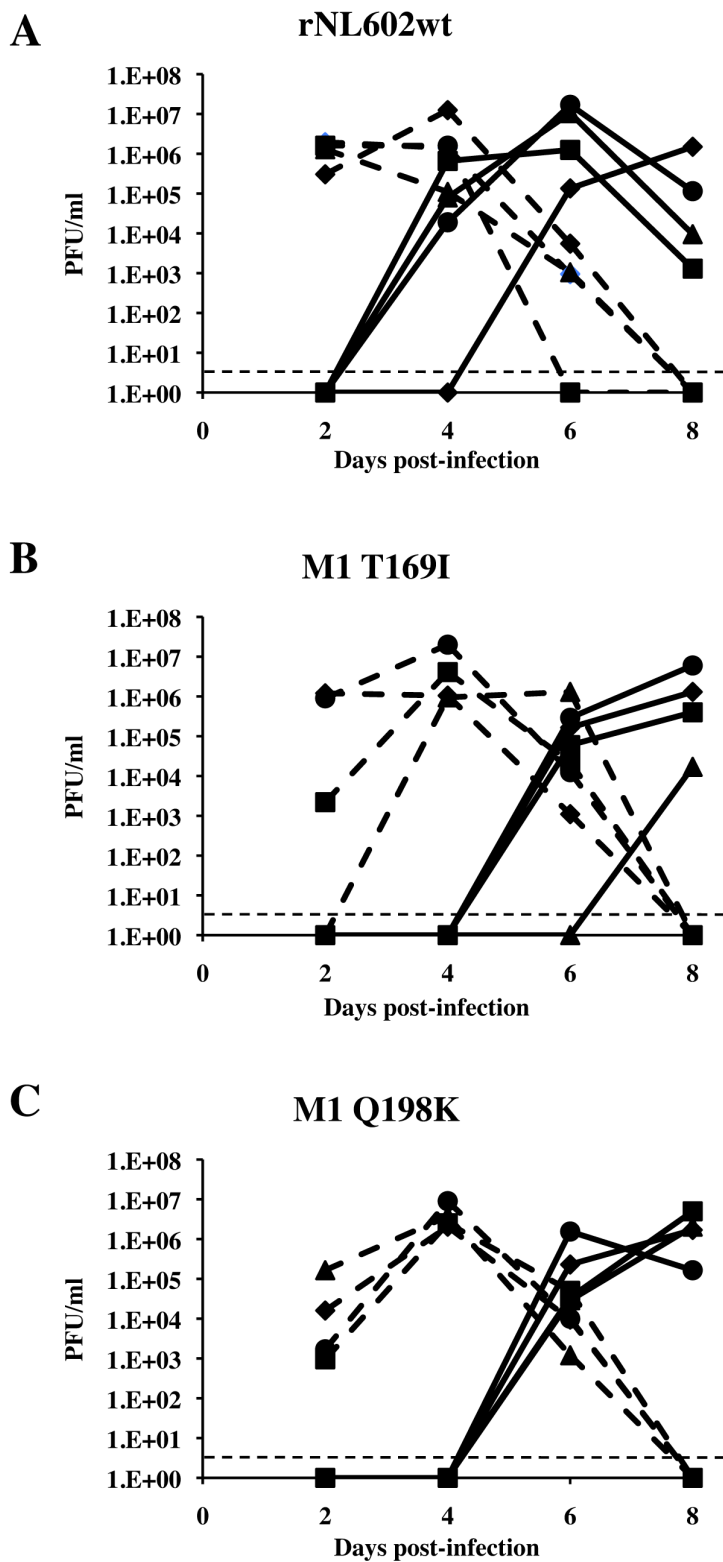


Figure 9.

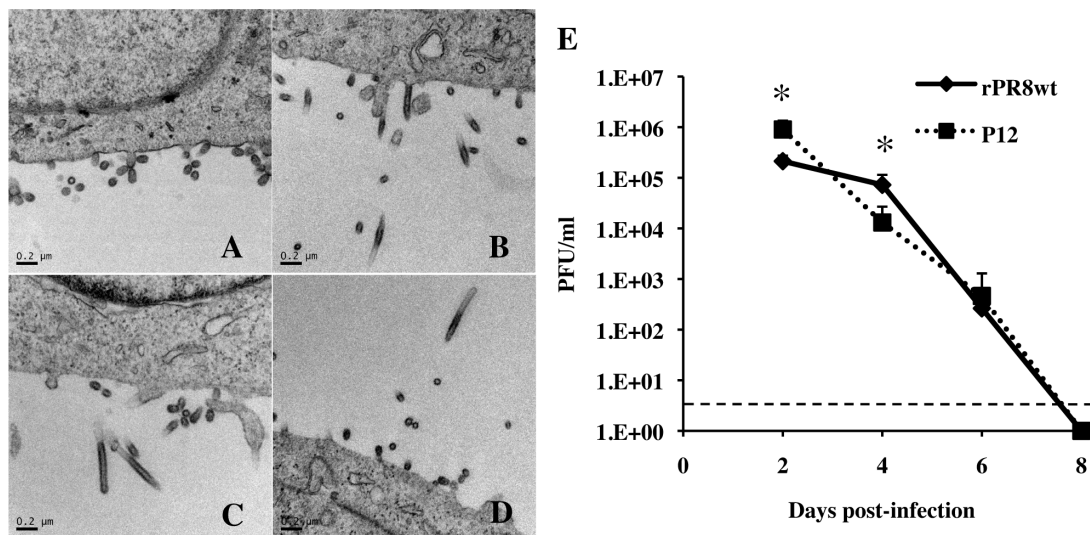


Figure 10.

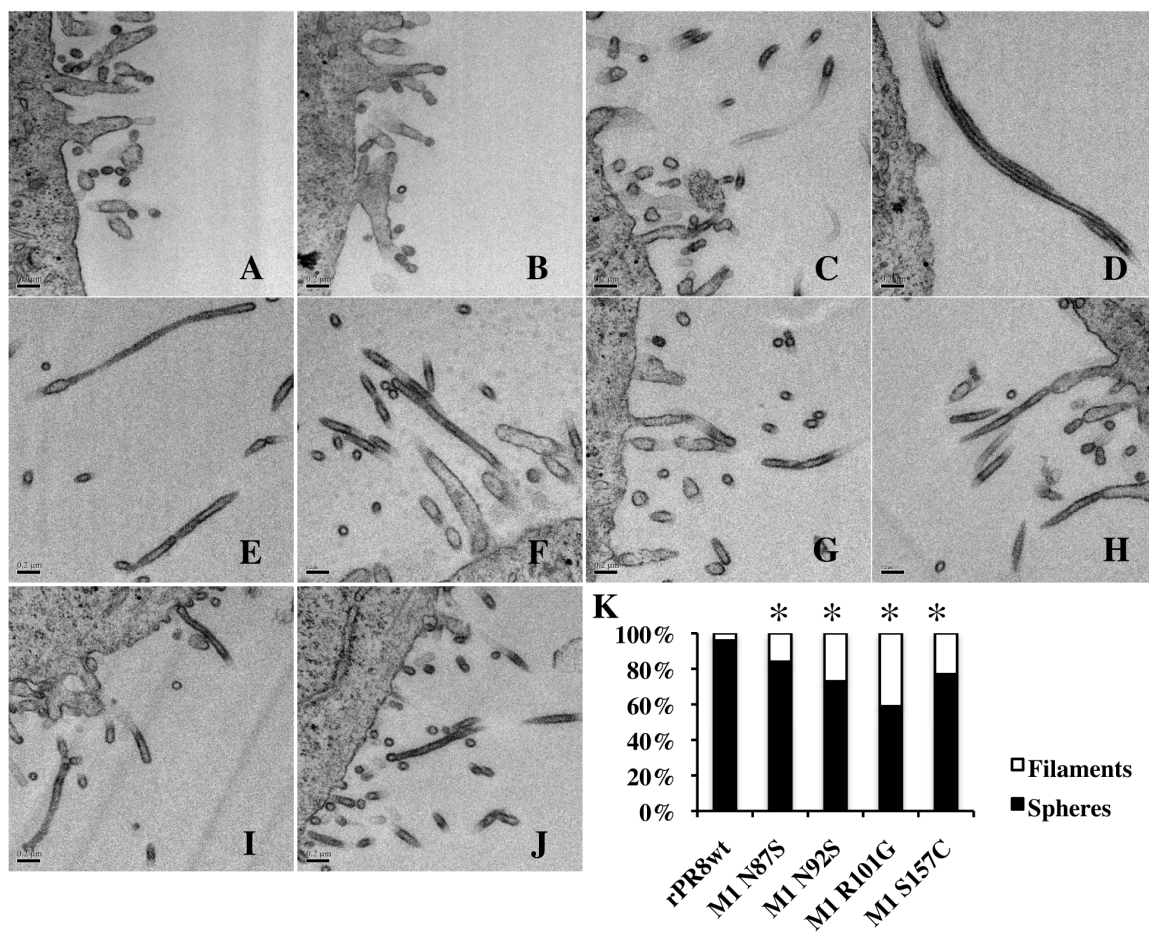


Figure 11.

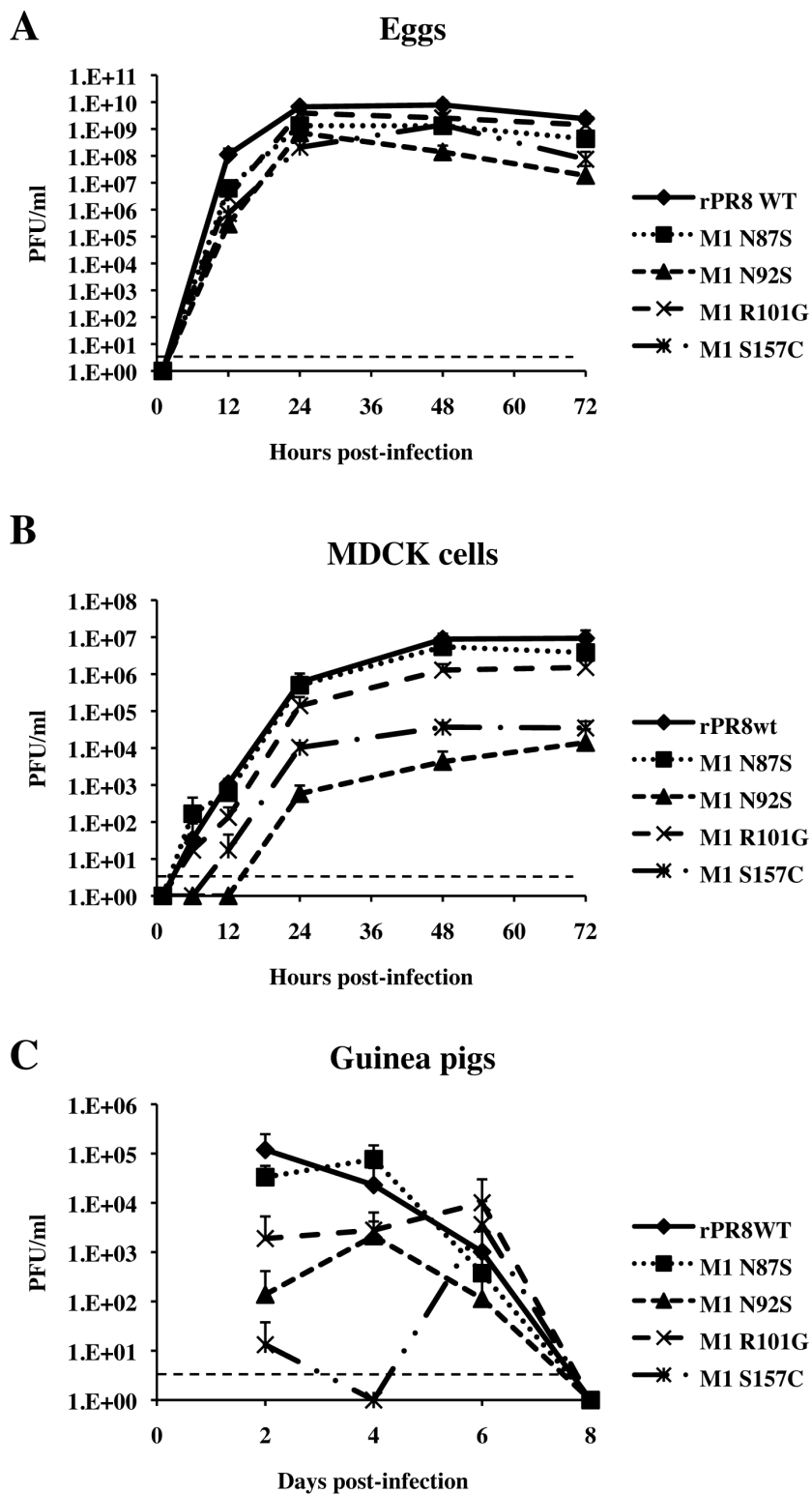
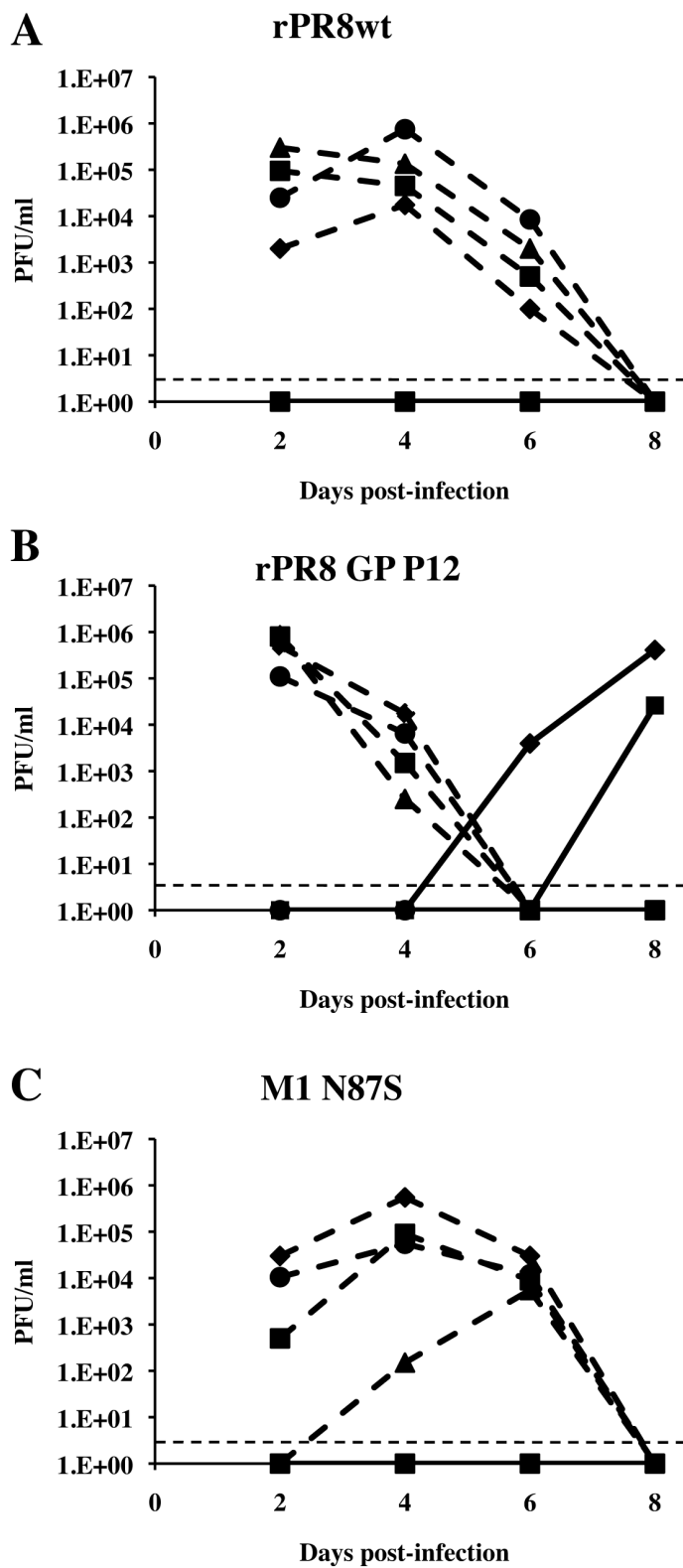


Figure 12.



Chapter 3: Filament-producing mutants of influenza A/Puerto Rico/8/1934 (H1N1) virus have higher neuraminidase activities than the spherical wild-type

Jill Seladi-Schulman, Patricia Campbell, Suganthi Suppiah, John Steel, and Anice C. Lowen

The work of this chapter has been submitted for publication in *PLOS One*.

Abstract

Influenza virus exhibits two morphologies – spherical and filamentous. Strains that have been grown extensively in laboratory substrates are comprised predominantly of spherical virions while clinical or low passage isolates produce a mixture of spheres and filamentous virions of varying lengths. The filamentous morphology can be lost upon continued passage in embryonated chicken eggs, a common laboratory substrate for influenza viruses. The fact that the filamentous morphology is maintained in nature but lost in favor of a spherical morphology *in ovo* suggests that filaments confer a selective advantage within the infected host that is not necessary for growth in laboratory substrates. Indeed, we have recently shown that filament-producing variant viruses are selected upon passage of the spherical laboratory strain A/Puerto Rico/8/1934 (H1N1) [PR8] in guinea pigs. Toward determining the nature of the selective advantage conferred by filaments, we sought to identify functional differences between spherical and filamentous particles. We compared the wild-type PR8 virus to two previously characterized recombinant PR8 viruses in which single point mutations within M1 confer a filamentous morphology. Our results indicate that these filamentous PR8 mutants have higher neuraminidase activities than the spherical PR8 virus. Conversely, no differences were observed in HAU:PFU or HAU:RNA ratios, binding avidity, sensitivity to immune serum in hemagglutination inhibition or plaque reduction assays, or virion stability at elevated temperatures. Based on these results, we propose that the pleomorphic nature of influenza virus particles is important for the optimization of neuraminidase functions *in vivo*.

Introduction

Influenza A virus (IAV) is an enveloped virus containing eight negative-sense RNA gene segments (1). It is the causative agent of seasonal epidemics of respiratory illness as well as occasional pandemics, the most recent of which occurred in 2009 (2). IAV is pleomorphic, producing virions of spherical and filamentous morphology (3). Strains that produce predominantly spherical or ovoid virions have typically been passaged many times within laboratory substrates, while filament-producing strains occur in primary or low passage isolates (4, 5). Filaments are of variable length and can be up to 30 μm long (6). Herein, we define filaments as any virion 300 nm in length or longer ($\geq 3\times$ the diameter of a typical spherical virion). Studies performed using reverse genetics systems have identified the M1 matrix protein as the major genetic determinant of virion morphology, however portions of the viral nucleoprotein (NP) as well as the cytoplasmic tails of the M2 ion channel, hemagglutinin (HA) and neuraminidase (NA) proteins have been shown to affect virion morphology as well (7-13).

Early observations showed that the filamentous morphology is gradually lost upon continued passage in embryonated chicken eggs in favor of a more spherical morphology (14, 15). The fact that filaments are maintained in nature while dispensable for growth in laboratory substrates suggests that the filamentous morphology provides a selective advantage within the infected host that is not necessary for growth in the laboratory. Previously, we showed that passaging of the spherical laboratory strain A/Puerto Rico/8/1934 (H1N1) [PR8] twelve times in guinea pigs led to the emergence of virions that are filamentous in morphology (5). Through sequencing of the M1 matrix gene of the passage 12 (P12) virus pool, we identified several coding mutations within M1.

Individual introduction of four of these amino acid changes using reverse genetics yielded mutant viruses that produced significantly more filaments than the wild-type [$p < 0.05$; difference in proportions test] (5).

While selection for a filamentous morphology through passaging in an animal host confirms an advantage of filamentous virions *in vivo*, the nature of the selective advantage remains unclear. In order to determine the advantage filament-producing viruses have over their spherical counterparts, we used recombinant wild-type PR8 [rPR8wt] and two previously characterized filamentous M1 mutants – rPR8 M1 N87S [N87S] and rPR8 M1 R101G [R101G] (5). These three viruses present an ideal system in which to address the differences between exclusively spherical and filament-producing IAV, for the following reasons: i) the mutant strains are highly similar genetically to the rPR8wt, simplifying the interpretation of results; ii) the mutations used arose naturally, minimizing the likelihood of disrupting viral functions through their introduction; and iii) the mutant viruses differ significantly from rPR8wt in terms of filament production. Thus, rPR8wt, N87S, and R101G viruses were analyzed in a series of *in vitro* assays. We hypothesized that functional differences between spherical and filamentous virions might arise due to their differing surface areas, and therefore focused our efforts on the two surface glycoproteins of IAV, HA and NA. We tested whether the HA avidity or NA activity per virion differed between the spherical rPR8wt virus and filament producing strains. In addition, the ratio of hemagglutination units (HAU) to plaque forming units (PFU), the ratio of HAU to RNA copies, and virion stability at elevated temperatures were investigated. Our findings suggest a role of the viral NA protein in the fitness advantage conferred by filamentous virion morphology: by two independent measures,

the two filamentous rPR8 mutants displayed a higher neuraminidase activity compared to rPR8wt, but did not differ significantly in binding avidity, inhibition of binding or plaque formation by antiserum, infectivity or thermostability.

Material and Methods

Ethics statement

This study was performed in accordance with the recommendations in the Guide for the Care and Use of Laboratory Animals of the National Institutes of Health. Animal husbandry and experimental procedures were approved by the Emory University Institutional Animal Care and Use Committee (IACUC protocol #2000719).

Viruses and cells:

The rPR8wt, rPR8 M1 N87S, and rPR8 M1 R101G viruses were generated using reverse genetics as previously described (16-18). Briefly, rPR8-based viruses were recovered following eight (pDZ) plasmid transfection of 293T cells and subsequent inoculation of transfected cells and culture medium into 9-11 day old embryonated chicken's eggs. Stocks of the rPR8 wild-type virus and mutants were generated in 9-11 day old embryonated chicken's eggs. Influenza A/Udorn/301/1972 (H3N2) virus was grown in MDCK cells. Influenza A/Anhui/1/2013 (H7N9) virus was grown in eggs under enhanced BSL3 containment and inactivated by addition of beta-propiolactone (BPL) prior to removal from the BSL3 facility.

Washed chicken red blood cells from Lampire Biological were used for all hemagglutination-based assays. MDCK cells, a kind gift of Peter Palese, were maintained in minimal essential medium supplemented with 10% fetal bovine serum and penicillin/streptomycin. 293T cells (ATCC), used for virus rescue by reverse genetics, were maintained in Dulbecco's minimal essential medium supplemented with 10% fetal bovine serum. Embryonated chickens' eggs were obtained from Hy-Line International and incubated at 37°C, with rocking, for 9-11 days prior to inoculation with IAV.

Red blood cell elution assay:

Each virus was standardized to a concentration of 128 hemagglutination units (HAU, defined as the reciprocal of the highest dilution of virus still allowing agglutination of red blood cells). Duplicate HA assays were then set up in parallel using serially diluted viruses and allowed to develop at 4°C. One set of plates was then transferred to 37°C (t = 0 hours) to trigger neuraminidase activity, while the second set of plates was left at 4°C to act as a negative control. Red blood cells were monitored for elution (visible as the formation of a red blood cell pellet at the bottom of the well) at the following time points: 1, 2, 3, 4, 6, and 8 hours.

Infectious titer comparison:

Viruses were diluted to concentration of 128 HAU. After confirming the HA titer, viruses were titrated in triplicate by plaque assay of 10-fold serial dilutions on MDCK cells. A Student *t*-test was used to compare the infectious titers of each mutant virus to rPR8wt virus.

C_q value comparison:

Viruses were diluted to concentration of 128 HAU. After confirming the HA titer, RNA was extracted from 160 µl of each diluted virus sample using the QIAamp Viral RNA Mini Kit (QIAGEN), according to the manufacturer's instructions. cDNA was generated using Maxima reverse transcriptase (Thermo Scientific) and a universal forward primer (GGCCAGCAAAAGCAGG). Quantitative PCR was then performed on a Bio-Rad CFX384 thermocycler using the cDNA as template, SsoFast EvaGreen Supermix (Bio-Rad), and primers specific for the NP segment (F: TATTCGTCTCAGGGAGCAAAAGCAGG (19) and R: CTGATTTCAGTGGCATTCTGGC). Each cDNA was analyzed in triplicate and the resulting cycle threshold (C_q) values were recorded. Average C_q values shown in Table 1 were calculated by first converting each C_q value to 2^(-C_q), calculating the arithmetic mean, and then taking the -log₂ of the arithmetic mean.

MUNANA neuraminidase activity assay:

Neuraminidase activity assays using the soluble substrate methylumbelliferyl N-acetylneuraminic acid (MUNANA) were performed as previously described by Campbell et al. (20). Virus was diluted to 5 x 10⁵ PFU/ml and 80 µl was added to each well of a black 96-well plate (CoStar). A sample of each diluted virus preparation was retained for quantification of viral RNA therein by RT-qPCR. Concentrations of MUNANA substrate ranging from 1.17 µM to 150 µM were used. When cleaved by the viral NA, MUNANA produces a fluorescent product. Fluorescence was quantified using a Biotek Synergy H1

plate reader every minute over the course of an hour. Fluorescence curves were then fitted to the Michaelis-Menton equation to determine values of V_{\max} (maximal enzyme velocity) and K_m (the Michaelis constant, the substrate concentration at which the reaction rate is half of V_{\max}). Each experiment included triplicate samples of each virus.

Virus concentration for Western blot analysis:

Each virus was purified from allantoic fluid collected from 9-11 day embryonated chicken eggs infected with 250 PFU of virus. Allantoic fluid was spun at 3,000 rpm for 10 minutes at 4°C in a Sorvall tabletop centrifuge after which the supernatant was transferred to ultracentrifuge tubes (Beckman Coulter). Samples were spun in an SW32 rotor at 10,000 rpm for 30 minutes at 4°C and supernatant was then transferred to a fresh tube where a 5-ml 30% sucrose cushion was added. Samples were spun in an SW32 rotor at 25,000 rpm for 2.5 hours at 4°C. All supernatant was removed and 100 µl of PBS was added to the virus pellet and allowed to resuspend at 4°C overnight.

NP normalization and Western blot:

Concentrated virus samples were denatured by boiling for 10 minutes and treated with PNGaseF (New England Biolabs) for 1 hour at 37°C to allow for deglycosylation. The amount of NP in each virus sample was quantified by polyacrylamide gel electrophoresis followed by Coomassie staining (GelCode Blue – Thermo Scientific) and analysis with Image Lab software (Bio-Rad). The volume of each sample used for western blotting was then normalized based on NP content. Samples were loaded on a 4-15% SDS gradient gel (Bio-Rad Mini Protean) and electrophoresed at 130 V for 1 hour and 5 minutes. Protein

was transferred (semi-dry) onto nitrocellulose membrane for 1 hour at 100 mA and blocking was performed overnight. NA was detected using a goat anti-NA primary antibody (BEI NR-9598) and a donkey anti-goat alexa 647-conjugated secondary antibody. NP was detected using a rabbit anti-NP primary antibody (a kind gift of Peter Palese) and a donkey anti-rabbit alexa 488-conjugated secondary antibody. Band intensity was quantified using Image Lab software (Bio-Rad).

Red blood cell-based avidity assay:

The red blood cell-based avidity assay was performed similarly to those described in (21). Briefly, a 1.3% solution of red blood cells in PBS was treated with a series of dilutions of *C. perfringens* neuraminidase (Sigma) for 30 minutes at 37°C. Neuraminidase concentrations incremented by 5 mU/ml for the PR8-based viruses and 10 mU/ml for the H3 and H7 subtype viruses. Treated red blood cells were then added to virus at a standardized concentration of 8 HAU in a v-bottom, 96-well plate. Hemagglutination was assessed after 2 hours at 4°C. To rule out the activity of the viral NA in interpreting results, virus was diluted in PBS containing oseltamivir carboxylate (GS4071) and the assay was allowed to develop at 4°C.

Trypsin-heat-periodate treatment:

In order to remove nonspecific inhibitors of hemagglutination, serum treatment was performed as outlined in (22). Briefly, serum was treated with L -1-Tosylamide-2-phenylethyl chloromethyl ketone (TPCK) trypsin for 30 minutes at 56°C. After cooling to room temperature, serum was then treated with 0.011 M metapotassium periodate (KIO₄)

for 15 minutes at room temperature. After KIO_4 treatment, serum was treated with 1% glycerol in PBS for 15 minutes at room temperature after which an 85% PBS solution was added to reach a final serum dilution of 1:10.

Hemagglutination inhibition (HI) assay:

Trypsin-heat-periodate-treated anti-PR8 guinea pig serum was diluted in PBS either 1:2 or 1:1.5 across a v-bottom, 96-well plate. Each virus was standardized to a concentration of 8 HAU and was then added to the diluted serum. Serum and virus were incubated together at 4°C for 30 minutes after which 0.5% red blood cells in PBS were added to each well. The assay was allowed to develop at 4°C. Naïve guinea pig serum was used as a negative control. The HI titers shown in Table 3 reflect HI activity above background levels.

Plaque reduction assay:

Each virus was diluted to approximately 250 PFU. Trypsin-heat-periodate treated anti-PR8 guinea pig serum was serially diluted 1:80, 1:160, 1:320, and 1:640 in PBS. Control serum obtained from a naïve guinea pig was also used. Virus was added to the diluted serum and incubated for 30 minutes at 37°C. The infectious titer of each serum/virus sample then quantified by plaque assay in MDCK cells. This assay was performed in triplicate.

Thermostability assay:

Each virus was diluted to approximately 1×10^6 PFU. Fifteen 120 μ l aliquots of each virus were incubated at 50°C and three aliquots of each virus were removed at 0, 15, 30, 60, and 120 minutes. Titers for each sample were quantified via plaque assay on MDCK cells.

Results

The rPR8 M1 N87S and rPR8 M1 R101G filamentous mutants have higher neuraminidase activity than rPR8wt virus.

The NA activity of the spherical and filament-producing viruses was first assessed by comparing rPR8wt, N87S, and R101G viruses in a red blood cell elution assay. To test our hypothesis that filamentous and spherical virions differ at the level of the whole virus particle, due to differing surface areas, we aimed to evaluate NA activity per virion rather than per NA protein. We therefore normalized virus input by hemagglutination titer rather than protein levels. Briefly, HA assays were set up in parallel using a standardized amount of virus (128 HAU) and allowed to develop at 4°C. At that point, one set of plates was transferred to 37°C. At this temperature, the viral NA is active and begins cleaving the sialic acids on the surface of the red blood cells, causing them to drop to the bottom of the well (elution). We monitored the plates for elution over the course of 8 hours. Progressive elution was observed at 37°C, while no elution was seen over the same time period at 4°C. We found that, when incubated with the R101G mutant virus, red blood cells eluted at a faster rate compared to those incubated with rPR8wt (Figure 1A). The

N87S mutant had a less marked phenotype than the R101G mutant, but also eluted red blood cells at a faster rate than the rPR8wt – particularly at the later time points (Figure 1B).

Equivalent HAU of the rPR8wt, rPR8 M1 N87S, and rPR8 M1 R101G viruses do not differ in infectivity or RNA copy number

To verify that differences in the amount of virus used for each assay did not account for the observed differences in elution, we evaluated both the PFU titer and RNA content of 128 HAU samples of rPR8wt, N87S, and R101G viruses. Each virus was diluted to 128 HAU and HA titers were confirmed. Diluted virus samples were then titrated in triplicate by plaque assay. The mutant viruses showed lower PFU titers compared to rPR8wt, but the differences were not statistically significant (Table 1). RNA was extracted from 160 μ l of each diluted virus and quantified by reverse transcription followed by quantitative PCR. C_q values obtained were consistent across all three viruses (Table 1). Thus, for all three viruses, the HAU to PFU and HAU to RNA copy number ratios were comparable. To assess the precision and consistency of the hemagglutination assay, we furthermore evaluated the PFU titers and relative RNA copy numbers of three 128 HAU samples of rPR8wt virus that had been obtained through independent dilution series. The average PFU titers obtained ranged from 1.66 to 1.78 $\times 10^8$ PFU/ml (n=3 per 128 HAU sample). The average C_q values were also very similar, ranging from 18.64 to 18.85. Taken together, these results indicate that the more rapid elution exhibited by the N87S and R101G viruses are unlikely to be due to greater input of these viruses relative to rPR8wt.

Table 1: 128 HAU of rPR8wt, rPR8 M1 N87S and rPR8 M1 R101G viruses comprise comparable infectious titers and genome copies

Virus	Infectious titer (PFU/ml) ^a	Average infectious titer (PFU/ml)	C _q value ^b	Average C _q value
rPR8wt	6.00 x 10 ⁷	1.15 x 10 ⁸	19.06	19.16
	1.55 x 10 ⁸		19.37	
	1.30 x 10 ⁸		19.08	
rPR8 M1 N87S	5.00 x 10 ⁷	7.60 x 10 ⁷	19.23	19.32
	5.00 x 10 ⁷		19.42	
	1.30 x 10 ⁸		19.32	
rPR8 M1 R101G	4.00 x 10 ⁷	7.80 x 10 ⁷	18.86	18.94
	6.50 x 10 ⁷		18.92	
	1.30 x 10 ⁸		19.04	

^a rPR8wt to rPR8 M1 N87S comparison (p = 0.38), rPR8wt to rPR8 M1 R101G comparison (p = 0.40). A two-tailed Student *t*-test was used to assess significance.

^b rPR8wt to rPR8 M1 N87S comparison (p = 0.23), rPR8wt to rPR8 M1 R101G comparison (p = 0.10). To assess significance, a two-tailed Student *t*-test was applied to values of 2^(-C_q).

The rPR8 M1 N87S and rPR8 M1 R101G filamentous mutants have higher neuraminidase activity in the MUNANA assay than rPR8wt virus.

To further confirm that the differing elution phenotypes observed were due to differing NA activities, we compared the spherical and filamentous rPR8 viruses using a MUNANA-based assay. MUNANA (methylumbelliferyl N-acetylneuraminic acid) is a soluble substrate that produces a fluorescent product when cleaved by the viral NA. For this assay, viruses were standardized to equivalent PFU and RNA titers and

concentrations of MUNANA substrate ranging from 1.17 μM to 150 μM were used. Levels of fluorescence were measured every minute over a sixty-minute period. The resulting fluorescence curves were then fitted to the Michaelis-Menton equation for calculation of K_m and V_{\max} values associated with each virus. It is important to note that, in line with our aim of evaluating NA enzyme kinetics per virion, NA protein levels contained within each virus sample were not normalized for this assay.

The results obtained correlated well with those observed from the red blood cell elution assay (Figure 2). The R101G mutant virus displayed the highest V_{\max} , followed by the N87S mutant. rPR8wt had the lowest V_{\max} (Table 2). The K_m for all three viruses was found to be consistent, as expected considering the NA protein is the same for all three viruses (Table 2). Based on the results of both the elution assay and the MUNANA assay, we concluded that the filament-producing M1 mutant viruses had a higher neuraminidase activity per virion than the spherical wild-type virus.

Table 2: rPR8 M1 N87S and rPR8 M1 R101G viruses have a higher neuraminidase activity than rPR8 wt virus in a MUNANA-based assay

Virus	V_{\max}	V_{\max} 95% confidence interval	K_m	K_m 95% confidence interval
rPR8wt	1040	978-1101	13.02	10.41-15.63
rPR8 M1 N87S	1434	1370-1497	13.15	11.17-15.14
rPR8 M1 R101G	1785	1669-1901	15.52	10.60-20.44

When standardized to NP protein levels, NA and M1 protein incorporation among rPR8wt, rPR8 M1 N87S, and rPR8 M1 R101G is similar.

Because filamentous virions can be much greater in size than spherical virions, a logical explanation for our NA activity results is that filamentous virions have more NA adorning their surface. Indeed, the consistent K_m values across all three viruses obtained from the MUNANA assay suggest that the intrinsic NA activity is unaffected. To test this hypothesis, we performed Western blots on concentrated virus preparations of rPR8wt, N87S, and R101G, and probed for NP, NA, and M1 proteins. The fluorescence intensity of bands was quantified using a Bio-Rad Chemidoc imager. NP and M1 were included as controls: due to its association with the viral genome, NP levels would be expected to be constant among viruses of differing morphology, while M1 levels would be expected to increase with surface area. For a given amount of NP, the filamentous mutant viruses did not show increased quantities of NA or M1 proteins in virions (Figure 3A and 3B). Similar results were obtained when inputs were normalized by viral RNA content, rather than normalization to NP (data not shown). Based on our inability to detect increases in M1:NP ratios for the filament-producing viruses relative to rPR8wt, we concluded that the Western blot assay used was not sufficiently sensitive to detect differences (or lack thereof) in NA or M1 incorporation. The preponderance of spherical viruses present in the N87S and R101G virus stocks most likely obscures any differences in protein content between spherical and filamentous particles.

No difference in binding avidity is observed between rPR8wt, rPR8 M1 N87S, and rPR8 M1 R101G.

After assessing the NA activity between spherical and filamentous viruses, we compared the function of the viral HA in a red blood cell-based avidity assay. We treated chicken

red blood cells with a series of dilutions of *C. perfringens* neuraminidase. This treatment removes α 2,3-, α 2,6- and α 2,8-linked sialic acids. Thus, red blood cells treated with higher concentrations of neuraminidase had fewer sialic acids on their surface than those treated with lower concentrations of neuraminidase. We then added a standardized amount of virus (8 HAU) to the treated red blood cells and allowed agglutination to occur. We found that the neuraminidase concentration that prevented agglutination was the same for the rPR8wt, N87S, and R101G viruses, indicating that red blood cell binding avidity is not affected by the changes in morphology seen with these viruses (Figure 4). Additionally, to validate that the assay was sufficiently sensitive to detect differences in red blood cell binding avidity, we compared avidity of the rPR8-based viruses to those of viruses with differing HA types (specifically, H3 and H7). We found that A/Udorn/301/1972 (H3N2) and BPL-inactivated A/Anhui/1/2013 (H7N9) virus had higher red blood cell binding avidities than the PR8-based viruses. From these results, we concluded that the changes in virion morphology mediated by the N87S and R101G mutations do not affect the binding avidity of rPR8 virus.

No difference in hemagglutination inhibition or plaque reduction was observed among rPR8wt, rPR8 M1 N87S, and rPR8 M1 R101G.

Next, we compared hemagglutination inhibition (HI) between rPR8wt, N87S, and R101G viruses, reasoning that, due to their increased size, filaments may be more difficult to neutralize than spheres. Using 1:2 dilutions of trypsin-heat-periodate treated anti-PR8 guinea pig immune serum and virus standardized to 8 HAU, we found no difference in HI between rPR8wt, N87S, and R101G (Table 3). Since we were working with populations

of mixed morphology, which may make differences between filaments and spheres difficult to detect, we sought to improve the sensitivity of the assay by using a series of 1:1.5 serum dilutions. Similar to the assays utilizing 1:2 dilutions, we observed little difference in HI between the spherical wild-type and filamentous mutants (Table 3).

Table 3: There are no differences in hemagglutination inhibition among rPR8wt, rPR8 M1 N87S, rPR8 M1 R101G viruses

Virus	1:2 serum dilutions			1:1.5 serum dilutions		
	HI titer ^a			HI titer ^a		
	A	B	C	A	B	C
rPR8wt	160	160	320	256	256	384
rPR8 M1 N87S	160	160	160	256	256	384
rPR8 M1 R101G	160	160	320	171	256	384

^a The reciprocal of the highest dilution of serum that prevented hemagglutination is shown for three replicates (A, B and C).

To further substantiate the observation that particle morphology did not affect the sensitivity of virus to immune serum, we also performed a plaque reduction assay. Briefly, trypsin-heat-periodate treated anti-PR8 guinea pig serum was diluted to 1:80, 1:160, 1:320, or 1:640 in PBS. The same dilutions of a naïve guinea pig serum were used as controls. Virus was diluted to approximately 250 PFU and incubated with the diluted serum for 30 minutes at 37°C. Following the incubation period, virus titer was determined in triplicate for each serum/virus sample by plaque assay in MDCK cells. Plaque numbers were compared to those obtained when virus was incubated with the control serum. While no significant reduction in plaque number was observed with 1:320 or higher dilutions of serum, all three viruses showed significant reductions with serum diluted

1:160 and 1:80 (Figure 5). Thus, the results from the HI assays and the plaque reduction assay agree and suggest that the selection of filamentous variants *in vivo* is not related to changes in HA avidity.

No difference in virion stability is observed between rPR8wt, rPR8 M1 N87S, and rPR8 M1 R101G.

Due to potential differences in the structure of the matrix layer (23), we hypothesized that filamentous and spherical viruses might differ in their sensitivity to environmental stresses, such as fluctuations in temperature. To test this hypothesis, we evaluated virion stability at high temperatures. Each virus was diluted to a concentration of 1×10^6 PFU and incubated at 50°C for one of the following lengths of time: 0, 15, 30, 60, or 120 minutes. Following heat exposure, the titer of each sample was quantified in triplicate via plaque assay in MDCK cells. All three viruses had similar infectious titers remaining at each time point, indicating that the observed changes in virion morphology do not affect virion stability at elevated temperatures (Figure 6).

Discussion

The fact that the filamentous morphology of IAV is maintained in nature but not in the laboratory suggests that filaments have a functional significance within the infected host. Due to the greater surface area of filaments relative to spheres, we hypothesized that functional differences between the two morphologies may lie with the HA and NA surface glycoproteins. We therefore focused our study on the HA and NA functions of strains with differing morphological phenotypes. We took advantage of two M1 point

mutants selected during serial adaptation of rPR8 virus to an animal host (5). By measuring particles in electron micrographs, the R101G mutant was previously shown to comprise 41% filamentous particles, while the N87S had 16% filaments and the rPR8wt virus had 6% filaments (5).

Our approach, focused on the surface of the virion, assumes that the internal components of spherical and filamentous particles are similar. Our results indicating comparable infectivity and RNA content per HAU for spherical and filament-producing strains supports this assumption. Similar results were also reported by Roberts et al. for the A/Udorn/301/1972 (H3N2) strain (10). Nevertheless, the literature contains conflicting reports on the genomic content of filaments versus spheres. Early studies suggested that filamentous virions could be polyploid (containing more than one copy of the genome) or contain more RNA than their spherical counterparts (24, 25). In contrast, a recent cryo-electron tomography study has shown that many longer filaments produced by A/Udorn/301/1972 (H3N2) virus lack RNPs (26). Lastly, sectioning TEM and cryo-electron tomography studies have shown that filamentous virions contain a single copy of the viral genome located at the apical tip of the budding virion (23, 27). These apparently contradictory results can be partially reconciled by noting that the absence of genomes from filamentous particles appears to apply mainly to very long filaments (26). In some cases, IAV strain specific differences in the properties of filaments may also play a role.

Our observations through two independent functional assays show that the two filament-producing rPR8 mutants have higher NA activities than the spherical rPR8wt virus. Replacement of the PR8 M segment with that of the filamentous 2009 pandemic strain A/Netherlands/602/2009 (H1N1) was also shown to increase both filament

production and NA activity compared to the rPR8wt virus (20). Now we show that significant increases in NA activity can be conferred through a single point mutation that changes virion morphology, thereby strengthening the causal link between morphology and NA activity. We predict that the increased NA activities associated with filament-containing virus preparations are due to greater numbers of NA proteins adorning the surface of filaments compared to spheres. We were not able to test this prediction robustly, however, due to limitations in the sensitivity of our Western blot assay. An alternative mechanism by which morphology could impact NA activity relates to the distribution of NA molecules on the virion surface. If filaments and spheres differ in terms of the positioning of NA on the particle, increased neuraminidase activity could be due to a cooperative effect mediated by greater NA protein clustering on filamentous virions. Consistent with this idea, clustering of NA at the tip of the virus particle proximal to the cell membrane has been reported (23, 28, 29). Such an arrangement was suggested to promote destruction of host cell receptors as the virus is budding.

Contrary to what was observed for NA activity, we found no difference in binding avidity to red blood cells between the spherical and filamentous rPR8 viruses. Similarly, we did not observe an appreciable difference in HI titer or in plaque reduction between spherical and filamentous viruses. These results suggest that the mechanism by which NA activity is increased for filament-producing viruses does not apply to HA. For example, if incorporation of both glycoproteins increases with filament size, then our data would suggest that avidity does not increase linearly with the valency of the virus particle. Lastly, we did not observe a difference in thermostability between spherical and filamentous viruses. Thus our data suggest that, at least in the PR8 background and in a

guinea pig host, the selective advantage of a filamentous morphology lies with increased NA activity.

Enhanced NA activity could be advantageous to the virus by promoting release from infected cells and/or spread within the respiratory tract to new target cells (30). Indeed, Roberts et al. suggested that increased amounts of NA protein per virion could aid movement through the mucus lining the airway (31). Additionally, increased NA activity was shown to improve transmission in guinea pigs (20, 32). Importantly, the M segment has been shown to affect virus transmission as well (20, 33). Whether this effect on transmission is directly mediated by viral morphology has not yet been established. However, the fact that a single point mutation in the M1 matrix protein can both significantly alter virion morphology and confer increased NA activity suggests a mechanism by which the M segment may affect transmission. We know from previous work that the rPR8 M1 N87S mutant virus, which has both a significantly more filamentous morphology as well as a higher NA activity than rPR8wt, is not transmissible by a contact route in the guinea pig transmission model (5). It is likely that N87S and the other individual point mutations identified through passaging need to be coupled with additional permissive mutations on the M segment and/or elsewhere in the genome to promote transmission (34).

In summary, we have shown that filament-producing viruses have a higher neuraminidase activity than their spherical counterparts. Other properties such as HA binding avidity, HI titer, and thermostability were unaffected by changes in virion morphology. The viruses used herein were single M1 point mutants generated on a PR8 background and produced significantly more filaments than rPR8wt. The fact that these

point mutations, when introduced individually, confer both a filamentous morphology and increased NA activity further strengthens the idea that the selective advantage conferred by filamentous virions lies in their increased NA activity over spherical virions.

Acknowledgements

This work was funded by the Centers for Excellence in Influenza Research and Surveillance (CEIRS) contract number HHSN266200700006C.

References

1. Palese P, Shaw ML. (2007) Orthomyxoviridae: the viruses and their replication. In: Knipe DM, Howley PM, editors. *Fields Virology* 5th edition. Philadelphia: Lippincott Williams & Wilkins. pp 1647-1689.
2. Novel Swine-Origin Influenza A (H1N1) Virus Investigation Team, Dawood FS, Jain S, Finelli L, Shaw MW, Lindstrom S, Garten RJ, Gubareva LV, Xu X, Bridges CB, Uyeki TM. (2009) Emergence of a novel swine-origin influenza A (H1N1) virus in humans. *N Engl J Med.* 360:2605-2615.
3. Chu CM, Dawson IM, Elford WJ. (1949) Filamentous forms associated with newly isolated influenza virus. *Lancet.* 1:602.
4. Itoh Y, Shinya K, Kiso M, Watanabe T, Sakoda Y, Hatta M, Muramoto Y, Tamura D, Sakai-Tagawa Y, Noda T, Sakabe S, Imai M, Hatta Y, Watanabe S, Li C, Yamada S, Fujii K, Murakami S, Imai H, Kakugawa S, Ito M, Takano R, Iwatsuki-Horimoto K, Shimojima M, Horimoto T, Goto H, Takahashi K, Makino A, Ishigaki H, Nakayama M, Okamatsu M,

- Takahashi K, Warshauer D, Shult PA, Saito R, Suzuki H, Furuta Y, Yamashita M, Mitamura K, Nakano K, Nakamura M, Brockman-Schneider R, Mitamura H, Yamazaki M, Sugaya N, Suresh M, Ozawa M, Neumann G, Gern J, Kida H, Ogasawara K, Kawaoka Y. (2009) In vitro and in vivo characterization of new swine-origin H1N1 influenza viruses. *Nature*. 460:1021-1025.
5. Seladi-Schulman J, Steel J, Lowen AC. (2013) Spherical influenza viruses have a fitness advantage in embryonated eggs, while filament-producing strains are selected in vivo. *Journal of Virol*. 87:13343-13353.
 6. Mosley VM, Wyckoff RW. (1946) Electron micrography of the virus of influenza. *Nature*. 157:263.
 7. Burleigh LM, Calder LJ, Skehel JJ, Steinhauer DA. (2005) Influenza A viruses with mutations in the M1 helix six domain display a wide variety of morphological phenotypes. *J Virol*. 79:1262-1270.
 8. Bourmakina SV, Garcia-Sastre A. (2003) Reverse genetics studies on the filamentous morphology of influenza A virus. *J Gen Virol*. 84:517-527.
 9. Elleman CJ, Barclay WS. (2004) The M1 matrix protein controls the filamentous phenotype of influenza A virus. *Virology*. 321:144-153.
 10. Roberts PC, Lamb RA, Compans RW. (1998) The M1 and M2 proteins of influenza A virus are important determinants in filamentous particle formation. *Virology*. 240:127-137.
 11. Jin H, Leser GP, Zhang J, Lamb RA. (1997) Influenza virus hemagglutinin and neuraminidase cytoplasmic tails control particle shape. *EMBO J*.

- 16:1236-1247.
12. Bialas KM, Bussey KA, Stone RL, Takimoto T. (2014) Specific nucleoprotein residues affect influenza virus morphology. *J Virol.* 88:2227-2234.
 13. Mitnaul LJ, Castrucci MR, Murti KG, Kawaoka Y. (1996) The cytoplasmic tail of influenza A virus neuraminidase (NA) affects NA incorporation into virions, virion morphology, and virulence in mice but is not essential for virus replication. *J Virol.* 70:873-879.
 14. Kilbourne ED, Murphy JS. (1960) Genetic studies of influenza viruses. I. Viral morphology and growth capacity as exchangeable genetic traits. Rapid in ovo adaptation of early passage Asian strain isolates by combination with PR8. *J Exp Med.* 111:387-406.
 15. Choppin PW, Murphy JS, Tamm I. (1960) Studies of two kinds of virus particles which comprise influenza A2 virus strains. III. Morphological characteristics: independence to morphological and functional traits. *J Exp Med.* 112:945-952.
 16. Fodor E, Devenish L, Engelhardt OG, Palese P, Brownlee GG, Garcia-Sastre A. (1999) Rescue of influenza A virus from recombinant DNA. *J Virol* 73:9679-9682.
 17. Steel J, Lowen AC, Mubareka S, Palese P. (2009) Transmission of influenza virus in a mammalian host is increased by PB2 amino acids 627K or 627E/701N. *PLoS Pathog.* 5:e100052.
 18. Quinlivan M, Zamarin D, Garcia-Sastre A, Cullinane A, Chambers T,

- Palese P. (2005) Attenuation of equine influenza viruses through truncations of the NS1 protein. *J Virol.* 79:8431-8439.
19. Hoffmann E, Stech J, Guan Y, Webster RG, Perez DR. (2001) Universal primer set for the full-length amplification of all influenza A viruses. *Arch Virol.* 146:2275-2289.
 20. Campbell PJ, Danzy S, Kyriakis CS, Deymier MJ, Lowen AC, Steel J. (2014) The M segment of the 2009 pandemic influenza virus confers increased NA activity, filamentous morphology, and efficient contact transmissibility to A/Puerto Rico/8/1934-based reassortant viruses. *Journal of Virol.* 88:3802-3814.
 21. Hensley SE, Das SR, Bailey AL, Schmidt LM, Hickman HD, Jayaraman A, Viswanathan K, Raman R, Sasisekharan R, Bennink JR, Yewdell JW. (2009) Hemagglutinin receptor binding avidity drives influenza A virus antigenic drift. *Science.* 326:734-736.
 22. Webster RG, Cox NJ, Sthor K. (2002) WHO manual on animal influenza diagnosis and surveillance. World Health Organization, Geneva, Switzerland:<http://www.who.int/csr/resources/publications/influenza/en/whocdscsrncs20025rev.pdf>.
 23. Calder LJ, Wasilewski S, Berriman JA, Rosenthal PB. (2010) Structural organization of a filamentous influenza A virus. *Proc Natl Acad Sci USA.* 107:10685-10690.
 24. Ada GL, Perry BT. (1958) Properties of the nucleic acid of the Ryan strain of filamentous influenza virus. *J Gen Virol.* 19:40-54.

25. Smirnov YA, Kuznetsova MA, Kaverin NV. (1991) The genetics aspects of influenza virus filamentous particle formation. *Arch Virol.* 118:279-284.
26. Vijayakrishnan S, Loney C, Jackson D, Suphamungmee W, Rixon FJ, Bhella D. (2013) Cryotomography of budding influenza A virus reveals filaments with diverse morphologies that mostly do not bear a genome at their distal end. *PLoS Pathog.* 9:e1003413.
27. Noda T, Sagara H, Yen A, Takada A, Kida H, Cheng RH, Kawaoka Y. (2006) Architecture of ribonucleoprotein complexes in influenza A virus particles. *Nature.* 439:490-492.
28. Murti KG, Webster RG. (1986) Distribution of hemagglutinin and neuraminidase on influenza virions as revealed by immunoelectron microscopy. *Virology.* 149:36-43.
29. Harris A, Cardone G, Winkler DC, Heymann JB, Brecher M, White JM, Steven AC. (2006) Influenza virus pleiomorphy characterized by cryoelectron tomography. *Proc Natl Acad Sci USA.* 103:19123-19127.
30. Matrosovich MN, Matrosovich TY, Gray T, Roberts NA, Klenk HD. (2004) Neuraminidase is important for the initiation of influenza virus infection in human airway epithelium. *J Virol.* 78:12665-1267.
31. Roberts PC, Compans RW. (1998) Host cell dependence of viral morphology. *Proc Natl Acad Sci USA.* 95:5746-5751.
32. Bouvier NM, Lowen AC, Palese P. (2008) Oseltamivir-resistant influenza A viruses are transmitted efficiently among guinea pigs by direct contact but not by aerosol. *J Virol.* 82:10052-10058.

33. Chou YY, Albrecht RA, Pica N, Lowen AC, Richt JA, Garcia-Sastre A, Palese P, Hai R. (2011) The M segment of the 2009 new pandemic H1N1 influenza virus is critical for its high transmission efficiency in the guinea pig model. *J Virol.* 85:11235-11241.
34. Gong LI, Suchard MA, Bloom JD. (2013) Stability-mediated epistasis constrains the evolution of an influenza protein. *Elife.* 2:e00631.

Figure Legends

Figure 1: rPR8 M1 R101G and rPR8 M1 N87S viruses elute red blood cells at a faster rate than rPR8wt virus. HA assays were set up using virus diluted to a concentration of 128 HAU. After the assays had developed, plates were transferred to 37°C to allow for red blood cell elution by the viral neuraminidase. A second set of plates remained at 4°C where no elution occurred (not shown). The results of three independent experiments are shown, with each experiment represented by a separate bar. Within each experiment, viruses were analyzed in triplicate (standard deviation for each virus = 0). “Units of elution” is defined as the reciprocal of the highest virus dilution showing elution. A) Elution of rPR8 M1 R101G virus is compared to that of rPR8wt virus. B) Elution of rPR8 M1 N87S virus is compared to that of rPR8wt virus.

Figure 2: rPR8 M1 R101G and rPR8 M1 N87S viruses have higher neuraminidase activity than rPR8wt virus. A) Neuraminidase enzyme kinetics. Virus input was standardized to 5×10^5 PFU and concentrations of MUNANA substrate ranging from

1.17 μM to 150 μM were used. Fluorescence generated at each time point (every minute over the course of 1 hour) was detected using a Biotek Synergy H1 plate reader. The resulting fluorescence curves were then fitted to the Michaelis-Menton equation. B) That equivalent amounts of each virus were used in the MUNANA assay was confirmed by RT-qPCR for the viral NP segment. The arithmetic mean ($n=3$) and standard deviation of $2^{-(C_q)}$ values were calculated and then converted back to a C_q scale by taking the \log_2 .

Figure 3: NA and M1 protein levels between rPR8wt, rPR8 M1 N87S, and rPR8 M1 R101G are similar when normalized to NP protein levels. Virus samples were concentrated via ultracentrifugation through a 30% sucrose cushion and resuspended in PBS. Samples were then deglycosylated and denatured, after which NP protein levels were standardized via Coomassie. For the Western blot, protein was detected using primary antibodies specific for NA, M1, and NP and fluorophore-conjugated secondary antibodies. All bands were quantified using Image Lab software (Bio-Rad).

Figure 4: rPR8wt, rPR8 M1 N87S, and rPR8 M1 R101G viruses have the same red blood cell binding avidity. Chicken red blood cells were treated with a series of dilutions of *C. perfringens* neuraminidase. Treated red blood cells were then added to a standardized amount of each virus (8 HAU) and allowed to develop at 4°C. The assay was run in triplicate (standard deviation for each virus = 0). The highest concentration of neuraminidase that still allowed agglutination by each virus is plotted.

Figure 5: There is no difference in plaque reduction among rPR8wt, rPR8 M1 N87S, and rPR8 M1 R101G viruses. Each virus was diluted to approximately 250 PFU. Trypsin-heat-periodate treated serum was diluted 1:80, 1:160, 1:320, and 1:640 in PBS. Virus was added to serum dilutions and incubated for 30 minutes at 37°C. Virus titer for each serum/virus sample was then quantified by plaque assay in MDCK cells. A) Titers of virus samples incubated with anti-PR8 guinea pig immune serum. B) Titers of virus incubated with naïve guinea pig serum or PBS alone, as indicated. The mean of three replicates is plotted, and error bars indicate standard deviation. * $p < 0.05$ compared to virus incubated with naïve serum. Dashed lines indicate limit of detection (5 PFU/ml).

Figure 6: No difference in virion stability at an elevated temperature was observed between rPR8wt, rPR8 M1 N87S, and rPR8 M1 R101G viruses. Each virus was diluted to 1×10^6 PFU and incubated in triplicate at 50°C for one of the following lengths of time: 0, 15, 30, 60, and 120 min. Results shown are the average of four separate assays performed in triplicate. The dotted line indicates the limit of detection.

Figure 1.

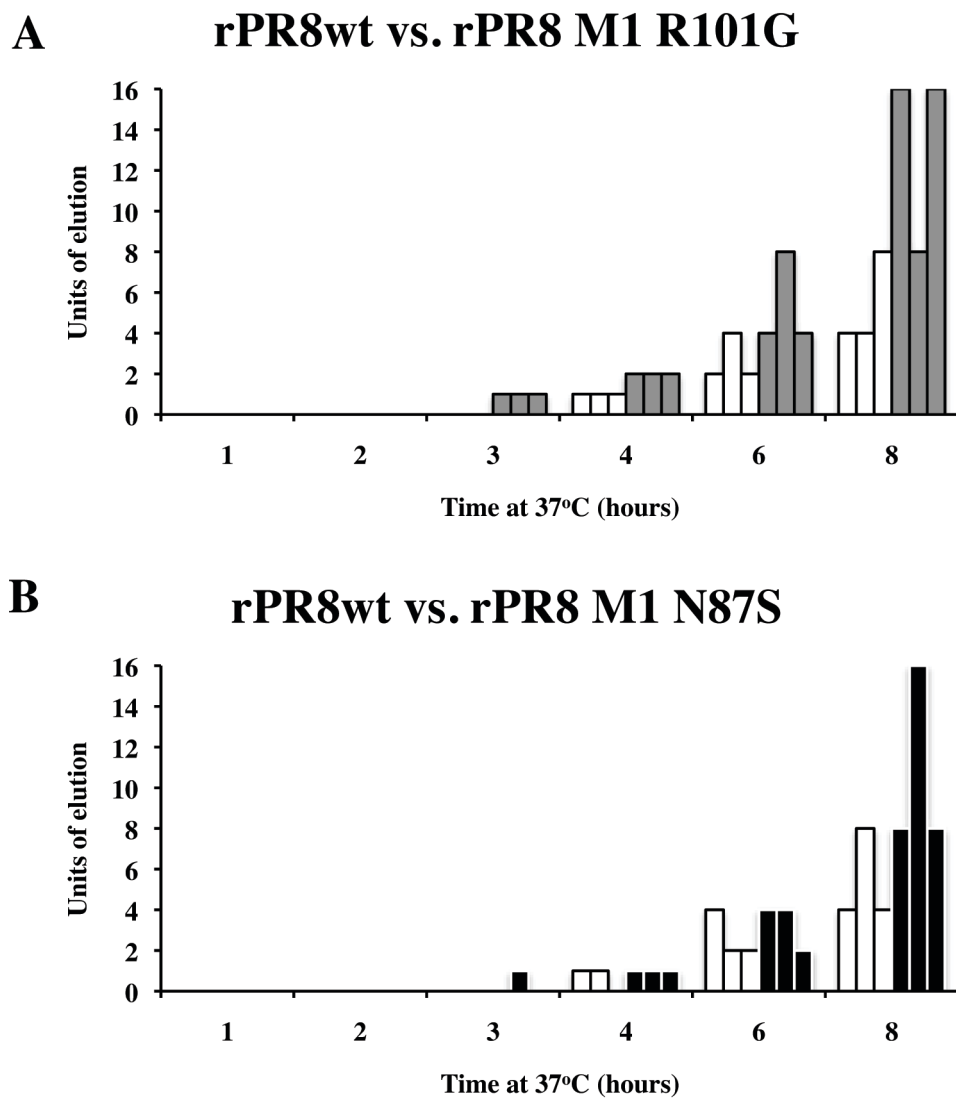


Figure 2.

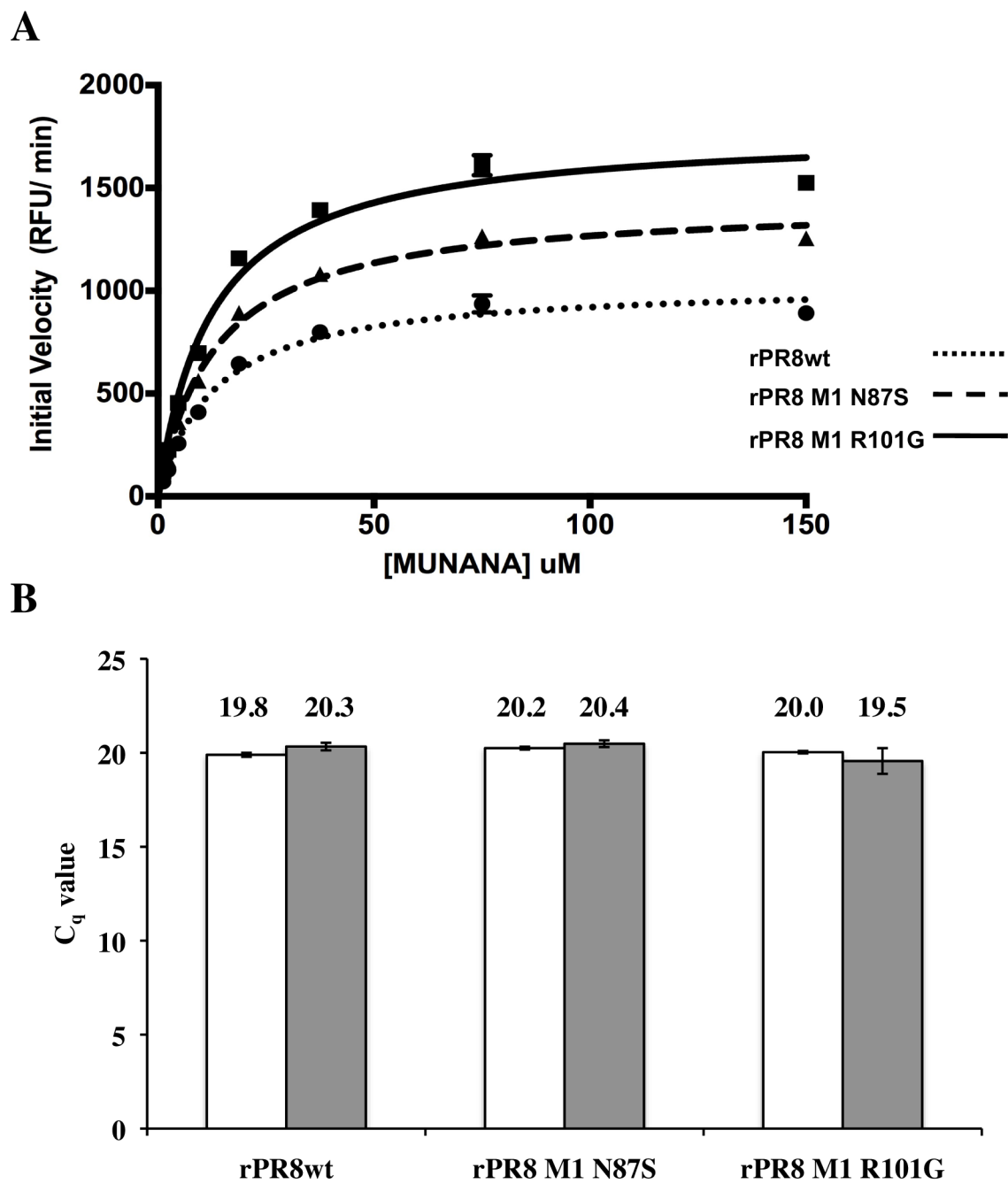


Figure 3.

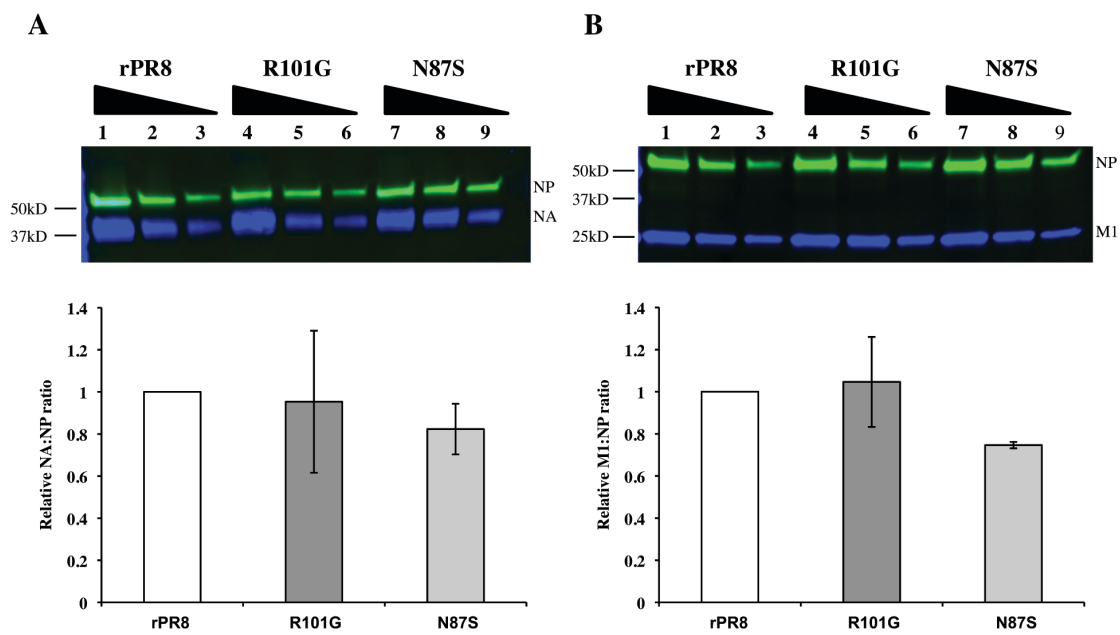


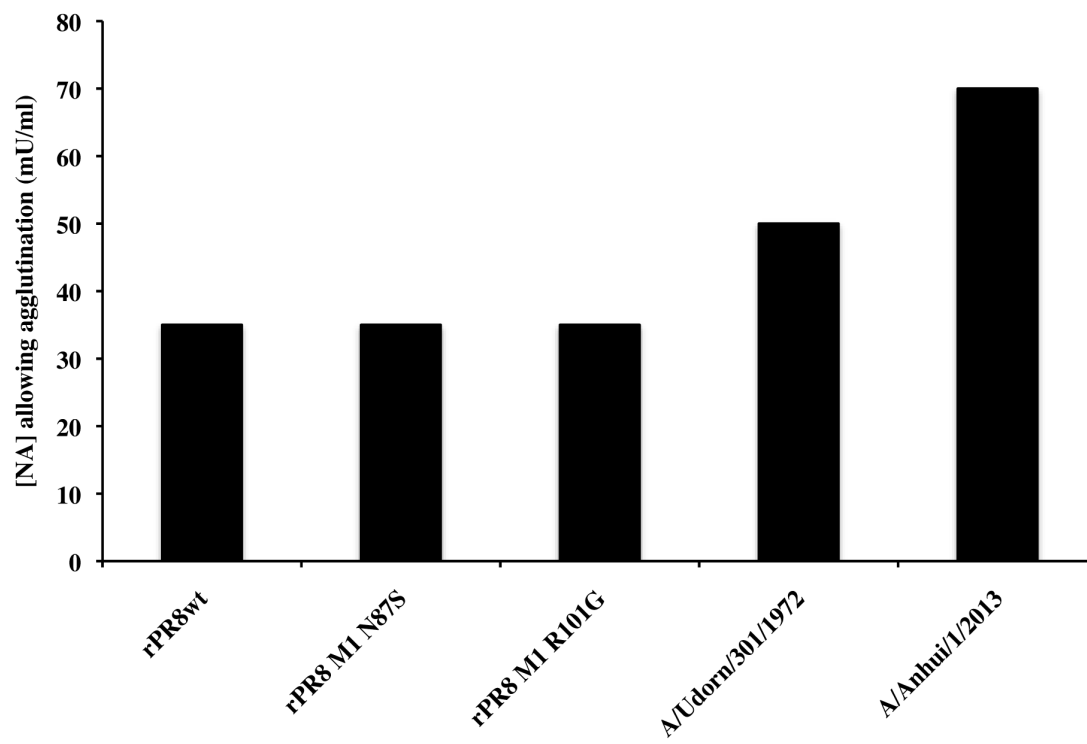
Figure 4.

Figure 5.

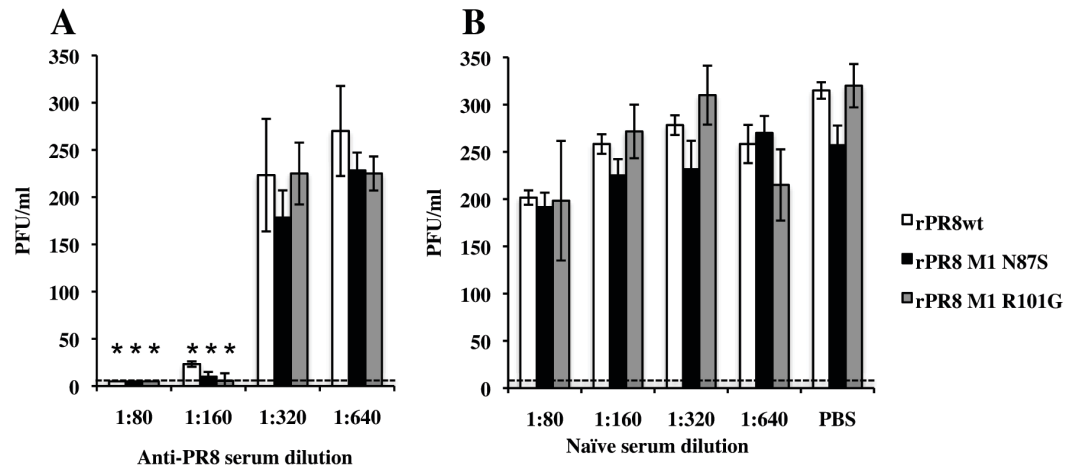
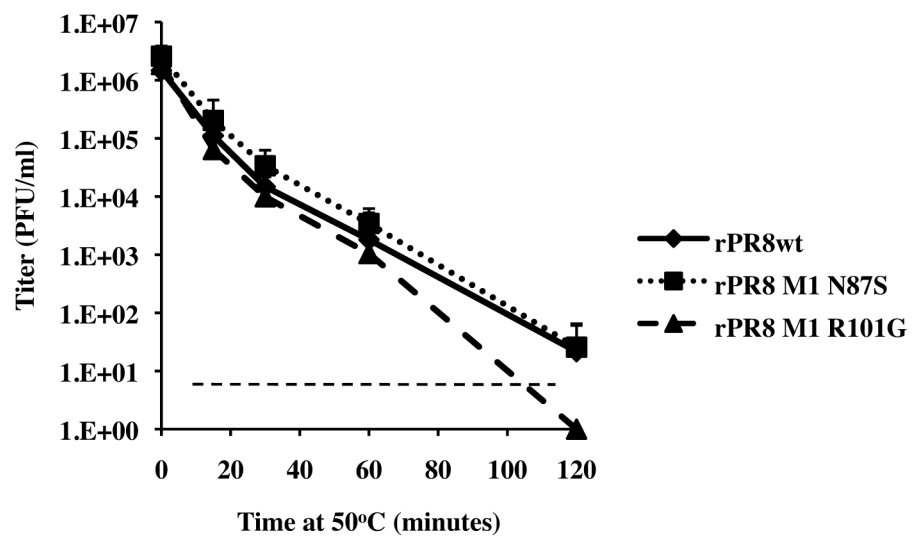


Figure 6.



Chapter 4: Supplementary Data – Paired Spherical and Filamentous Viruses

Introduction

In order to test the hypothesis that spherical viruses have a selective advantage in laboratory substrates while filament-producing strains have an advantage *in vivo*, we used reverse genetics to generate paired spherical and filamentous viruses. The mutations introduced were identified from published literature reporting molecular determinants of virion morphology (12, 20, 112). The amino acid changes employed were originally identified through alanine scanning mutagenesis or the introduction of reciprocal changes into spherical and filamentous virus backgrounds, at sites where these strains were found to differ. For our work, the M1 K102A mutation was introduced into the spherical rPR8 strain to generate a filament-producing mutant virus (rPR8fil). Three point mutations (A41V, R95K, and E204D) were introduced into the M1 protein of the filament-producing strain rNL602, producing a mutant virus that formed predominantly spherical virions. The growth of these paired spherical and filamentous viruses were then compared in eggs, MDCK cells, HTBE cells, and guinea pigs.

Materials and Methods

Viruses and cells:

The rPR8, rPR8fil, rNL602, and rNL60sph viruses were generated using reverse genetics as previously described. In brief, rNL602-based viruses were recovered by 8 (pHW) plasmid transfection of 293T cells and subsequent co-culture with MDCK cells. rPR8-

based viruses were recovered by 8 (pDZ) plasmid transfection of 293T cells and subsequent injection of transfected cells and culture medium into 9-11 day old embryonated chicken's eggs. The rPR8 and rPR8fil viruses were grown in 9-11 day old embryonated chicken eggs while the rNL602 and rNL602sph viruses were grown in MDCK cells. Embryonated chicken eggs were incubated at 37°C for 9-11 days prior to inoculation. MDCK cells were maintained in minimal essential medium (MEM) supplemented with 10% fetal bovine serum (FBS) and penicillin/streptomycin. 293T cells (used for virus rescue) were maintained in Dulbecco's minimal essential medium (DMEM) supplemented with 10% FBS. Human tracheo-bronchial (HTBE) cells obtained from Lonza were thawed and seeded into two T75 flasks containing bronchial epithelial cell growth medium (BEGM). Upon reaching 70-80% confluency, cells were trypsinized, counted, and seeded onto collagen-coated transwell filters. Gray's medium, composed of BEGM media plus Lonza Single Quots and DMEM media plus Lonza Single Quots combined in equal volumes, was added to both the top and bottom chambers. At 100% confluency, an air-liquid interface was created by removing the medium from the top chamber. Gray's medium supplemented with retinoic acid was then added to the bottom chamber to allow for differentiation. Upon differentiation cells were maintained by adding fresh Gray's medium plus retinoic acid every 2-3 days.

Virus concentration and visualization via transmission electron microscopy

Embryonated chicken eggs were infected with 250 PFU/egg for rPR8-based viruses and 2500 PFU/egg for rNL602-based viruses. Eggs were incubated at 37°C for 48 hours before being placed at 4°C to kill the embryos. Allantoic fluid was harvested the

following day. Following collection, blood cells and debris were pelleted by centrifugation of allantoic fluid in a Sorval tabletop centrifuge at 3,000 rpm for 10 minutes at 4°C. To further clarify the sample, supernatant was transferred to a centrifuge tube (Beckman Coulter) and spun in a SW32 rotor at 10,000 rpm for 30 minutes at 4°C. Supernatant was then transferred to a fresh centrifuge tube and a 5-ml 30% sucrose cushion was added to the bottom. Sample was then spun in an SW32 rotor at 25,000 rpm for 2.5 hours at 4°C. Supernatant was then carefully aspirated and 100 µl of PBS was added to the virus pellet and incubated overnight to allow gentle resuspension of the virus.

Following resuspension, samples were dialyzed in PBS for six hours using the Slide-A-Lyzer Dialysis Kit (10 MWCO membrane – Thermo Scientific). Buffer was changed once after the first hour and again after the second hour. Dialyzed samples were then taken to the Emory Robert P. Apkarian Integrated Electron Microscopy Core where they were added to grids and stained with methylamine tungstate. After sample preparation, grids were imaged at 75 kV using a Hitachi H-7500 transmission electron microscope.

Growth curves:

Growth curves in embryonated chicken eggs were performed using three eggs/virus/time point. Each egg was infected with 250 PFU of virus for rPR8-based viruses and 2500 PFU of virus for rNL602-based viruses. At each time point (12, 24, 48, and 72 hours post-infection), eggs were placed at 4°C to halt virus growth and allantoic fluid was collected from chilled eggs the following day. Growth curves in MDCK cells were performed in triplicate using an MOI of 0.001 PFU/cell. Tissue culture supernatant was

collected at the following time points: 1, 6, 12, 24, 48, and 72 hours post-infection. Growth curves in HTBE cells were performed in triplicate using an MOI of 0.05 PFU/cell for rPR8-based viruses and an MOI of 0.001 PFU/cell for rNL602-based viruses. At each time point (1, 6, 12, 24, 48, 72, and 96 hours post-infection) 200 μ l of PBS was added to the apical surface of the cells and collected after an incubation period of 30 minutes. Following growth analyses in all three substrates, virus titers were quantified by plaque assay on MDCK cells.

Growth experiments in guinea pigs:

Female Hartley strain guinea pigs were obtained from Charles River Laboratories. For each virus, four animals were infected intranasally with 1000 PFU in 300 μ l of PBS. Nasal washes were collected in 1 ml PBS at days 2, 4, 6, and 8 post-infection and virus titer was determined via plaque assay in MDCK cells.

Results

rPR8fil produces filaments but is generally attenuated in all substrates tested

Reverse genetics was used to introduce the K102A mutation into the rPR8 M1 protein. The K102A mutation was previously identified via alanine-scanning mutagenesis and was shown to confer robust filament formation (20). Visualization of purified rPR8wt and rPR8fil virions by transmission electron microscopy revealed that while rPR8wt produces predominantly spherical virions, rPR8fil produces filamentous virions of varying lengths (Figure 1). In order to investigate the idea that the filament-producing

morphology provides a selective advantage *in vivo* while a spherical morphology provides a selective advantage in laboratory substrates, we performed growth curves with rPR8 and rPR8fil in four different substrates. The first two substrates were embryonated chicken eggs, the substrates believed to select for spherical virions. The second two substrates were HTBE primary cells and the guinea pig animal model. We predicted that the filament-producing rPR8fil mutant would have an advantage in these two substrates. We found that the rPR8wt had a growth advantage over the rPR8fil mutant in embryonated chicken eggs and MDCK cells (Figure 2). Given the fact that passage in laboratory substrates had been shown to select for predominantly spherical virions, this was what we had expected. When we performed growth curves in the HTBE primary cell line and in the guinea pig, however, we found that not only was the rPR8fil mutant attenuated in the HTBE cells, but did not initiate a productive infection in guinea pigs from the 1000 PFU dose used (Figure 3). As such, we concluded that the mutation introduced (M1 K102A) to confer a filament-producing morphology to rPR8wt was generally attenuating.

rNL602sph produces predominantly spherical virions but is attenuated in all substrates tested

Reverse genetics was used to introduce three point mutations (A41V, R95K, and E204D) into the M1 protein of rNL602. A41V was identified as an antibody escape mutant of the filament-producing Udorn strain, and was found to confer a spherical morphology in that background (112). Both R95K and E204D were found to impact morphology through introducing amino acids found in the spherical WSN strain into the Udorn M1 (12).

Imaging of purified samples of rNL602wt and rNL602sph revealed fewer virions per grid than the rPR8-based viruses, due to poorer growth of the rNL602-based viruses in laboratory substrates. Nevertheless, filamentous virions were detected in the rNL602wt samples while predominantly spherical virions were observed in the rNL602sph samples (Figure 4).

Next we compared the growth of rNL602wt and rNL602sph in embryonated chicken eggs, MDCK cells, and HTBE primary cells. We found that the rNL602sph mutant grew comparably to the filament-producing rNL602wt virus in embryonated chicken eggs and was attenuated in MDCK cells (Figure 5A and 5B). Additionally, in HTBE cells, the rNL602sph mutant showed a delayed growth phenotype when compared to rNL602wt (Figure 3C). Based on the results of these experiments, the growth of the two viruses was not compared in the guinea pig model.

Conclusions

Taken together, it was concluded that the mutations introduced to generate the paired spherical and filamentous viruses could be attenuating in ways unrelated to morphology. To identify mutations that affect morphology of both rPR8 and rNL602 viruses, while minimizing the probability of those mutations interfering with viral functions, we performed serial passaging experiments aimed at the selection of morphology altering mutations (127).

Figure Legends

Figure 1: rPR8wt is predominantly spherical in morphology while rPR8fil produces filamentous virions. TEM of egg grown virus. Eggs were infected with 250 PFU/egg for each virus. Magnification = 40KX

Figure 2. rPR8fil is attenuated in laboratory substrates. A) Growth in eggs. Eggs were infected with 250 PFU of the indicated viruses. B) Growth in MDCK cells. Cells were infected at an MOI of 0.001 PFU/cell. Growth curve was performed in triplicate and viral titer was determined by plaque assay in MDCK cells. The dotted line indicates the limit of detection.

Figure 3. rPR8fil is attenuated in a primary cells and in guinea pigs. A) Growth in HTBE cells. Cells were infected at an MOI of 0.05 PFU/ml. B) Shedding from guinea pig nasal passages. Guinea pigs were infected intranasally with 1000 PFU of the indicated viruses. Nasal washes were taken at days 2, 4, 6, and 8 post-infection. Growth curve was performed in triplicate and viral titer was determined by plaque assay in MDCK cells. The dotted line indicates the limit of detection.

Figure 4: rNL602wt produces filamentous virions while the rNL602sph mutant produces spherical virions. TEM of egg grown virus. Eggs were infected with 2500 PFU/egg for each virus. Magnification = 200KX

Figure 5. rNL602sph is attenuated in all substrates. A) Growth in eggs. Eggs were infected with 2500 PFU of the indicated viruses. B) Growth in MDCK cells. Cells were infected at an MOI of 0.001 PFU/cell. C) Growth in HTBE cells. Cells were infected at an MOI of 0.001 PFU/ml. Growth curve was performed in triplicate and viral titer was determined by plaque assay in MDCK cells. The dotted line indicates the limit of detection.

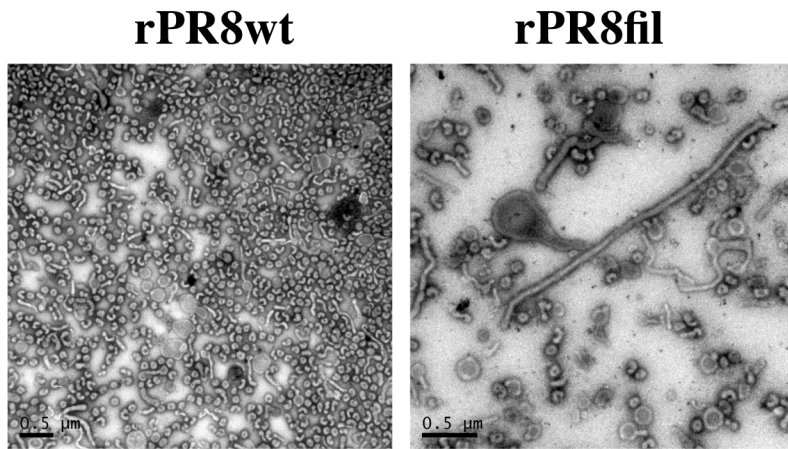
Figure 1.

Figure 2.

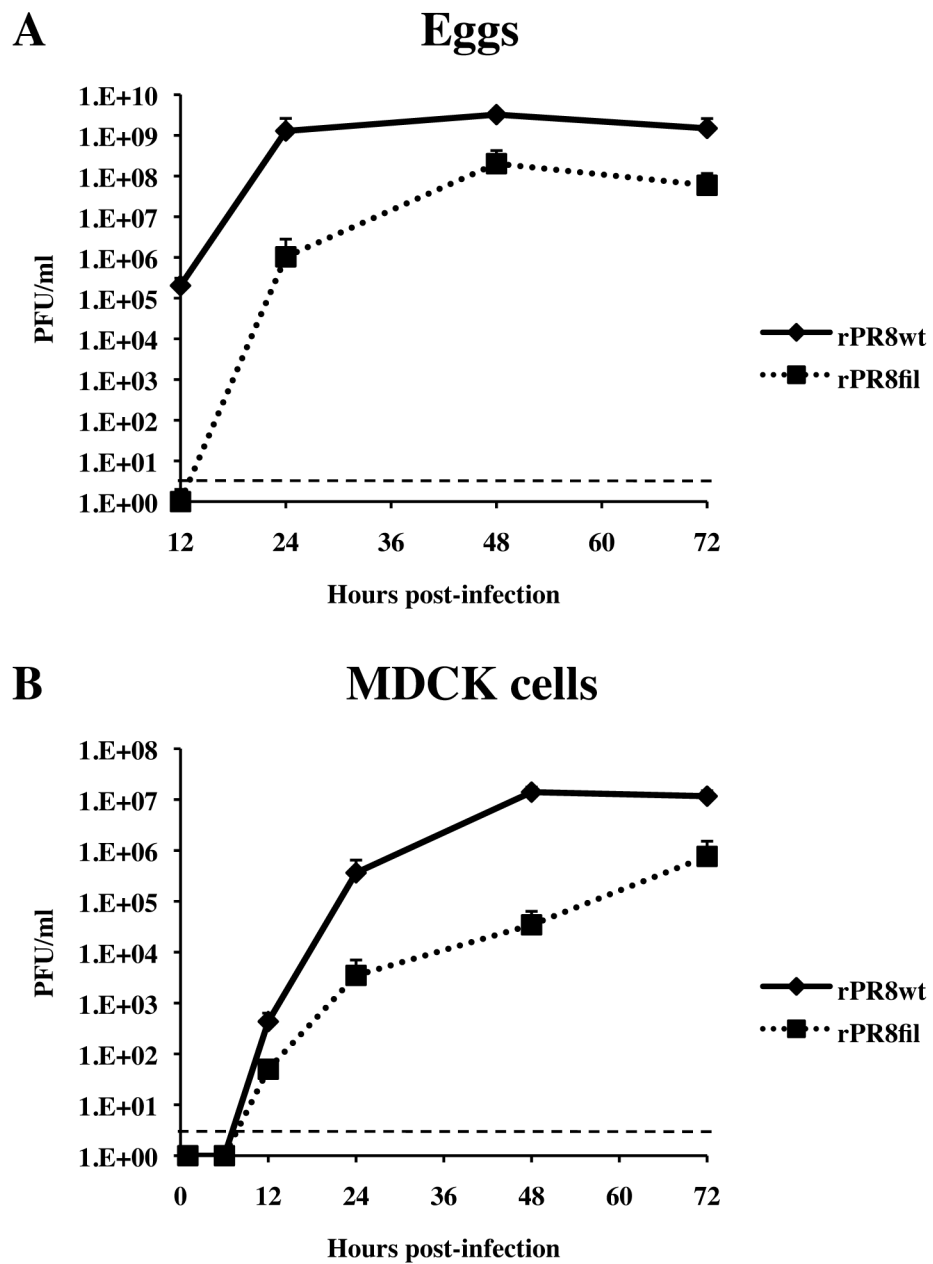


Figure 3.

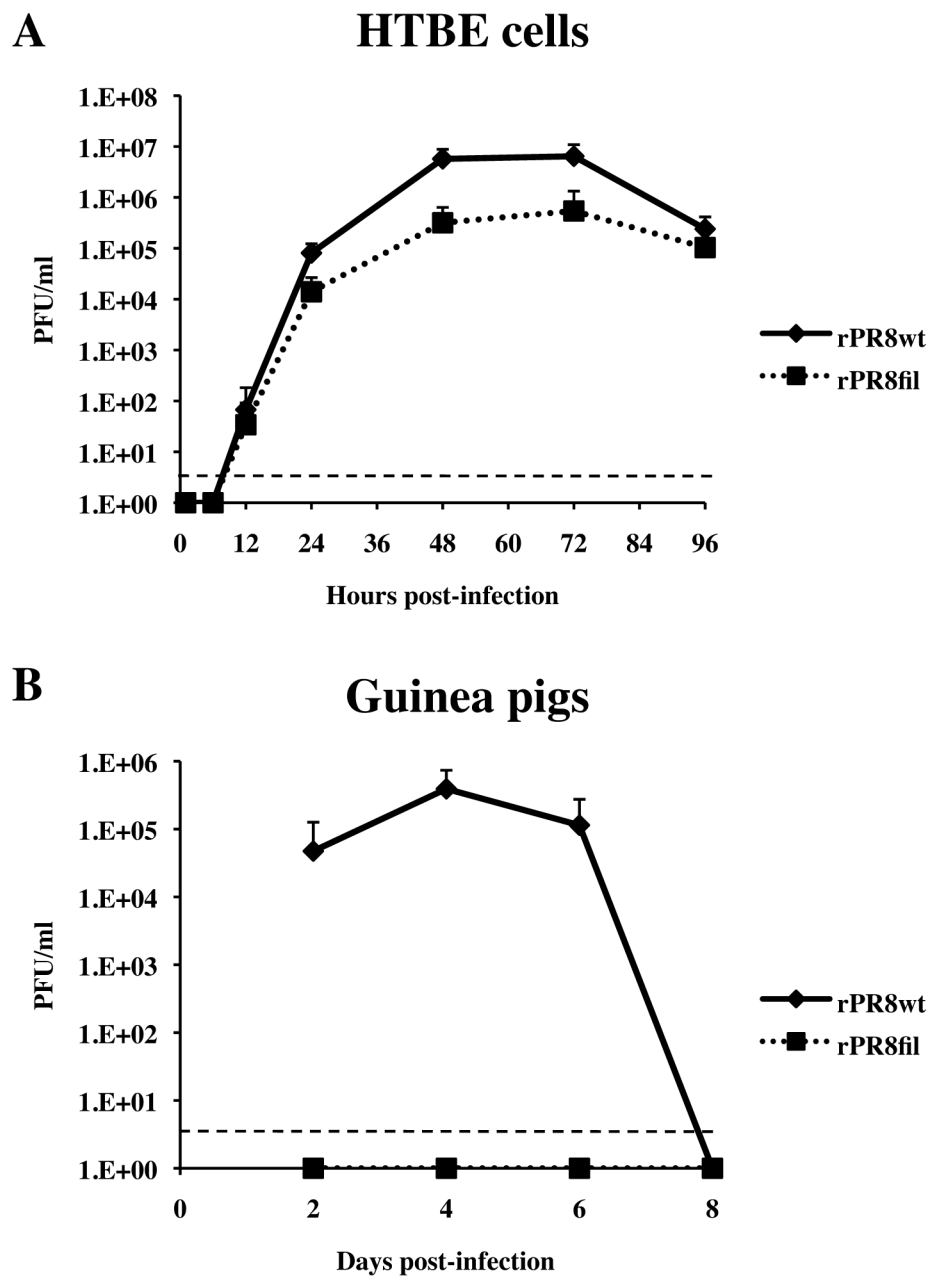


Figure 4.

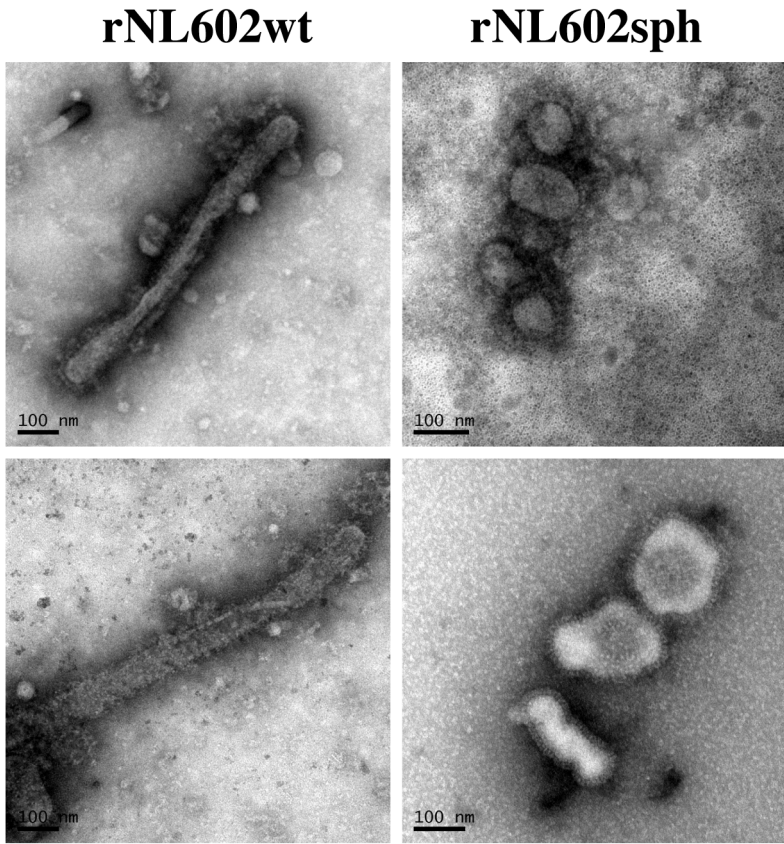
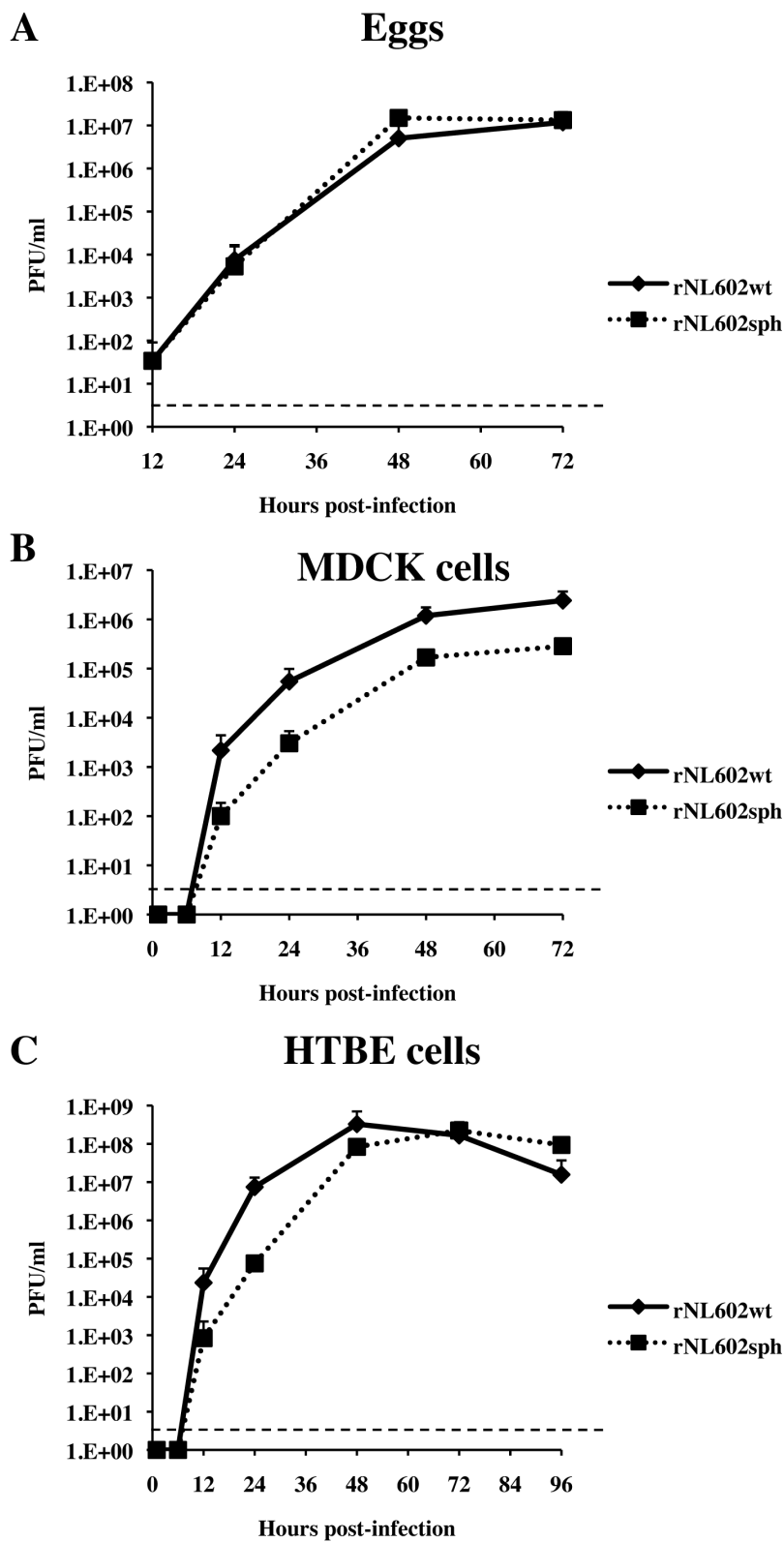


Figure 5.



Chapter 5: Discussion and Future Directions

Introduction of artificial mutations previously shown to affect viral morphology results in general attenuation

Despite early observations that IAV produces virions of both spherical and filamentous morphologies, with the filament-forming morphology lost upon passage in laboratory substrates, little progress has been made in defining the functional roles that virions of each morphology play. That filaments are maintained in nature but not in the laboratory suggested that they provide an advantage within the infected host that is not necessary for growth within laboratory substrates such as embryonated chicken eggs or cell culture. Several different groups have previously identified various amino acid residues within the M1 matrix protein to be important in determining IAV morphology. Through studying escape mutants to an anti-M2 antibody, Roberts et al. found position 41 in M1 to be important in morphology determination (112). In a later study using mutant viruses generated via reverse genetics, Bourmakina and Garcia-Sastre found positions 95 and 204 to affect morphology (12). Position 41, however, was not found to affect particle shape in this study. In a second reverse genetics study, Elleman and Barclay found position 41 to affect morphology while position 95 did not (39). Lastly, through alanine-scanning mutagenesis Burleigh et al. found mutations at position 102 to affect virion shape (20). However, we found that introducing these previously characterized mutations into our own viruses (rPR8 and rNL602) resulted in general attenuation in all substrates tested. Indeed, many of these mutations were identified through artificial means such as alanine-scanning mutagenesis or through introduction of amino acid residues found in viruses of

the opposite morphology. It should also be noted that the K102A mutation lies within the nuclear localization sequence of the M1 matrix protein. Mutation of the lysine residue at position 102 in the M1 protein was previously found to drastically affect viral growth while mutation of some of the surrounding residues (such as R101) had a lesser effect on viral fitness (77). We concluded that interpretation of our results obtained with spherical and filamentous viruses carrying these artificial mutations was complicated by the potential for these mutations to disrupt the viral life cycle in ways unrelated to morphology. We reasoned that a better method to identify naturally occurring mutations that affect IAV morphology was to undertake serial passage experiments in laboratory substrates and *in vivo*.

An exclusively spherical morphology is not necessary for growth in laboratory substrates, while filament formation is selected through passaging *in vivo*

While we observed that passaging of the clinical strain M5081 in embryonated chicken eggs led to the emergence of a significantly more spherical morphology, we found that the 2009 pandemic strain rNL602 both retained a filament-forming morphology and had a growth advantage in eggs. Taken together, it appears that conversion to a predominantly spherical morphology is not necessary for improved growth in eggs, although in some cases (i.e. M5081) changes in morphology will occur. This could be due to strain-specific requirements for morphology change. Indeed, the laboratory strains Udorn and A/Victoria/3/1975 (H3N2) [Victoria] have retained their filament-forming phenotype despite being grown extensively in laboratory substrates. Despite the maintenance of filaments by egg passaged rNL602 virus, sequencing of plaque clones

isolated from the EP10 rNL602 lines revealed two point mutations in the M1 matrix protein that confer a predominantly spherical morphology to this virus. The fact that these mutations were detected indicates that some morphology transition took place, despite limited detection of spherical virions by thin-section TEM. It should be noted that both mutations identified, M1 T169I and M1 Q198K, occur at highly conserved positions in the M1 matrix protein and have not been previously characterized as having an effect on IAV morphology. However, a GenBank search indicates the presence of T169I in a pre-2009 swine strain (A/swine/Ontario/53518/03 [H1N1]) and Q198K in two post-2009 human strains (A/Boston/685/2009 [H1N1] and A/Hawaii/07/2010 [H1N1]). Whether these mutations affect morphology in their respective strains is unknown.

Through sequencing of the guinea pig P12 virus pool, we were able to identify several point mutations in M1 that conferred robust filament formation to rPR8. As with the mutations identified through egg passaging, the mutations identified through passaging in the guinea pig occur at highly conserved residues in M1, although we did find the presence of N87S (A/swine/Iowa/46519_1/2007 [H1N1]), R101G (A/swine/Iowa/15/1930 [H1N1]), and S157C (A/swine/Iowa/H04YS2/2004 [H1N1], A/swine/Iowa/H03G1/2003 [H1N1], and A/swine/Iowa/H03LJ10/2003 [H1N1]) in several pre-2009 swine strains. Again, the morphology of the strains is unknown. The fact that a filamentous morphology was selected for through passaging of a spherical laboratory strain (rPR8) in an animal host indicates that filaments confer a selective advantage within the infected host that is not necessary for growth in laboratory substrates.

Filament-forming rPR8 M1 mutant viruses have a higher neuraminidase activity compared to rPR8wt virus

The next goal of the project was to assess the functional nature of the selective advantage conferred by filamentous virions. Due to the large surface area of filaments relative to spheres, we hypothesized that the differences between the two morphologies would lie in the activity of the viral NA or in HA binding. As such, we performed a series of functional assays aimed at assessing the NA activity, HA binding avidity, sensitivity to hemagglutination inhibition and neutralization with PR8 antiserum, and thermostability between spherical and filament-producing strains. The viruses we chose to compare were rPR8 and two filament-producing mutants, M1 N87S and M1 R101G. This is an ideal system in which to assess the functional differences between spherical and filament-producing IAV strains, as the viruses are nearly identical to each other genetically, the mutant viruses produce significantly more filaments than rPR8wt, and the mutations arose naturally through passaging. Implicit in our approach of focusing on the outer surface of the virion is an assumption that the internal components of spherical and filamentous virions are similar. The fact that both the infectious titer per HAU and RNA count per HAU is similar among the spherical wild-type and two filamentous mutants lends support to this assumption. It should also be noted that in a study comparing the filament-producing Udorn strain to spherical Udorn variants, Roberts et al made similar observations as to the infectivity of filaments versus spheres (112).

The results obtained through two separate functional assays (red blood cell elution assay and MUNANA assay) indicate that both N87S and R101G have a higher NA activity than the spherical rPR8wt virus. In contrast to our observations regarding NA activity, we

found no difference in binding avidity to red blood cells, HI titer, plaque reduction, or thermostability. Thus, our data suggest that, at least in the PR8 background, the selective advantage of filamentous virions may lie with increased NA activity as compared to spherical virions.

Possible mechanisms promoting increased neuraminidase activity observed in filament-forming strains

The most likely explanation for the higher NA activity of filament-producing viruses is that filamentous virions have increased amounts of NA adorning the surface of the virion. Certainly, the fact that the K_m of rPR8wt, N87S, and R101G was found to be consistent indicates that there is no overall change in NA enzyme activity. In order to determine the level of NA incorporation among the three viruses, we performed Western blots and standardized input to NP levels. This method of standardization operates under the assumption that each virion should contain a single copy of the viral genome and thus should have similar NP levels regardless of particle size. However, we found that when input was standardized to NP content, NA incorporation appeared to be consistent among the three viruses (Chapter 3, Figure 3). This observation could be due to several factors, the first and most simple of which could be that filaments do not in fact incorporate more NA than spheres. Indeed, cryoelectron tomography studies have indicated that NA clusters on the proximal end of the budding filament (22). Close proximity to the surface of the cell would indeed promote more efficient particle release. Thus, the increase in NA activity could be due to a cooperative effect mediated by the close clustering of the NA molecules rather than an overall increase in incorporation. Alternative explanations for

our Western blot results are also possible. Perhaps using NP incorporation as a method of standardization may not be optimal. Reports as to the nature of the organization of viral RNPs within filamentous virions have been conflicting. Early studies suggested that filamentous virions could be polyploid (containing more than one copy of the genome) or contain more RNA than their spherical counterparts (1, 135). In contrast, a recent cryotomography study has shown that many very long filaments produced by Udorn lack RNPs (150). Further, sectioning TEM and cryoelectron tomography studies have shown that, despite their length, filamentous virions contain a single copy of the viral genome located at the apical tip of the budding virion (22, 101). Going forward, perhaps standardization by HAU would be more ideal for evaluating protein incorporation, as we have shown that both infectious titer and RNA count are similar across all three viruses. Another important point to consider is that filaments always coexist with a large population of spherical virions – typically greater than 50% of the population. In addition, those particles that are classified as filaments can be of variable length – from 300 nm to 30 μ m long (94). It could be that our assay is not sensitive enough to detect differences in protein incorporation if 50% or more of the population consists of spherical virions.

As such, a method to efficiently separate spherical and filamentous virions would be advantageous in further analyzing the functional differences between the two morphologies. Initially, we attempted to achieve this through sucrose gradient centrifugation, aiming to separate the spherical and filamentous populations of rPR8wt and R101G, with the intention of analyzing each population separately in functional assays. We found that, not only was virion integrity greatly compromised through

repeated centrifugation steps, but that separation of spheres and filaments was not efficient, as large clumps of spherical virions were present in the same fractions as filamentous virions.

A more promising method was aimed at analysis of rPR8wt, R101G, and N87S in the absence of filaments and involved running virus that had been amplified in eggs through a 0.22 μm filter. Because we define filaments as any virion greater than 300 nm in length, most if not all of the filaments present in the allantoic fluid would be absent from the filtered sample. We found that, when we compared filtered and non-filtered samples of R101G to rPR8wt in the red blood cell elution assay, the filtered R101G sample eluted red blood cells at a rate identical to rPR8wt. Non-filtered R101G eluted red blood cells at a higher rate than both rPR8wt and filtered R101G. (Figure 1A) Thus, it appeared that removing filaments from the R101G mutant virus reduced the red blood cell elution rate to the levels observed with rPR8wt, implying that the enhanced elution rate observed in the case of R101G was due to the presence of significantly more filamentous virions relative to wild-type. It should be noted, however, that when filtered N87S was compared to non-filtered N87S and rPR8wt, that the filtered N87S exhibited elution activity below levels of rPR8wt (Figure 1B). Due to the semi-quantitative nature of the red blood cell elution assay, we wished to confirm the observed results using the MUNANA neuraminidase activity assay. We found that all filtered viruses (including a control filtered rPR8wt) had much lower NA activity than the non-filtered viruses (Figure 2). The results obtained from comparing the filtered and non-filtered viruses in the elution assay appeared promising, however the MUNANA assay results using the same viruses suggested that the filtration process damaged the surface glycoproteins. Indeed, perhaps

the size of the filter (0.22 μm) is too small for even spherical virions to move through undamaged. In future experiments, we will test filters with a larger pore size, such as 0.45 μm and filters made up of different material. Confirmation that filtered filament-producing viruses have NA activity similar to that of predominantly spherical viruses would lend additional weight to the hypothesis that the presence of filaments confers an advantage through increased NA activity.

Possible benefits of increased neuraminidase activity to viral fitness

An increase in NA activity could increase viral fitness through a number of different mechanisms. First, an increase in NA activity would promote a more efficient release from the infected cell. Second, the mucins of the airway contain sialic acid residues to which influenza viruses bind (130), limiting the productivity of the infection. It has been proposed that an increase in NA activity would enable the virus to move more efficiently through this mucus in order to infect new cells (112).

The hypothesis that increased NA activity reduces sensitivity to inhibition by mucus could be tested using a method similar to a neutralization assay (Figure 3). Once fully differentiated, human tracheo-bronchial epithelial (HTBE) cells produce large amounts of mucus. This mucus would be collected and serially diluted in PBS, after which virus would be added. Following incubation with virus, MDCK cells would be infected and samples taken at 24, 48, and 72 hours post-infection. If increased NA activity prevents mucus inhibition, then viruses with a higher NA activity (such as N87S and R101G) would grow in the presence of more concentrated mucus, compared to viruses with lower NA activity.

A third means by which NA activity could increase viral fitness is through improved transmission. This mechanism may be related to one or both of the possible mechanisms described above. Higher NA activity has been associated with improved transmission in the guinea pig and ferret models (38, 63, 72). Viruses carrying NA inhibitor resistance mutations, which lower NA activity, were found to transmit more poorly than viruses lacking resistance.

Studies using the 2009 IAV pandemic strains have indicated that the M segment plays a role in improved transmission (23, 24, 30). Whether this effect on transmission is directly related to the viral morphology has not yet been firmly established. We have shown that our spherical rNL602 mutants show delayed transmission in the guinea pig model, indicating that a filamentous morphology is not absolutely necessary for transmission. Similarly, the filamentous N87S mutant virus is not transmissible by contact in the guinea pig model. Therefore, filament formation alone is not sufficient for transmission to occur. Our data do not suggest a role for virion morphology in determining transmission phenotype. However, the data do not exclude this possibility either. The rNL602wt virus is highly transmissible in the guinea pig model while rPR8wt is completely non-transmissible. Taken together, while changes in morphology were not sufficient to alter transmission phenotypes, morphology may contribute to transmission in the appropriate context.

The fact that the rPR8 guinea pig P12 virus transmitted to 2 of 4 exposed animals, while the N87S mutant did not transmit, indicates that additional permissive mutations on the M segment and/or the other genome segments are required to promote transmission. As such, we are interested in assessing within what genetic context filamentous mutations

arise *in vivo* and whether or not they contribute to a transmissible phenotype. In order to do this, we plan to sequence the full genomes of clonal virus isolates derived from the guinea pig P12 virus stock. Specifically, we will pick plaques from MDCK cells infected with the rPR8 guinea pig P12 virus and extract the viral RNA. Following generation of cDNA, high-resolution melt (HRM) analysis will be performed using primers designed to allow detection of the N87S mutation (Figure 4). HRM analysis hinges on the fact that sequence differences between two double-stranded DNA molecules will confer differences in melting properties. Thus, double-stranded DNA is labeled with a fluorescent dye that will cease fluorescing when the DNA melts into a single-stranded state. Therefore, we will be able to use this method to identify samples containing the N87S mutation. N87S was chosen because the rPR8 M1 mutant virus carrying this mutation was the most fit of the single mutants characterized. When a sample is identified as positive for N87S, we will sequence the entire viral genome to identify additional mutations. These mutations will then be introduced into both the rPR8wt and rPR8 M1 N87S backgrounds and contact transmission assessed in the guinea pig model. We believe these experiments will reveal the context in which the N87S filament-forming mutations arose and allow testing of whether this morphology altering mutation improves transmission when introduced in that context.

Overall summary and conclusions

In summary, we have shown that filament formation is selected for through passaging within an animal host, indicating that the filamentous morphology provides a fitness advantage within the host. Through the use of a panel of functional assays, we have

observed that filamentous M1 point mutants of rPR8 have a higher neuraminidase activity than the wild-type virus. Additionally, properties such as HA binding avidity, sensitivity to serum, and thermostability were not affected by changes in virion morphology. These observations strengthen the hypothesis that the selective advantage conferred by filamentous virions is due to their increased NA activity over spherical virions.

Figure Legends

Figure 1: Filtered rPR8 M1 N87S and rPR8 M1 R101G mutant viruses elute red blood cells at a similar or lower rate compared to rPR8wt. rPR8 M1 N87S and rPR8 M1 R101G were grown up in embryonated chicken eggs. After harvesting, the allantoic fluid was run through a 0.22 μm filter. Elution assays were then set up as described in Chapter 3. Within each experiment, viruses were analyzed in triplicate (standard deviation for each virus = 0). “HA units of elution” is defined as the HAU eluted at each time point. A) Elution of rPR8 M1 R101G filtered virus is compared to that of rPR8wt and rPR8 M1 R101G non-filtered virus. B) Elution of rPR8 M1 N87S filtered virus is compared to that of rPR8wt virus and rPR8 M1 N87S non-filtered virus.

Figure 2: Filtered rPR8wt, rPR8 M1 N87S, and rPR8 M1 R101G have negligible neuraminidase activity when compared to non-filtered viruses in the MUNANA assay. Neuraminidase enzyme kinetics. MUNANA assay was performed as described in Chapter 3.

Figure 3: Mucus-based neutralization assay. A) Mucus will be collected from fully differentiated human tracheo-bronchial epithelial (HTBE) cells. B) Once collected, 1:2 serial dilutions of mucus will be made in PBS. C) Spherical wild-type (rPR8) and filament-forming mutant viruses (N87S and R101G) will be incubated with the mucus dilutions. D) Following incubation with mucus, samples will be used to infect MDCK cells. Tissue culture supernatant will be collected 24, 48, and 72 hours post-infection and neutralization titer will be determined via HA assay. Neutralization titer is reported as the reciprocal of the highest mucus dilution that allows viral growth.

Figure 4: Identification of additional mutations in N87S-containing clones using HRM analysis. MDCK cells will be infected with rPR8 guinea pig P12 virus. The resulting plaques will be picked and resuspended in PBS. Viral RNA will be extracted from plaque plugs and cDNA will be generated. High-resolution melt analysis will be performed on all samples utilizing primers designed to detect the N87S mutation. Samples containing N87S will have different melting properties from samples in which N87S is absent. This difference will be reflected by the resulting melt curves. Samples positive for N87S will be sequenced in full and any additional mutations identified will be introduced into both the rPR8wt and rPR8 M1 N87S viruses using reverse genetics. Following virus rescue and sequence verification, transmission will be assessed in the guinea pig contact transmission model.

Figure 1.

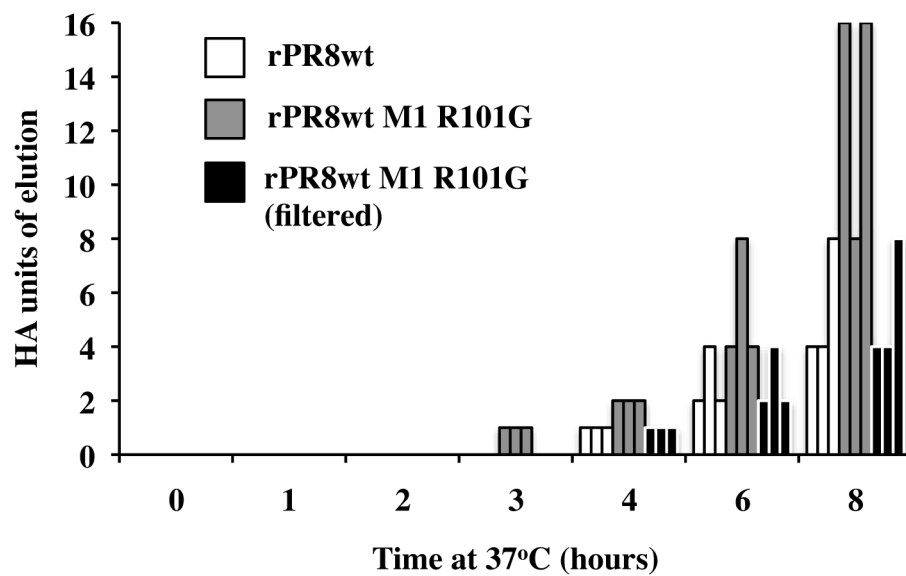
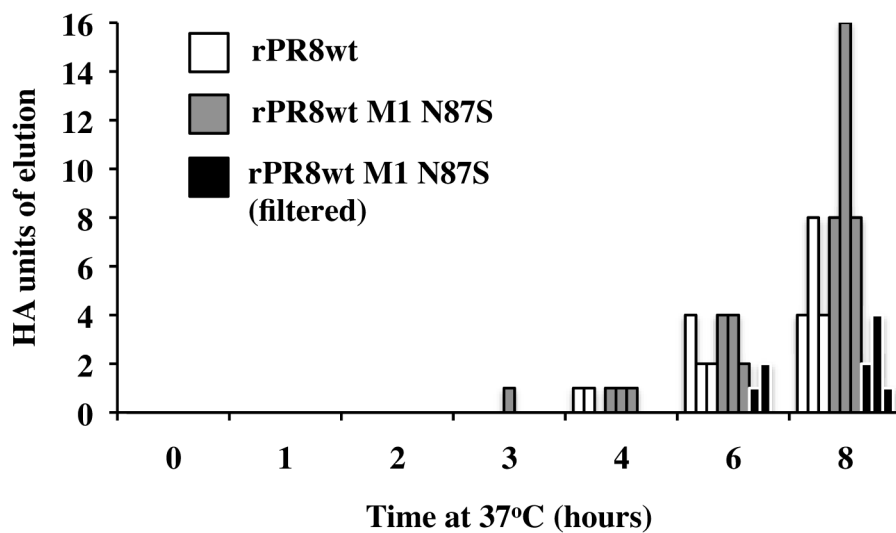
A**B**

Figure 2.

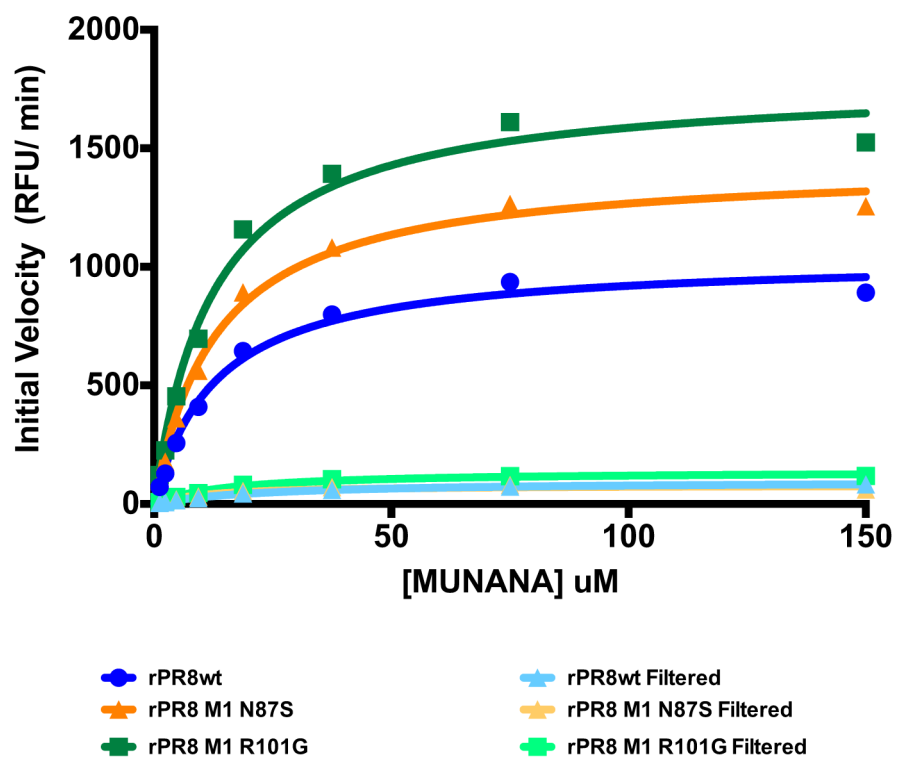


Figure 3.

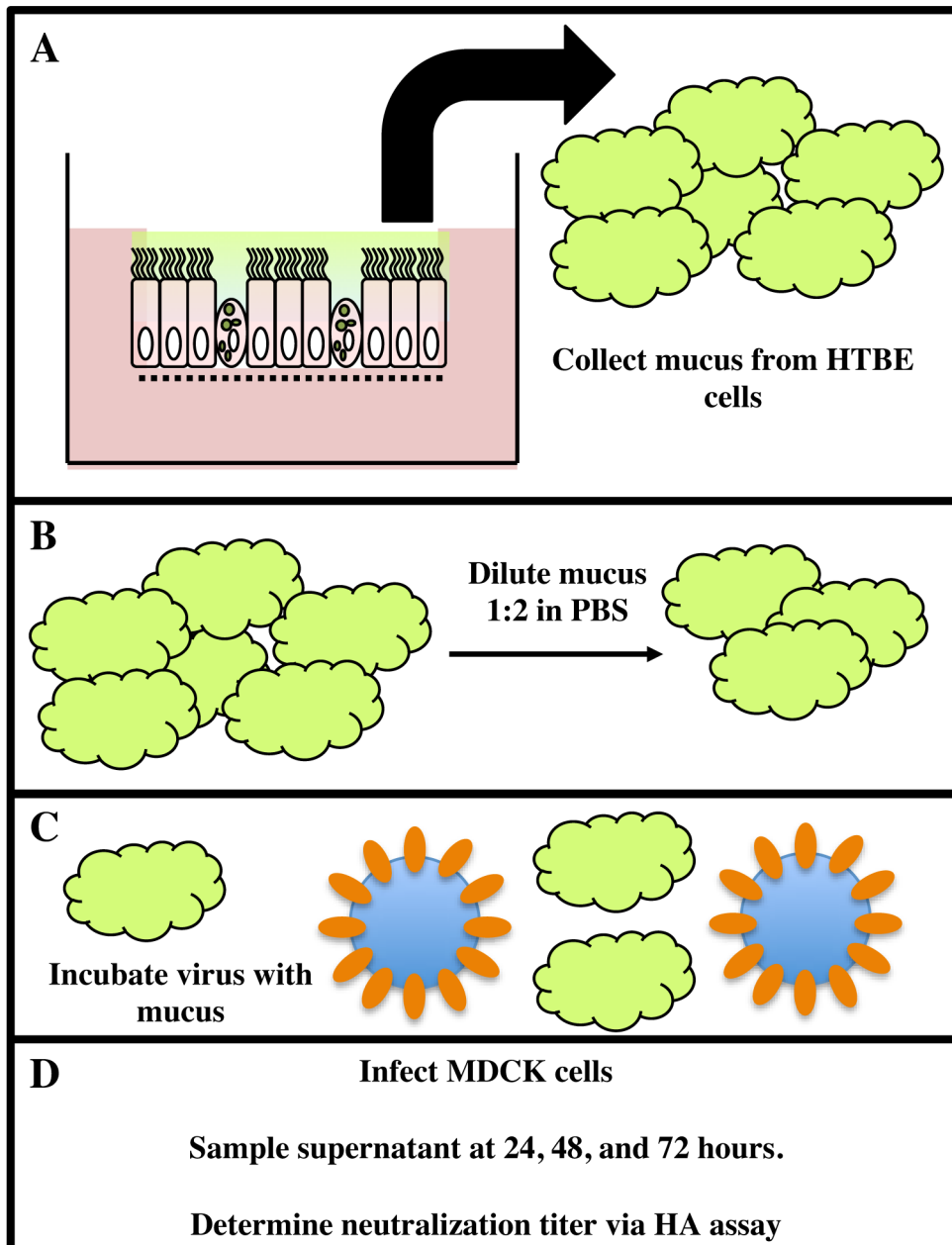
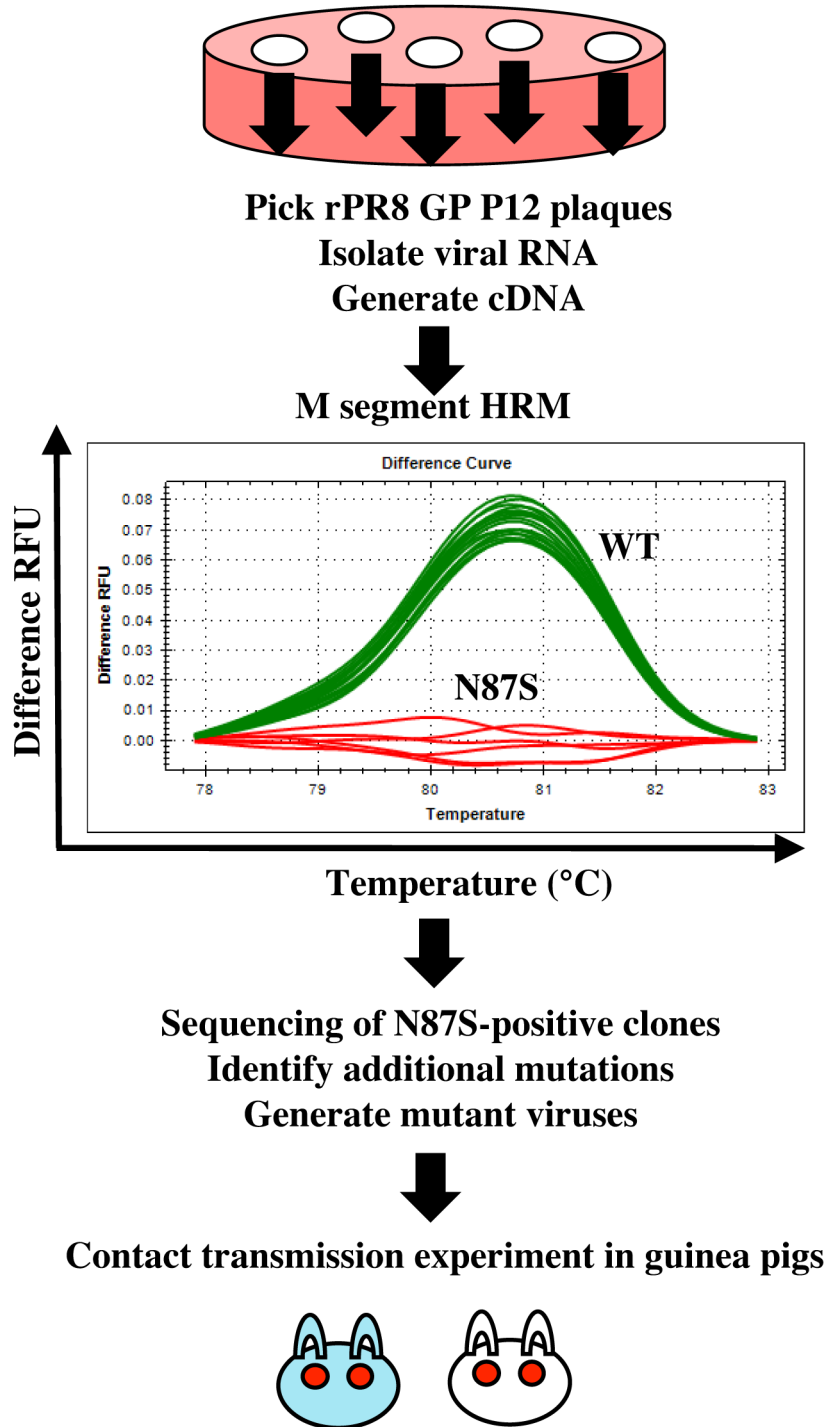


Figure 4.



References

1. **Ada GL and Perry BT.** 1958. Properties of the nucleic acid of the Ryan strain of filamentous influenza virus. *J Gen Virol* **19**: 40-54.
2. **Akarsu H, Burmeister WP, Petosa C, Petit I, Muller CW, Ruigrok RW, and Baudin F.** 2003. Crystal structure of the M1 protein-binding domain of the influenza A virus nuclear export protein (NEP/NS2). *EMBO J* **22**: 4646-4655.
3. **Ali A, Avalos RT, Ponimaskin E, and Nayak DP.** 2000. Influenza virus assembly: effect of influenza virus glycoproteins on the membrane association of M1 protein. *J Virol* **74**: 8709-8719.
4. **Amorim MJ, Bruce EA, Read EK, Foeglein A, Mahen R, Stuart AD, and Digard P.** 2011. A Rab11- and microtubule-dependent mechanism for cytoplasmic transport of influenza A virus viral RNA. *J Virol* **85**: 4143-4156.
5. **Arzt S, Baudin F, Barge A, Timmins P, Burmeister WP, and Ruigrok RW.** 2001. Combined results from solution studies on intact influenza virus M1 protein and from a new crystal form of its N-terminal domain show that M1 is an elongated monomer. *Virology* **279**: 439-446.
6. **Avilov SV, Moisy D, Naffakh N, and Cusack S.** 2012. Influenza A virus progeny vRNP trafficking in live infected cells studied with the virus-encoded fluorescently tagged PB2 protein. *Vaccine* **30**: 7411-7417.
7. **Azoulay-Dupuis E, Lambre CR, Soler P, Moreau J, and Thibon M.** 1984. Lung alterations in guinea-pigs infected with influenza virus. *J Comp Pathol* **94**: 273-283.

8. **Baskin CR, Bielefeldt-Ohmann H, Tumpey TM, Sabourin PJ, Long JP, Garcia-Sastre A, Tolnay AE, Albrecht R, Pyles JA, Olson PH, Aicher LD, Rosenzweig ER, Murali-Krishna K, Clark EA, Kotur MS, Fornek JL, Proll S, Palermo RE, Sabourin CL, and Katze MG.** 2009. Early and sustained innate immune response defines pathology and death in nonhuman primates infected by highly pathogenic influenza virus. *Proc Natl Acad Sci USA* **106**: 3455-3460.
9. **Bateman AC, Busch MG, Karasin AI, Bovin N, and Olsen CW.** 2008. Amino acid 226 in the hemagglutinin of H4N6 influenza virus determines binding affinity for alpha2,6-linked sialic acid and infectivity levels in primary swine and human respiratory epithelial cells. *J Virol* **82**: 8204-8209.
10. **Baudin F, Petit I, Weissenhorn W, and Ruigrok RW.** 2001. In vitro dissection of the membrane and RNP binding activities of influenza virus M1 protein. *Virology* **281**: 102-108.
11. **Bialas KM, Bussey KA, Stone RL, and Takimoto T.** 2014. Specific nucleoprotein residues affect influenza virus morphology. *J Virol* **88**: 2227-2234.
12. **Bourmakina SV and Garcia-Sastre A.** 2003. Reverse genetics studies on the filamentous morphology of influenza A virus. *J Gen Virol* **84**: 517-527.
13. **Bouvier NM, Lowen AC, and Palese P.** 2008. Oseltamivir-resistant influenza A viruses are transmitted efficiently among guinea pigs by direct contact but not by aerosol. *J Virol* **82**: 10052-10058.
14. **Bridges CB, Kuehnert MJ, and Hall CB.** 2003. Transmission of influenza: implications for control in health care settings. *Clin Infect Dis* **37**: 1094-1101.

15. **Brown IH, Harris PA, McCauley JW, and Alexander DJ.** 1998. Multiple genetic reassortment of avian and human influenza A viruses in European pigs, resulting in the emergence of an H1N2 virus of novel genotype. *J Gen Virol* **79**: 2947-2955.
16. **Bruce EA, Digard P, and Stuart AD.** 2010. The Rab11 pathway is required for influenza A virus budding and filament formation. *J Virol* **84**: 5848-5859.
17. **Brundage JF and Shanks GD.** 2008. Deaths from bacterial pneumonia during 1918-1919 influenza pandemic. *Emerg Infect Dis* **14**: 1193-1199.
18. **Bui M, Wills EG, Helenius A, and Whittaker GR.** 2000. Role of the influenza virus M1 protein in nuclear export of viral ribonucleoproteins. *J Virol* **74**: 1781-1786.
19. **Bui M, Whittaker G, and Helenius A.** 1996. Effect of M1 protein and low pH on nuclear transport of influenza virus ribonucleoproteins. *J Virol* **70**: 8391-8401.
20. **Burleigh LM, Calder LJ, Skehel JJ, and Steinhauer DA.** 2005. Influenza A viruses with mutations in the M1 helix six domain display a wide variety of morphological phenotypes. *J Virol* **79**: 1262-1270.
21. **Bussey KA, Bousse TL, Desmet EA, Kim B, and Takimoto T.** 2010. PB2 residue 271 plays a key role in enhanced polymerase activity of influenza A viruses in mammalian host cells. *J Virol* **84**: 4395-4406.
22. **Calder LJ, Wasilewski S, Berriman JA, and Rosenthal PB.** 2010. Structural organization of a filamentous influenza A virus. *Proc Natl Acad Sci USA* **107**: 10685-10690.

23. **Campbell PJ, Danzy S, Kyriakis CS, Deymier MJ, Lowen AC, and Steel J.** 2014. The M segment of the 2009 pandemic influenza virus confers increased NA activity, filamentous morphology, and efficient contact transmissibility to A/Puerto Rico/8/1934-based reassortant viruses. *Journal of Virol* **88**: 3802-3814.
24. **Campbell PJ, Kyriakis CS, Marshall N, Suppiah S, Seladi-Schulman J, Danzy S, Lowen AC, and Steel J.** 2014. Residue 41 of the Eurasian avian-like swine influenza A virus matrix protein modulates virion filament length and efficiency of contact transmission. *J Virol* **88**: 7569-7577.
25. **Chen BJ, Leser GP, Jackson D, and Lamb RA.** 2008. The influenza virus M2 protein cytoplasmic tail interacts with the M1 protein and influences virus assembly at the site of virus budding. *J Virol* **82**: 10059-10070.
26. **Chen BJ, Leser GP, Morita E, and Lamb RA.** 2007. Influenza virus hemagglutinin and neuraminidase, but not the matrix protein, are required for assembly and budding of plasmid-derived virus-like particles. *J Virol* **81**: 7111-7123.
27. **Chen R and Holmes EC.** 2006. Avian influenza virus exhibits rapid evolutionary dynamics. *Mol Biol Evol* **23**: 2336-2341.
28. **Choppin PW, Murphy JS, and Stoeckenius W.** 1961. The surface structure of influenza virus filaments. *Virology* **13**: 548-550.
29. **Choppin PW, Murphy JS, and Tamm I.** 1960. Studies of two kinds of virus particles which comprise influenza A2 virus strains. III. Morphological characteristics: independence to morphological and functional traits. *J Exp Med* **112**: 945-952.

30. **Chou YY, Albrecht RA, Pica N, Lowen AC, Richt JA, Garcia-Sastre A, Palese P, and Hai R.** 2011. The M segment of the 2009 new pandemic H1N1 influenza virus is critical for its high transmission efficiency in the guinea pig model. *J Virol* **85**: 11235-11241.
31. **Chu CM, Dawson IM, and Elford WJ.** 1949. Filamentous forms associated with newly isolated influenza virus. *Lancet* **1**: 602.
32. **Chutinimitkul S, Herfst S, Steel J, Lowen AC, Ye J, van Riel D, Schrauwen EJ, Bestebroer TM, Koel B, Burke DF, Sutherland-Cash KH, Whittleston CS, Russell CA, Wales DJ, Smoth DJ, Jonges M, Meijer A, Koopmans M, Rimmelzwaan GF, Kuiken T, Osterhaus AD, Garcia-Sastre A, Perez DR, and Fouchier RA.** 2010. Virulence-associated substitution D222G in the hemagglutinin of 2009 pandemic influenza A(H1N1) virus affects receptor binding. *J Virol* **84**: 11802-11813.
33. **Connor RJ, Kawaoka Y, Webster RG, and Paulson JC.** 1994. Receptor specificity in human, avian, and equine H2 and H3 virus isolates. *Virology* **205**: 17-23.
34. **Cros JF, Garcia-Sastre A, and Palese P.** 2005. An unconventional NLS is critical for the nuclear import of the influenza A virus nucleoprotein and ribonucleoprotein. *Virology* **6**: 205-213.
35. **de Vries E, Tscherne DM, Wienholts MJ, Cobos-Jimenez V, Scholte F, Garcia-Sastre A, Rottier PJ, and de Haan CA.** 2011. Dissection of the influenza A virus endocytic routes reveals macropinocytosis as an alternative entry pathway. *PLoS Pathog* **7**: e1001329.

36. **Dias A, Bouvier D, Crepin T, McCarthy AA, Hart DJ, Baudin F, Cusack S, and Ruigrok RW.** 2009. The cap-snatching endonuclease of influenza virus polymerase resides in the PA subunit. *Nature* **458**: 914-918.
37. **Dourmashkin RR and Tyrrell DA.** 1974. Electron microscopic observations on the entry of influenza virus into susceptible cells. *J Gen Virol* **24**: 129-141.
38. **Duan S, Boltz DA, Seiler P, Li J, Bragstad K, Nielsen LP, Webby RJ, Webster RG, and Govorkova EA.** 2010. Oseltamivir-resistant pandemic H1N1/2009 influenza virus possesses lower transmissibility and fitness in ferrets. *PLoS Pathog* **6**: e1001022.
39. **Elleman CJ and Barclay WS.** 2004. The M1 matrix protein controls the filamentous phenotype of influenza A virus. *Virology* **321**: 144-153.
40. **Enami M and Enami K.** 1996. Influenza virus hemagglutinin and neuraminidase glycoproteins stimulate the membrane association of the matrix protein. *J Virol* **70**: 6653-6657.
41. **Gabriel G, Dauber B, Wolff T, Planz O, Klenk HD, and Stech J.** 2005. The viral polymerase mediates adaptation of an avian influenza virus to a mammalian host. *Proc Natl Acad Sci USA* **102**: 18590-18595.
42. **Gao Y, Zhang Y, Shinya K, Deng G, Jiang Y, Li Z, Guan Y, Tian G, Li Y, Shi J, Liu L, Zeng X, Bu Z, Xia X, Kawaoka Y, and Chen H.** 2009. Identification of amino acids in HA and PB2 critical for the transmission of H5N1 avian influenza viruses in a mammalian host. *PLoS Pathog* **5**: e1000709.

43. **Garcia-Sastre A and Palese P.** 1995. The cytoplasmic tail of the neuraminidase protein of influenza A virus does not play an important role in the packaging of this protein into viral envelopes. *Virus Res* **37**: 37-47.
44. **Garten RJ, Davis CT, Russell CA, Shu B, Lindstrom S, Balish A, Sessions WM, Xu X, Skepner E, Deyde V, Okomo-Adhiambo M, Gubareva L, Barnes J, Smith CB, Emery SL, Hillman MJ, Rivaller P, Smagala J, de Graaf M, Burke DF, Fouchier RA, Pappas C, Alpuche-Aranda CM, Lopez-Gatell H, Olivera H, Lopez I, Myers CA, Faix D, Blair PJ, Yu C, Keene KM, Dotson PD Jr, Boxrud D, Sambol AR, Abid SH, St George K, Bannerman T, Moore AL, Stringer DJ, Blevins P, Demmler-Harrison GJ, Ginsberg M, Kriner P, Waterman S, Smole S, Guevara HF, Belongia EA, Clark PA, Beatrice ST, Donis R, Katz J, Finelli L, Bridges CB, Shaw M, Jernigan DB, Uyeki TM, Smith DJ, Klimov AI, and Cox NJ.** 2009. Antigenic and genetic characteristics of swine-origin 2009 A(H1N1) influenza viruses circulating in human. *Science* **325**: 197-201.
45. **Glaser L, Stevens J, Zamarin D, Wilson IA, Garcia-Sastre A, Tumpey TM, Basler CF, Taubenberger JK, and Palese P.** 2005. A single amino acid substitution in 1918 influenza virus hemagglutinin changes receptor binding specificity. *J Virol* **79**: 11533-11536.
46. **Goldsmith CS, Metcalfe MG, Rollin DC, Shieh WJ, Paddock CD, Xu X, and Zaki SR.** 2011. Ultrastructural characterization of pandemic (H1N1) 2009 virus. *Emerg Infect Dis* **17**: 2056-2059.

47. **Gomez-Puertas P, Albo C, Perez-Pastrana E, Vivo A, and Portela A.** 2000. Influenza virus matrix protein is the major driving force in virus budding. *J Virol* **74**: 11538-11547.
48. **Gregoriades A and Frangione B.** 1981. Insertion of influenza M protein into the viral lipid bilayer and localization of site of insertion. *J Virol* **40**: 323-328.
49. **Guilligay D, Tarendeau F, Resa-Infante P, Coloma R, Crepin T, Sehr P, Lewis J, Ruigrok RW, Ortin J, Hart DJ, and Cusack S.** 2008. The structural basis for cap binding by influenza virus polymerase subunit PB2. *Nat Struct Mol Biol* **15**: 500-506.
50. **Hamilton BS, Whittaker GR, and Daniel S.** 2012. Influenza virus-mediated membrane fusion: determinants of hemagglutinin fusogenic activity and experimental approaches for assessing virus fusion. *Viruses* **4**: 1144-1168.
51. **Harris A, Forouhar F, Qiu S, Sha B, and Luo M.** 2001. The crystal structure of the influenza virus matrix protein M1 at neutral pH: M1-M1 protein interfaces can rotate in the oligomeric structures of M1. *Virology* **289**: 34-44.
52. **Hause BM, Collin EA, Liu R, Huang B, Sheng Z, Lu W, Wang D, Nelson EA, and Li F.** 2014. Characterization of a novel influenza virus in cattle and Swine: proposal for a new genus in the Orthomyxoviridae family. *MBio* **5**: e00031-14.
53. **Herfst S, Schrauwen EJ, Linster M, Chutinimitkul S, de Wit E, Munster VJ, Sorrell EM, Bestebroer TM, Burke DF, Smith DJ, Rimmelzwaan GF, Osterhaus AD, and Fouchier RA.** 2012. Airborne transmission of influenza A/H5N1 virus between ferrets. *Science* **336**: 1534-1541.

54. **Herz C, Stavnezer E, Krug R, and Gurney T Jr.** 1981. Influenza virus, an RNA virus, synthesizes its messenger RNA in the nucleus of infected cells. *Cell* **26**: 391-400.
55. **Imai M, Watanabe T, Masato H, Das SC, Ozawa M, Shinya K, Zhong G, Hanson A, Katsura H, Watanabe S, Li C, Kawakami E, Yamada S, Kiso M, Suzuki Y, Maher EA, Neumann G, and Kawaoka Y.** 2012. Experimental adaptation of an influenza H5 HA confers respiratory droplet transmission to a reassortant H5 HA / H1N1 virus in ferrets. *Nature* **486**: 420-428.
56. **Itoh Y Shinya K, Kiso M, Watanabe T, Sakoda Y, Hatta M, Muramoto Y, Tamura D, Sakai-Tagawa Y, Noda T, Sakabe S, Imai M, Hatta Y, Watanabe S, Li C, Yamada S, Fujii K, Murakami S, Imai H, Kakugawa S, Ito M, Takano R, Iwatsuki-Horimoto K, Shimojima M, Horimoto T, Goto H, Takahashi K, Makino A, Ishigaki H, Nakayama M, Okamatsu M, Takahashi K, Warshauer D, Shult PA, Saito R, Suzuki H, Furuta Y, Yamashita M, Mitamura K, Nakano K, Nakamura M, Brockman-Schneider R, Mitamura H, Yamazaki M, Sugaya N, Suresh M, Ozawa M, Neumann G, Gern J, Kida H, Ogasawara K, and Kawaoka Y.** 2009. In vitro and in vivo characterization of new swine-origin H1N1 influenza viruses. *Nature* **460**: 1021-1025.
57. **Iwatsuki-Horimoto K, Horimoto T, Noda T, Kiso M, Maeda J, Watanabe S, Muramoto Y, Fujii K, and Kawaoka Y.** 2006. The cytoplasmic tail of the influenza A virus M2 protein plays a role in viral assembly. *J Virol* **80**: 5233-5240.

58. **Jackson DA, Caton AJ, McCready SJ, and Cook PR.** 1982. Influenza virus RNA is synthesized at fixed sites in the nucleus. *Nature* **296**: 366-368.
59. **Jin H, Leser GP, and Lamb RA.** 1994. The influenza virus hemagglutinin cytoplasmic tail is not essential for virus assembly or infectivity. *EMBO J* **13**: 5504-5515.
60. **Jin H, Leser GP, Zhang J, and Lamb RA.** 1997. Influenza virus hemagglutinin and neuraminidase cytoplasmic tails control particle shape. *EMBO J* **16**: 1236-1247.
61. **Jo S, Kawaguchi A, Takizawa N, Morikawa Y, Momose F, and Nagata K.** 2010. Involvement of vesicular trafficking system in membrane targeting of the progeny influenza virus genome. *Microbes Infect* **12**: 1079-1084.
62. **Johnson NP and Mueller J.** 2002. Updating the accounts: global mortality of the 1918-1920 "Spanish" influenza pandemic. *Bull Hist Med* **76**: 105-115.
63. **Kaminski MM, Ohnemus A, Staeheli P, and Rubbenstroth D.** 2013. Pandemic 2009 H1N1 influenza A virus carrying a Q136K mutation in the neuraminidase gene is resistant to zanamivir but exhibits reduced fitness in the guinea pig transmission model. *J Virol* **87**: 1912-1915.
64. **Kash JC, Tumpey TM, Proll SC, Carter V, Perwitasari O, Thomas MJ, Basler CF, Palese P, Taubenberger JK, Garcia-Sastre A, Swayne DE, and Katze MG.** 2006. Genomic analysis of the increased host immune and cell death responses induced by 1918 influenza virus. *Nature* **443**: 578-581.

65. **Kawaoka Y, Krauss S, and Webster RG.** 1989. Avian-to-human transmission of the PB1 gene of influenza A viruses in the 1957 and 1968 pandemics. *J Virol* **63**: 4603-4608.
66. **Ketha KM and Atreya CD.** 2008. Application of bioinformatics-coupled experimental analysis reveals a new transport-competent nuclear localization signal in the nucleoprotein of influenza A virus strain. *BMC Cell Biol* **9**: 22.
67. **Kilbourne ED and Murphy JS.** 1960. Genetic studies of influenza viruses. I. Viral morphology and growth capacity as exchangeable genetic traits. Rapid in ovo adaptation of early passage Asian strain isolates by combination with PR8. *J Exp Med* **111**: 387-406.
68. **Kobasa D, Jones SM, Shinya K, Kash JC, Copps J, Ebihara H, Hatta Y, Kim JH, Halfmann P, Hatta M, Feldmann F, Alimonti JB, Fernando L, Li Y, Katze MG, Feldmann H, and Kawaoka Y.** 2007. Aberrant innate immune response in lethal infection of macaques with the 1918 influenza virus. *Nature* **445**: 319-323.
69. **Krenn BM, Egorov A, Romanovskaya-Romanko E, Wolschek M, Nakowitsch S, Ruthsatz T, Kiefmann B, Morokutti A, Humer J, Geiler J, Cinati J, Michaelis M, Wressnigg N, Sturlan S, Ferko B, Batishchev OV, Indenbom AV, Zhu R, Kastner M, Hinterdorfer P, Kiselev O, Muster T, and Romanova J.** 2011. Single HA2 mutation increases the infectivity and immunogenicity of a live attenuated H5N1 intranasal influenza vaccine candidate lacking NS1. *PLoS One* **6**: e18577.

70. **Kwon YK, Lipatov AS, and Swayne DE.** 2009. Bronchointerstitial pneumonia in guinea pigs following inoculation with H5N1 high pathogenicity avian influenza virus. *Vet Pathol* **46**: 138-141.
71. **Lai JC, Chan WW, Kien F, Nicholls JM, Peiris JS, and Garcia JM.** 2010. Formation of virus-like particles from human cell lines exclusively expressing influenza neuraminidase. *J Gen Virol* **91**: 2322-2330.
72. **Lakdawala SS, Lamirande EW, Suguitan AL, Jr., Wang W, Santos CP, Vogel L, Matsuoka Y, Lindsley WG, Jin H, and Subbarao K.** 2011. Eurasian-origin gene segments contribute to the transmissibility, aerosol release, and morphology of the 2009 pandemic H1N1 influenza virus. *PLoS Pathog* **7**: e1002443.
73. **Lamb RA, Lai CJ, and Choppin PW.** 1981. Sequences of mRNAs derived from genome RNA segment 7 of influenza virus: colinear and interrupted mRNAs code for overlapping proteins. *Proc Natl Acad Sci USA* **78**: 4170-4174.
74. **Latham T and Galarza JM.** 2001. Formation of wild-type and chimeric influenza virus-like particles following simultaneous expression of only four structural proteins. *J Virol* **75**: 6154-6165.
75. **Leser GP and Lamb RA.** 2005. Influenza virus assembly and budding in raft-derived microdomains: a quantitative analysis of the surface distribution of HA, NA, and M2 proteins. *Virology* **342**: 215-227.
76. **Li Q, Sun X, Li Z, Liu Y, Vavricka CJ, Qi J, and Gao GF.** 2012. Structural and functional characterization of neuraminidase-like molecule N10 from bat influenza A virus. *Proc Natl Acad Sci USA* **109**: 18897-18902.

77. **Liu T and Ye Z.** 2002. Restriction of viral replication by mutation of the influenza virus matrix protein. *J Virol* **76**: 13055-13061.
78. **Lowen AC, Mubareka S, Steel J, and Palese P.** 2007. Influenza virus transmission is dependent on relative humidity and temperature. *PLoS Pathog* **3**: 1470-1476.
79. **Lowen AC, Mubareka S, Tumpey TM, Garcia-Sastre A, and Palese P.** 2006. The guinea pig as a transmission model for human influenza viruses. *Proc Natl Acad Sci USA* **103**: 9988-9992.
80. **Ma W, Liu Q, Bawa B, Qiao C, Qi W, Shen H, Chen Y, Ma J, Li X, Webby RJ, Garcia-Sastre A, and Richt JA.** 2012. The neuraminidase and matrix genes of the 2009 pandemic influenza H1N1 virus cooperate functionally to facilitate efficient replication and transmissibility in pigs. *J Gen Virol* **93**: 1261-1268.
81. **Maines TR, Lu XH, Erb SM, Edwards L, Guarner J, Greer PW, Nguyen DC, Szretter KJ, Chen LM, Thawatsupha P, Chittaganpitch M, Waicharoen S, Nguyen DT, Nguyen T, Nguyen HH, Kim JH, Hoang LT, Kang C, Phuong LS, Lim W, Zaki S, Donis RO, Cox NJ, Katz JM, and Tumpey TM.** 2005. Avian influenza (H5N1) viruses isolated from humans in Asia in 2004 exhibit increased virulence in mammals. *J Virol* **79**: 11788-11800.
82. **Mair CM, Ludwig K, Herrmann A, and Sieben C.** 2014. Receptor binding and pH stability - how influenza A virus hemagglutinin affects host-specific virus infection. *Biochim Biophys Acta* **1838**: 1153-1168.

83. **Martin K and Helenius A.** 1991. Nuclear transport of influenza virus ribonucleoproteins: the viral matrix protein (M1) promotes export and inhibits import. *Cell* **67**: 117-130.
84. **Matlin KS, Reggio H, Helenius A, and Simons K.** 1981. Infectious entry pathway of influenza virus in a canine kidney cell line. *J Cell Biol* **91**: 601-613.
85. **Matrosovich MN, Gambaryan AS, Teneberg S, Piskarev VE, Yamnikova SS, Lvov DK, Robertson JS, and Karlsson KA.** 1997. Avian influenza A viruses differ from human viruses by recognition of sialyloligosaccharides and gangliosides and by a high conservation of the HA receptor-binding site. *Virology* **233**: 224-234.
86. **Matrosovich MN, Matrosovich TY, Gray T, Roberts NA, and Klenk HD.** 2004. Neuraminidase is important for the initiation of influenza virus infection in human airway epithelium. *J Virol* **78**: 12665-12667.
87. **McCown MF and Pekosz A.** 2006. Distinct domains of the influenza A virus M2 protein cytoplasmic tail mediate binding to the M1 protein and facilitate infectious virus production. *J Virol* **80**: 8178-8189.
88. **Mehle A and Doudna JA.** 2009. Adaptive strategies of the influenza virus polymerase for replication in humans. *Proc Natl Acad Sci USA* **106**: 21312-21326.
89. **Mitnaul LJ, Castrucci MR, Murti KG, and Kawaoka Y.** 1996. The cytoplasmic tail of influenza A virus neuraminidase (NA) affects NA incorporation into virions, virion morphology, and virulence in mice but is not essential for virus replication. *J Virol* **70**: 873-879.

90. **Molinari NA, Ortega-Sanchez IR, Messonnier ML, Thompson WW, Wortley PM, Weintraub E, and Bridges CB.** 2007. The annual impact of seasonal influenza in the US: measuring disease burden and costs. *Vaccine* **25**: 5086-5096.
91. **Momose F, Sekimoto T, Ohkura T, Jo S, Kawaguchi A, Nagata K, and Morikawa Y.** 2011. Apical transport of influenza A virus ribonucleoprotein requires Rab11-positive recycling endosome. *PLoS One* **6**: e21123.
92. **Moren DM, Taubenberger JK, and Fauci AS.** 2008. Predominant role of bacterial pneumonia as a cause of death in pandemic influenza: implications for pandemic influenza preparedness. *J Infect Dis* **198**: 962-970.
93. **Morgan C, Rose HM, and Moore DH.** 1956. Structure and development of viruses observed in the electron microscope. III. Influenza virus. *J Exp Med* **104**: 171-182.
94. **Mosley VM and Wyckoff RW.** 1946. Electron micrography of the virus of influenza. *Nature* **157**: 263.
95. **Mukaigawa J and Nayak DP.** 1991. Two signals mediate nuclear localization of influenza virus (A/WSN/33) polymerase basic protein 2. *J Virol* **65**: 245-253.
96. **Murti KG and Webster RG.** 1986. Distribution of hemagglutinin and neuraminidase on influenza virions as revealed by immunoelectron microscopy. *Virology* **149**: 36-43.
97. **Nakajima N, Hata S, Sato Y, Tobiume M, Katano H, Kaneko K, Nagata N, Kataoka M, Aina A, Hasegawa H, Tashiro M, Kuroda M, Odai T, Urasawa N, Ogino T, Hanaoka H, Watanabe M, and Sata T.** 2010. The first autopsy case of pandemic influenza (A/H1N1pdm) virus infection in Japan: detection of a

- high copy number of the virus in type II alveolar epithelial cells by pathological and virological examination. *Jpn J Infect Dis* **63**: 67-71.
98. **Nath ST and Nayak DP.** 1990. Mol Cell Biol 10: 4139-4145, Function of two discrete regions is required for nuclear localization of polymerase basic protein 1 of A/WSN/33 influenza virus (H1N1). **10**: 4139-4145
99. **Neumann G, Hughes MT, and Kawaoka Y.** 2000. Influenza A virus NS2 protein mediates vRNP nuclear export through NES-independent interaction with hCRM1. *EMBO J* **19**: 6751-6788.
100. **Nieto A, de la Luna S, Barcena J, Portela A, and Ortin J.** 1994. Complex structure of the nuclear translocation signal of influenza virus polymerase PA subunit. *J Gen Virol* **75**: 29-36.
101. **Noda T, Sagara H, Yen A, Takada A, Kida H, Cheng RH, and Kawaoka Y.** 2006. Architecture of ribonucleoprotein complexes in influenza A virus particles. *Nature* **439**: 490-492.
102. **Novel Swine-Origin Influenza A (H1N1) Virus Investigation Team, Dawood FS, Jain S, Finelli L, Shaw MW, Lindstrom S, Garten RJ, Gubareva LV, Xu X, Bridges CB, and Uyeki TM.** 2009. Emergence of a novel swine-origin influenza A (H1N1) virus in humans. *N Engl J Med* **360**: 2605-2615.
103. **O'Neill RE, Jaskunas R, Blobel G, Palese P, and Moroianu J.** 1995. Nuclear import of influenza virus RNA can be mediated by viral nucleoprotein and transport factors required for protein import. *J Biol Chem* **270**: 22701-22704.

104. **O'Neill RE, Talon J, and Palese P.** 1998. The influenza virus NEP (NS2 protein) mediates the nuclear export of viral ribonucleoproteins. *EMBO J* **17**: 288-296.
105. **Palese P and Shaw ML.** 2007. Orthomyxoviridae: the viruses and their replication, p. 1647-1689. *In* Knipe DM and Howley PM, (ed). *Fields Virology* 5th edition. Lippincott Williams & Wilkins, Philadelphia, PA.
106. **Pica N and Bouvier NM.** 2012. Environmental factors affecting the transmission of respiratory viruses. *Curr Opin Virol* **2**: 90-95.
107. **Pinto LH, Holsinger LJ, and Lamb RA.** 1992. Influenza virus M2 protein has ion channel activity. *Cell* **69**: 517-528.
108. **Plotch SJ, Bouloy M, Ulmanen I, and Krug RM.** 1981. A unique cap(m⁷GpppXm)-dependent influenza virion endonuclease cleaves capped RNAs to generate the primers that initiate viral RNA transcription. *Cell* **23**: 847-858.
109. **Poch O, Sauvaget I, Delarue M, and Tordo N.** 1989. Identification of four conserved motifs among the RNA-dependent polymerase encoding elements. *EMBO J* **8**: 3867-3874.
110. **Roberts KL, Leser GP, Ma C, and Lamb RA.** 2013. The amphipathic helix of influenza A virus M2 protein is required for filamentous bud formation and scission of filamentous and spherical particles. *J Virol* **87**: 9973-9982.
111. **Roberts PC and Compans RW.** 1998. Host cell dependence of viral morphology. *Proc Natl Acad Sci USA* **95**: 5746-5751.

112. **Roberts PC, Lamb RA, and Compans RW.** 1998. The M1 and M2 proteins of influenza A virus are important determinants in filamentous particle formation. *Virology* **240**: 127-137.
113. **Rogers GN and D'Souza BL.** 1989. Receptor binding properties of human and animal H1 influenza virus isolates. *Virology* **173**: 317-322.
114. **Rogers GN, Paulson JC, Daniels RS, Skehel JJ, Wilson IA, and Wiley DC.** 1983. Single amino acid substitutions in influenza haemagglutinin change receptor binding specificity. *Nature* **304**: 76-78.
115. **Rossman JS, Jing X, Leser GP, Balannik V, Pinto LH, and Lamb RA.** 2010. Influenza virus m2 ion channel protein is necessary for filamentous virion formation. *J Virol* **84**: 5078-5088.
116. **Rossman JS, Jing X, Leser GP, and Lamb RA.** 2010. Influenza virus M2 protein mediates ESCRT-independent membrane scission. *Cell* **142**: 902-913.
117. **Rossman JS and Lamb RA.** 2011. Influenza virus assembly and budding. *Virology* **411**: 229-236.
118. **Ruigrok RW, Barge A, Durrer P, Brunner J, Ma K, and Whittaker GR.** 2000. Membrane interaction of influenza virus M1 protein. *Virology* **267**: 289-298.
119. **Rust MJ, Lakadamyali M, Zhang F, and Zhuang X.** 2004. Assembly of endocytic machinery around individual influenza viruses during viral entry. *Nat Struct Mol Biol* **11**: 567-573.

120. **Scheiffele P, Roth MG, and Simons K.** 1997. Interaction of influenza virus haemagglutinin with sphingolipid-cholesterol membrane domains via its transmembrane domain. *EMBO J* **16**: 5501-5508.
121. **Schmidt NW, Mishra A, Wang J, DeGrado WF, and Wong GC.** 2013. Influenza virus A M2 protein generates negative Gaussian membrane curvature necessary for budding and scission. *J Am Chem Soc* **135**: 13710-13719.
122. **Schnell JR and Chou JJ.** 2008. Structure and mechanism of the M2 proton channel of influenza A virus. *Nature* **451**: 591-595.
123. **Scholtissek C, Rohde W, Von Hoyningen V, and Rott R.** 1978. On the origin of the human influenza virus subtypes H2N2 and H3N2. *Virology* **87**: 13-20.
124. **Schulman JL.** 1968. The use of an animal model to study transmission of influenza virus infection. *Am J Public Health Nations Health* **58**: 2092-2096.
125. **Schulman JL and Kilbourne ED.** 1963. Experimental transmission of influenza virus infection in mice. II. Some factors affecting the incidence of transmitted infection. *J Exp Med* **118**: 267-275.
126. **Schulze IT.** 1970. The structure of influenza virus. I. The polypeptides of the virion. *Virology* **42**: 890-904.
127. **Seladi-Schulman J, Steel J, and Lowen AC.** 2013. Spherical influenza viruses have a fitness advantage in embryonated eggs, while filament-producing strains are selected in vivo. *Journal of Virol* **87**: 13343-13353.
128. **Sha B and Luo M.** 1997. Structure of a bifunctional membrane-RNA binding protein, influenza matrix protein M1. *Nat Struct Biol* **4**: 239-244.

129. **Shapiro GI, Gurney T Jr, and Krug RM.** 1987. Influenza virus gene expression: control mechanisms at early and late times of infection and nuclear-cytoplasmic transport of virus-specific RNAs. *J Virol* **61**: 764-773.
130. **Sheehan JK, Thornton DJ, Somerville M, and Carlstedt I.** 1991. Mucin structure: The structure and heterogeneity of respiratory mucus glycoproteins. *Am Rev Respir Dis* **144**: S4-9.
131. **Shelton H, Roberts KL, Molesti E, Temperton N, and Barclay WS.** 2013. Mutations in haemagglutinin that affect receptor binding and pH stability increase replication of a PR8 influenza virus with H5 HA in the upper respiratory tract of ferrets and may contribute to transmissibility. *J Gen Virol* **94**: 1220-1229.
132. **Sheng ZM, Chertow DS, Ambroggio X, McCall S, Przygodzki RM, Cunningham RE, Maximova OA, Kash JC, Morens DM, and Taubenberger JK.** 2011. Autopsy series of 68 cases dying before and during the 1918 influenza pandemic peak. *Proc Natl Acad Sci USA* **108**: 16416-16421.
133. **Sieczkarski SB and Whittaker GR.** 2002. Influenza virus can enter and infect cells in the absence of clathrin-mediated endocytosis. *J Virol* **76**: 10455-10464.
134. **Simpson-Holley M, Ellis D, Fisher D, Elton D, McCauley J, and Digard P.** 2002. A functional link between the actin cytoskeleton and lipid rafts during the budding of filamentous influenza virions. *Virology* **301**: 212-225.
135. **Smirnov YA, Kuznetsova MA, and Kaverin NV.** 1991. The genetics aspects of influenza virus filamentous particle formation. *Arch Virol* **118**: 279-284.
136. **Smith GJ, Vijaykrishna D, Bahl J, Lycett SJ, Worobey M, Pybus OG, Ma SK, Cheung CL, Raghvani J, Bhatt S, Peiris JS, Guan Y, and Rambaut A.**

2009. Origins and evolutionary genomics of the 2009 swine-origin H1N1 influenza A epidemic. *Nature* **459**: 1122-1125.
137. **Sorrell EM, Wan H, Araya Y, Song H, and Perez DR.** 2009. Minimal molecular constraints for respiratory droplet transmission of an avian-human H9N2 influenza A virus. *Proc Natl Acad Sci USA* **106**: 7565-7570.
138. **Steel J, Lowen AC, Mubareka S, and Palese P.** 2009. Transmission of influenza virus in a mammalian host is increased by PB2 amino acids 627K or 627E/701N. *PLoS Pathog* **5**: e1000252.
139. **Tambunan US and Ramdhan.** 2010. Identification of sequence mutations affecting hemagglutinin specificity to sialic acid receptor in influenza A virus subtypes. *Bioinformatics* **5**: 244-249.
140. **Tamerius JD, Shaman J, Alonso WJ, Bloom-Feshbach K, Uejio CK, Comrie A, and Viboud C.** 2013. Environmental predictors of seasonal influenza epidemics across temperate and tropical climates. *PLoS Pathog* **9**: e1003194.
141. **Tang X and Chong KT.** 2009. Histopathology and growth kinetics of influenza viruses (H1N1 and H3N2) in the upper and lower airways of guinea pigs. *J Gen Virol* **90**: 386-391.
142. **Tarendeau F, Boudet J, Guilligay D, Mas PJ, Bougault CM, Boulo S, Baudin F, Ruigrok RW, Daigle N, Ellenberg J, Cusack S, Simorre JP, and Hart DJ.** 2007. Structure and nuclear import function of the C-terminal domain of influenza virus polymerase PB2 subunit. *Nat Struct Mol Biol* **14**: 229-233.
143. **Thangavel RR and Bouvier NM.** 2014. Animal models for influenza virus pathogenesis, transmission, and immunology. *J Immunol Methods* **1759**: 112-114.

144. **Tian C, Gao PF, Pinto LH, Lamb RA, and Cross TA.** 2003. Initial structural and dynamic characterization of the M2 protein transmembrane and amphipathic helices in lipid bilayers. *Protein Sci* **12**: 2597-2605.
145. **Tong S, Li Y, Rivaillier P, Conrardy C, Castillo DA, Chen LM, Recuenco S, Ellison JA, Davis CT, York IA, Turmelle AS, Moran D, Rogers S, Shi M, Tao Y, Well MR, Tang K, Rowe LA, Sammons S, Xu X, Frace M, Lindblade KA, Cox NJ, Anderson LJ, Rupprecht CE, and Donis RO.** 2012. A distinct lineage of influenza A virus from bats. *Proc Natl Acad Sci USA* **109**: 4269-4274.
146. **Tong S, Zhu X, Li Y, Shi M, Zhang J, Bourgeois M, Yang H, Chen X, Recuenco S, Gomez J, Chen LM, Johnson A, Tao Y, Dreyfus C, Yu W, McBride R, Carney PJ, Gilbert AT, Chang J, Guo Z, Davis CT, Paulson JC, Stevens J, Rupprecht CE, Holmes EC, Wilson IA, and Donis RO.** 2013. New world bats harbor diverse influenza A viruses. *PLoS Pathog* **9**: e1003657.
147. **Tumpey TM, Maines TR, Van Hoeven N, Glaser L, Solorzano A, Pappas C, Cox NJ, Swayne DE, Palese P, Katz JM, and Garcia-Sastre A.** 2007. A two-amino acid change in the hemagglutinin of the 1918 influenza virus abolishes transmission. *Science* **315**: 655-659.
148. **Van Hoeven N, Belser JA, Szretter KJ, Zeng H, Staeheli P, Swayne DE, Katz JM, and Tumpey TM.** 2009. Pathogenesis of 1918 pandemic and H5N1 influenza virus infections in a guinea pig model: antiviral potential of exogenous alpha interferon to reduce virus shedding. *J Virol* **83**: 2851-2861.
149. **Van Hoeven N, Pappas C, Belser JA, Maines TR, Zeng H, Garcia-Sastre A, Sasisekharan R, Katz JM, and Tumpey TM.** 2009. Human HA and polymerase

subunit PB2 proteins confer transmission of an avian influenza virus through the air. *Proc Natl Acad Sci USA* **106**: 3366-3371.

150. **Vijaykrishnan S, Loney C, Jackson D, Suphamungmee W, Rixon FJ, and Bhella D.** 2013. Cryotomography of budding influenza A virus reveals filaments with diverse morphologies that mostly do not bear a genome at their distal end. *PLoS Pathog* **9**: e1003413.
151. **Ward AC, Castelli LA, Lucantoni AC, White JF, Azad AA, and Macreadie IG.** 1995. Expression and analysis of the NS2 protein of influenza A virus. *Arch Virol* **140**: 2067-2073.
152. **Watanabe K, Handa H, Mizumoto K, and Nagata K.** 1996. Mechanism for inhibition of influenza virus RNA polymerase activity by matrix protein. *J Virol* **70**: 241-247.
153. **Webby RJ, Rossow K, Erickson G, Sims Y, and Webster R.** 2004. Multiple lineages of antigenically and genetically diverse influenza A virus co-circulate in the United States swine population. *Virus Res* **103**: 67-73.
154. **Webby RJ, Swenson SL, Krauss SL, Gerrish PJ, Goyal SM, and Webster RG.** 2000. Evolution of swine H3N2 influenza viruses in the United States. *J Virol* **74**: 8243-8251.
155. **Weber F, Kochs G, Gruber S, and Haller O.** 1998. A classical bipartite nuclear localization signal on Thogoto and influenza A virus nucleoproteins. *Virology* **250**: 9-18.
156. **Webster RG, Bean WJ, Gorman OT, Chambers TM, and Kawaoka Y.** 1992. Evolution and ecology of influenza A viruses. *Microbiol Rev* **56**: 152-179.

157. **Whittaker G, Bui M, and Helenius A.** 1996. Nuclear trafficking of influenza virus ribonucleoproteins in heterokaryons. *J Virol* **70**: 2743-2756.
158. **Worobey M, Han GZ, and Rambaut A.** 2014. Genesis and pathogenesis of the 1918 pandemic H1N1 influenza A virus. *Proc Natl Acad Sci USA* **22**: 8107-8112.
159. **Wright PF, Neumann G, and Kawaoka Y.** 2007. Orthomyxoviruses, p. 1691-1740. *In* Knipe DM, Howley PM, Griffin DE, Lamb RA, Straus SE, Martin MA, and Roizman B, (ed), *Fields Virology* 5th edition. Lippincott Williams & Wilkins, Philadelphia, PA.
160. **Wu WW, Sun YH, and Pante N.** 2007. Nuclear import of influenza A viral ribonucleoprotein complexes is mediated by two nuclear localization sequences on viral nucleoprotein. *Virology* **4**: 49.
161. **Yamada S, Suzuki Y, Suzuki T, Le MQ, Nidom CA, Sakai-Tagawa Y, Muramoto Y, Ito M, Kiso M, Horimoto T, Shinya K, Sawada T, Kiso M, Usui T, Murata T, Lin Y, Hay A, Haire LF, Stevens DJ, Russell RJ, Gamblin SJ, Skehel JJ, and Kawaoka Y.** 2006. Haemagglutinin mutations responsible for the binding of H5N1 influenza A viruses to human-type receptors. *Nature* **444**: 378-382.
162. **Yasuda J, Nakada S, Kato A, Toyoda T, and Ishihama A.** 1993. Molecular assembly of influenza virus: association of the NS2 protein with virion matrix. *Virology* **196**: 249-255.
163. **Ye Z, Robinson D, and Wagner RR.** 1995. Nucleus-targeting domain of the matrix protein (M1) of the influenza virus. *J Virol* **69**: 1964-1970.

164. **Yen HL, Liang CH, Wu CY, Forrest HL, Ferguson A, Choy KT, Jones J, Wong DD, Cheung PP, Hsu CH, Li OT, Yuen KM, Chan RW, Poon LL, Chan MC, Nicholls JM, Krauss S, Wong CH, Guan Y, Webster RG, Webby RJ, and Peiris M.** 2011. Hemagglutinin-neuraminidase balance confers respiratory-droplet transmissibility of the pandemic H1N1 influenza virus in ferrets. *Proc Natl Acad Sci USA* **108**: 14264-14269.
165. **Yuan P, Bartlam M, Lou Z, Chen S, Zhou J, He X, Lv Z, Ge R, Li X, Deng T, Fodor E, Rao Z, and Liu Y.** 2009. Crystal structure of an avian influenza polymerase PA(N) reveals an endonuclease active site. *Nature* **458**: 909-913.
166. **Zaraket H, Bridges OA, Duan S, Baranovich T, Yoon SW, Reed ML, Salomon R, Webby RJ, Webster RG, and Russell CJ.** 2013. Increased acid stability of the hemagglutinin protein enhances H5N1 influenza virus growth in the upper respiratory tract but is insufficient for transmission in ferrets. *J Virol* **87**: 9911-9922.
167. **Zaraket H, Bridges OA, and Russell CJ.** 2013. The pH of activation of the hemagglutinin protein regulates H5N1 influenza replication and pathogenesis in mice. *J Virol* **87**: 4826-4834.
168. **Zhang J, Leser GP, Pekosz A, and Lamb RA.** 2000. The cytoplasmic tails of the influenza virus spike glycoproteins are required for normal genome packaging. *Virology* **269**: 325-334.
169. **Zhang J and Lamb RA.** 1996. Characterization of the membrane association of the influenza virus matrix protein in living cells. *Virology* **225**: 255-266.

170. **Zhu X, Yang H, Guo Z, Yu W, Carney PJ, Li Y, Chen LM, Paulson JC, Donis RO, Tong S, Stevens J, and Wilson IA.** 2012. Crystal structures of two subtype N10 neuraminidase-like proteins from bat influenza A viruses reveal a diverged putative active site. *Proc Natl Acad Sci USA* **109**: 18903-18908.
171. **Zvonarjev AY and Ghendon YZ.** 1980. Influence of membrane (M) protein on influenza A virus virion transcriptase activity in vitro and its susceptibility to rimantadine. *J Virol* **33**: 583-586.